EVALUATION OF TURBULENT FORCED CONVECTION HEAT TRANSFER AND PRESSURE DROP OF NANOFLUIDS FLOW IN DIFFERENT CLOSED CONDUIT CONFIGURATIONS

ALI HASSAN ABDELRAZEK ELSAYED

FACULTY OF ENGINEERING
UNIVERSITY OF MALAYA
KUALA LUMPUR

2021

EVALUATION OF TURBULENT FORCED CONVECTION HEAT TRANSFER AND PRESSURE DROP OF NANOFLUIDS FLOW IN DIFFERENT CLOSED CONDUIT CONFIGURATIONS

ALI HASSAN ABDELRAZEK ELSAYED

THESIS SUBMITTED IN FULFILMENT OF THE REQUIREMENTS FOR THE DEGREE OF DOCTOR OF PHILOSOPHY

**FACULTY OF ENGINEERING
UNIVERSITY OF MALAYA
KUALA LUMPUR**

2021

UNIVERSITY OF MALAYA

ORIGINAL LITERARY WORK DECLARATION

Name of Candidate: ALI HASSAN ABDELRAZEK ELSAYED

Matric No: 17013157/1

Name of Degree: Doctor of Philosophy

Title of Thesis ("Evaluation of Turbulent Forced Convection Heat Transfer and Pressure Drop of Nanofluids Flow in Different Closed Conduit Configurations"):

Field of Study: Heat Transfer (Mechanics and Metal Work)

I do solemnly and sincerely declare that:

(1) I am the sole author/writer of this Work.
(2) This Work is original.
(3) Any use of any work in which copyright exists was done by way of fair dealing and for permitted purposes and any excerpt or extract from, or reference to or reproduction of any copyrighted work has been disclosed expressly and sufficiently and the title of the Work and its authorship have been acknowledged in this Work.
(4) I do not have any actual knowledge, nor do I ought reasonably to know that the making of this work constitutes an infringement of any copyrighted work.
(5) I hereby assign all and every right in the copyright to this Work to the University of Malaya ("UM"), who henceforth shall be owner of the copyright in this Work and that any reproduction or use in any form or by any means whatsoever is prohibited without the written consent of UM having been first had and obtained.
(6) I am fully aware that if in the course of making this work, I have infringed any copyright whether intentionally or otherwise, I may be subject to legal action, or any other action as may be determined by UM.

Candidate's Signature   Date:

Subscribed and solemnly declared before,

Witness's Signature   Date:

Name:

Designation:

ABSTRACT

Nanofluids are a relatively new class of fluids consisting of a base fluid with suspended nano-sized particles (1–100 nm). Nanofluids are suggested as a favorable convective medium because the thermal conductivity of the suspensions is typically an order-of-magnitude higher than those of normal fluids such as water. In convection heat transfer applications, some researchers reported that enhancing the convection heat transfer coefficient is directly proportional to nanofluids' thermal conductivity increment. In contrast, others said that the nanofluid thermal conductivity is not the critical parameter for enhancing convection heat transfer. Therefore, experimental and numerical work was conducted in the current study to evaluate the thermal performance of different nanofluids in different pipe geometries with the same hydraulic diameter. Three different aqua-based nanofluids of weight concentrations 0.05%, 0.075%, and 0.1% were prepared using the two-step method. One nanofluid was prepared from composite nanoparticles, composed of 60 % Al_2O_3 and 40% f-MWCNTs by weight. The second one was prepared from the Al_2O_3, and the third nanofluid was prepared from SiO_2 nanoparticles. All the nanofluids showed an excellent dispersion in the stability test over one month, and their thermophysical properties were evaluated experimentally except the specific heat, which was calculated theoretically. The experimental work was conducted using a test rig containing circular and square test sections of 10 mm hydraulic diameter exposed to a uniform heat flux on their outer surfaces. The inlet flow temperature was kept constant at 30 °C in all the runs. All experimental work was done under steady-state fully developed turbulent flow conditions with the Reynolds number range of 6000-11000. The results obtained experimentally showed that the Prandtl number has the most significant effect compared to the thermal conductivity on the Nusselt number and the convection heat transfer coefficient. The numerical work was conducted to evaluate the heat transfer and pressure drop through the same geometries in the experimental work in addition to an

annular heat exchanger of the same hydraulic diameter and an eccentricity range from 0.0 to 0.6. The continuity, momentum, and energy equations were solved using the finite volume approach available in the ANSYS-Fluent commercial software with the same flow and boundary conditions as the experimental work. The results obtained numerically were in good agreement with those obtained experimentally for the circular and square pipes. The annular pipe's model was validated with some empirical correlations, shown an average error of less than 10%. All the results obtained numerically confirmed the experimental findings. Finally, the thermal performance evaluation showed that the distilled water (DW) has the highest thermal performance, and the lower nanofluid concentration has also shown the higher thermal performance.

Keywords: Hybrid Nanofluids; Metal-oxide Nanofluids; Eccentric pipe heat exchanger; Forced Turbulent flow; CFD modeling.

ABSTRAK

Nanofluids atau cecair-nano adalah kelas cecair yang agak baru yang terdiri daripada cecair asas dengan zarah bersaiz nano yang terkandung (1-100 nm) di dalamnya. Nanofluids adalah dijangka menjadi sebagai medium konvektif yang baik dan sesuai bergantung kepada fakta bahawa kekonduksian haba kandungan tersebut biasanya adalah mengikut urutan-magnitud lebih tinggi daripada cecair biasa seperti air. Dalam aplikasi pemindahan haba konveksi atau perolakan, sesetengah penyelidik melaporkan bahawa peningkatan pekali pemindahan haba perolakan adalah berkadaran secara langsung dengan kenaikan kekonduksian haba cecair-nano manakala, yang lain melaporkan bahawa kekonduksian haba cecair-nano bukanlah parameter utama untuk meningkatkan pemindahan haba perolakan. Oleh itu, satu eksperimen dan kerja berangka telah dijalankan dalam kajian ini untuk menilai prestasi haba cecair-nano yang berbeza di dalam geometri paip yang berbeza yang mempunyai diameter hidraulik yang sama. Tiga cecair-nano berasaskan air yang berbeza kepekatan berat 0.05 %, 0.075 %, dan 0.1% telah disediakan menggunakan kaedah dua langkah: cecair-nano pertama telah disediakan dari partikel-nano hibrid, terdiri daripada 60% daripada Al_2O_3 dan 40% dengan beratf-MWCNTs, yang kedua telah disediakan dari Al_2O_3, dan yang ketiga disediakan dari partikle-nano SiO_2. Semua cecair-nano menunjukkan penyebaran yang sangat baik dalam ujian kestabilan dalam tempoh satu bulan dan sifat termofizikal mereka telah dinilai secara eksperimen kecuali haba-tentu yang telah dikira secara teoritikal. Kerja-kerja eksperimen dijalankan menggunakan pelantar ujian mengandungi bahagianujian berbentuk pekeliling dan persegi diameter hidraulik 10 mm yang terdedah kepada flux haba seragam pada permukaan luaran mereka dan suhu aliran masuk ditetapkan berterusan pada 30 °C dalam semua larian. Semua eksperimen telah dilakukan di bawah keadaan mantap dengan keadaan aliran bergelora sepenuhnya dengan julat nombor Reynolds 6000-11000. Keputusan yang diperolehi secara eksperimen menunjukkan

bahawa nombor Prandtl mempunyai kesan terbesar kepada nombor Nusselt dan pekali pemindahan haba perolakan juga, sebagai tambahan kepada kesan kekonduksian haba. Kerja-kerja berangka itu dijalankan untuk menilai pemindahan haba dan penurunan tekanan melalui geometri yang sama dalam kerja-kerja eksperimen sebagai tambahan kepada penukar haba annular dengan diameter hidraulik yang sama dan julat eksentrisiti dari 0.0 hingga 0.6. Kesinambungan (kontuniti), momentum, dan persamaan tenaga diselesaikan menggunakan pendekatan isi padu terhingga yang terdapat dalam perisian komersial ANSYS-Fluent dengan aliran dan keadaan sempadan yang sama seperti dalam kerja eksperimen. Keputusan yang diperolehi secara berangka adalah dalam sama dengan apa yang diperolehi secara eksperimen untuk paip keliling dan paip persegi, dan keputusan model anular paip. telah disahkan dengan beberapa korelasi empirikal, menunjukkan kesilapan purata kurang daripada 10%. Kesemua keputusan yang diperolehi secara berangka mengesahkan penemuan eksperimen. Akhirnya, penilaian prestasi haba menunjukkan bahawa air suling mempunyai prestasi haba tertinggi dan kepekatan cecair-nano yang lebih rendah juga menunjukkan prestasi haba yang lebih tinggi.

Kata kunci: Nanofluid Hybrid; Nanofluid logam-oksida; Penukar haba eksentrik; Aliran Turbulen Terpaksa; Pemodelan CFD.

ACKNOWLEDGEMENTS

TABLE OF CONTENTS

LIST OF FIGURES

LIST OF TABLES

LIST OF SYMBOLS AND ABBREVIATIONS

a	:	Outer to inner diameter ratio in the annular heat exchanger
a^*	:	Inner to outer diameter ratio in the annular heat exchanger
Al_2O_3	:	Aluminum Oxide
A_c	:	Cross-section area, m^2
A_s	:	Total heat transfer surface area, m^2
C	:	Total mass fraction of nanofluid
C_f	:	Friction coefficient
C_i	:	Mass fraction of nanomaterial "i"
C_p	:	Specific Heat, J /kg. K
D	:	Nominal diameter of circular tube, mm
D_h	:	Hydraulic Tube Diameter, $= (4A_c / p)$ m
D_{ins}	:	Diameter of insulation layer, mm
d_p	:	Nanoparticle Diameter, μm
DW	:	Distilled Water
E	:	Eccentric distance or displacement of inner cylinder/ m
e^*	:	Dimensionless eccentricity $= e/(R_o\text{-}R_i)$
f	:	Friction factor
H	:	Head produced by the pump, m
h	:	Convection heat transfer coefficient, W/ $m.^2$ K
I	:	Current, Amp.
I.P	:	Performance index
K	:	Thermal Conductivity, W/ m. K
k	:	Turbulent kinetic energy
L	:	Tube Computational Length, mm

L_s	:	Side length of square tube, m
m_{pi}	:	Mass of the nanomaterial "i" in the mixture of nanopowder, gm
m_{pt}	:	Total mass of different nanomaterials in the hybrid nanofluid
Nu	:	Nusselt number
P	:	Pressure, Pa
p	:	Perimeter, m
Pr	:	Prandtl Number
Q	:	Heat transfer rate, W
q''	:	Heat Flux, W/ m^2
Re	:	Reynolds number
R_i	:	Inner tube radius, m
R_o	:	Outer tube radius, m
SiO_2	:	Silicon Oxide
T	:	Temperature, K
T_b	:	Fluid bulk temperature, K
T_{in}	:	Inlet temperature, K
T_o	:	Outlet temperature, K
T_w	:	Tube wall temperature, K
u	:	Velocity component in x direction, m/ s
v	:	Velocity component in y direction, m/ s
V	:	Mean flow velocity, m/ s
ΔV	:	Voltage difference, V
$\dot{V}$	:	Volume flow rate, m^3
$\dot{W}$	:	Hydraulic pumping power, W

Greek symbols

| α_{th} | : | Thermal diffusivity of the fluid, m^2 /s |

γ	:	Specific weight of the fluid, N/ m^3
ε	:	Turbulent dissipation rate, m^2/ s^2
λ_i	:	Weight percentage of single nanomaterial in the hybrid nanofluid
μ	:	Dynamic viscosity, N.m/ s
μ_t	:	Eddy viscosity, N.m/ s
ν	:	Momentum diffusivity or Kinematic viscosity, m^2/ s
ρ	:	Density, kg/ m^3
τ	:	Shear stress, Pa
φ	:	Nanoparticles volume fraction (%)
ω	:	Nanoparticles weight concentration (%)

Subscript

ann	:	Annular
b	:	Bulk
bf	:	Base fluid
cir	:	Circular
in	:	Inlet
ins	:	Insulation
nf	:	Nanofluid
o	:	Outlet
s	:	Solid
sq	:	Square
t	:	Turbulence
th	:	Thermal
f	:	Fluid
p	:	Particles
w	:	Wall

LIST OF APPENDICES

CHAPTER 1: INTRODUCTION

1.1   Concepts and definitions

The heating and cooling of flowing fluids inside closed conduits is the most common and essential process in all industrial and engineering applications. Therefore, the ways to enhance the heat exchangers effectiveness are many and miscellaneous; either by changing the system parameters such as shape, size, design, and flow conditions, or by controlling the working fluid (Heat transfer medium) properties such as density, specific heat, viscosity, and thermal conductivity. The enhancement of fluid thermal properties was the most concerning issue attracting scientists' attention for many decades since Maxwell (1891) tried to break the fundamentals by dispersing millimeter-sized metal particles in some liquids to increase their thermal conductivity.

The great modern scientific revolution taught us that, at some stage, one would reach the molecular level and even the atomic level, below which the physical and chemical properties are entirely different from those of the original material. For example, the thermal conductivity of single-walled carbon nanotubes (diameters ranging from 0.4 to 50 nm) at room temperature could be an order of magnitude higher than that of copper. Therefore, carbon nanotubes (CNTs) have been considered as a candidate material for applications that require a high heat flux (Zhang, 2007). As a result, the need for studying the behavior of different materials in the nanoscale is continuously increasing.

Nanofluids are defined as a suspension of nanoparticles in a base fluid (Saidur et al., 2011). In common meaning, Nanofluids are a relatively new class of fluids that consist of a base fluid with suspended Nano-sized particles (1–100 nm). Those Nanoparticles may come from metals (e.g., Al, Cu, and Au), metal oxides (e.g., Aluminum oxide, Silicon oxide, Zirconium oxide), metal carbides, metal nitrides, and carbon derivatives (e.g., Diamond, Graphene, Fullerene, and CNT).While base fluids may be distilled water

or organic liquids such as different refrigerants, liquid fuels, lubricant oils, and ethylene-glycol (Sarkar et al., 2015).

According to Siginer and Wang (1995), using of Nanofluids in heat transfer applications has many advantages compared to conventional heat transfer, such as:

- High specific surface area and therefore more heat transfer surface between particles and fluids.

- High dispersion stability with a predominant Brownian motion of particles.

- Reduced pumping power as compared to pure liquid to achieve equivalent heat transfer intensification.

- Reduced particle clogging as compared to conventional slurries, thus promoting system miniaturization.

Nanofluid is being suggested as a convective medium because the thermal conductivity of the solid material particles is typically an order of magnitude higher than those of normal fluids such as water. Therefore, it is expected that a suspension of nano-sized solid particles in a base fluid, even at low volume concentrations, will cause a significant increase in its thermal performance. Many researchers such as (Kakaç & Pramuanjaroenkij, 2009; Sarkar et al., 2015; Trisaksri & Wongwises, 2007; X.-Q. Wang & Mujumdar, 2007; Wen et al., 2009; Yu et al., 2008) concluded that: the percentage increase in convective heat transfer coefficient (W/m^2.K) is generally more significant than the percentage increase in thermal conductivity (W/m.K) of the same nanofluid. Moreover, various studies were performed either experimentally or numerically to evaluate the use of nanofluids in the different applications of convection heat transfer performance since Pak and Choi (1998) started the first experimental investigation on convection heat transfer using nanofluids. Many researchers had reported enhancing convection heat transfer, but these enhancement levels are still a subject of debate, as

reported by Choi et al. (2014). They referred to many of the valued authors used a different definition for Nusselt number of nanofluid as Nu is multiplied by the magnification factor of $\left(k_{nf} \big/ k_{bf} \right)$ Which means the Nusselt number of nanofluids has been evaluated based on the thermal conductivity of the base fluids instead of nanofluids. Therefore, a wrong assessment of nanofluids as a convective medium may be presented.

As it is well known from the basic knowledge of heat transfer, the heat transfer by convection depends on two linked processes; diffusion and advection, and many properties are affecting them. Some of those properties have a positive effect, while others are affected negatively when using nanofluids. Therefore, Studying the whole aggregated factors affecting either diffusion rate or advection rate helps to understand the phenomenon well and leads to a better selection of nanofluid type for each engineering application.

1.2   Objectives

1. To synthesize and characterize nanocomposite materials in different mixing ratios and different weight concentrations.

2. To investigate the effect of nanofluid thermal conductivity compared to the thermal and momentum diffusivities on the convection heat transfer and friction loss.

3. To compare the performance of metal oxides nanofluid and a hybrid nanofluid of metal oxide and carbon-based nanoparticles through circular, square, and annular cross-section pipes of the same hydraulic diameters.

4. To analyze the heat transfer and fluid flow characteristics through an annular pipe of different vertical eccentricities using metal oxides and hybrid nanofluids.

1.3   Thesis layout

This thesis contains five chapters, including the chapter of the introduction.

- Chapter two is the literature review that presents a survey about the different methods of nanofluids preparation, nanofluids stability, the thermal and rheological properties of nanofluids. Moreover, the previous studies of the forced turbulent convection using nanofluids and the purpose of the current study are presented.

- Chapter three presents the methodology of the current study, including the preparation and characterization methods of the nanofluids with all instruments used as well. In addition, the experimental setup and its component. The numerical models and the critical assumptions for all the configurations are also included in this chapter.

- Chapter four presents the results and discussion, including the nanofluids' thermophysical properties and validation curves of the experimental and numerical work. The heat transfer and friction loss analysis for the experimental and numerical work are presented. Moreover, the performance analysis of all nanofluids in different pipe configurations, either experimentally or numerically, is presented.

- Chapter five contains the general conclusions of the present work.

The thesis also contains two appendices:

- Appendix A contains discussion about calibration of the test section, from which the current setup is based.

- Appendix B describes the uncertainty and error analysis.

CHAPTER 2: LITERATURE REVIEW

2.1 Background

As the heat transfer phenomenon is part of all human life activities, the studies on heat transfer enhancement did not stop all the time. Even inventions that may lead humanity to new horizons do not become applicable until the related heat transfer problems have been solved. Improvement of design and shapes of heat transfer devices made great leaps forward, and the revolution rises with the invention of micro-scale devices. In contrast, the convection heat transfer mediums do not achieve the same improvement level. Nanofluids are considered as the new revolution in heat transfer medium through the last two decades. In this chapter, a literature survey on the studies about different preparation methods; and the impact of their thermal properties on heat transfer and pressure drop are presented either in experimental or numerical studies.

2.2 Nanofluids preparation

The first and most crucial step in using nanofluid is the preparation of nanofluid, where it directly affects the value of thermal conductivity of nanofluid. The preparation of nanofluid has two ways: one-step preparation and two-step preparation.

2.2.1 One-step preparation

The preparation of nanofluid using the one-step method makes nanofluids more stable and achieve uniform dispersion of nanoparticles in the base fluid than the two-step method. The one-step process simultaneously makes and disperses the particles in the liquid, as done by Eastman et al. (2001) in preparing Cu/ethylene glycol nanofluids. As reported by Sridhara and Satapathy (2011), preparation of nanofluid by one-step method consists of direct evaporation and condensation of the nanoparticulate materials in the base liquid are obtained to produce stable nanofluids. Kanaras et al. (2002) used chemical reduction to make nanofluids. They prepared cuprous oxide nanofluids by

reducing copper acetate chemically using glucose in the presence of sodium lauryl sulfate (SLS). Kumar et al. (2009) also used chemical reduction to produce copper (Cu) nanofluids by reducing copper sulfate pentahydrate chemically in the presence of SLS in water. Submerged arc nanoparticle synthesis system (SANSS) was considered in preparing nanofluid (Lo et al., 2005; Lo et al., 2007). A pure metal rod is submerged in a dielectric liquid inside a vacuum chamber and passes an electric power to produce a very high temperature (from 6000 °C to 12000 °C), that can melt and vaporize the metal rod. The vaporized metal undergoes nucleation, growth, and condensation resulting in nanoparticles dispersed in the base fluid.

The metal nanoparticles are also dispersed directly into base fluid without needing to be dispersant by Laser ablation. Many researchers (Kim et al., 2009; Lee et al., 2012; Phuoc et al., 2007) used such technique to produce nanofluids from submerged metals such Cu, Ag, and Au into various base fluids (e.g., water and lubricant oils) by focusing a pulsed laser beam with a biconvex lens onto the submerged metal in the base fluid. Lee et al. (2012) prepared Cu/water nanofluid at a concentration of 0.001 vol.% by laser ablation method with Cu pellets.

Microwave irradiation is another technique used to prepare nanofluid as a one-step method. Reduction of $CuSO_4 \cdot 5H_2O$ by $NaH_2PO_2 \cdot H_2O$ in ethylene glycol (EG) under microwave irradiation produced copper nanofluid as reported by Zhu et al. (2004). This technique was applied to prepare silver nanofluid with oil and ethanol as base fluids (Bönnemann et al., 2005; Singh & Raykar, 2008). Yang et al. (2009) developed a general protocol to transfer metal ions from an aqueous solution to an organic medium called the phase transfer method. In such a method, the reactant migrates from one phase into another phase where the reaction occurs.

As reported by Wang et al. (2013), the combination between phase transfer technology and wet chemistry method for the synthesis of nanoparticles is an effective way for the preparation of nanofluids which helps to get the advantage of overcoming the problems associated with the insolubility of precursor materials in base fluids during the preparation of nanofluids. Kumar et al. (2004) applied the phase transfer method using A simple process based on amine chemistry. They applied this technique to transfer platinum nanoparticles from an aqueous to an organic solution. Wang et al. (2010) applied a similar way by using alkyl amine as a surfactant to transfer Au and Ag from aqueous to an organic phase. Graphene oxide nanosheets (GONs) were successfully transferred from water to n-octane after modification by the alkylamine (Yu et al., 2011).

Despite being that the one-step method helps reduce the aggregation of nanoparticles and achieves long-term nanofluids stability, it has some disadvantages. It cannot synthesize nanofluids on a large scale, the cost is also high, and the most critical defect is the remaining of the residual reactants in the nanofluids due to incomplete reaction or stabilization (Yu & Xie, 2012).

2.2.2 Two-step preparations

The two-step method is considered the most widespread and economical method to produce nanofluids on a large scale because nanopowder synthesis techniques have been scaled up to industrial production levels (Yu & Xie, 2012). In such method, nanoparticles, nanofibers, nanotubes, and any other nanomaterials used, are first produced as dry powders by chemical or physical methods (e.g., milling, grinding, and sol-gel and vapor phase methods). Then, the dispersion process is the second processing step to produce homogeneous colloids from nanoparticles and the host fluid. The dispersion process can be done with the help of intensive magnetic force agitation, ultrasonic agitation, high-shear mixing, homogenizing, and ball milling (Yu & Xie, 2012). Eastman et al. (2001)

reported that the two-step method is more suitable for preparing nanofluids with oxide nanoparticles than those with metallic nanoparticles. Figure 2-1 shows the preparation processes of nanofluids by a two-step method.
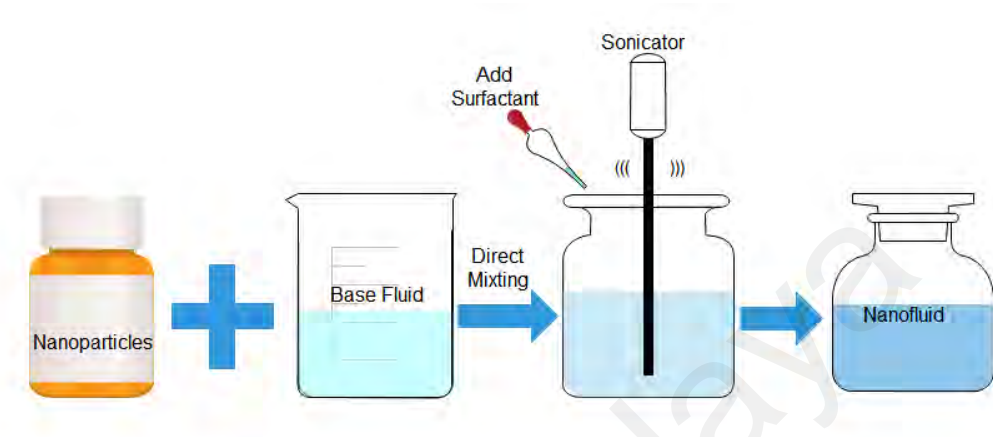
Figure 2-1: Two-step preparation processes of nanofluid.

Dispersion stability is one of the biggest challenges till now despite the great efforts devoted to overcoming it. Various approaches such as mechanical stirring, ultrasonic treatment, charging the nanoparticles' surfaces, and chemical treatment of surfaces using surfactants have improved dispersion stability (Yu et al., 2017).

2.3 Stability of nanofluids

2.3.1 Dispersing challenges

Stability is related directly to the dispersion and settlement of nanoparticles in the host fluid. It affects the flow pattern or clogging of microchannels and directly affects the thermal conductivity of nanofluid (Yu & Xie, 2012). So, it is considered a vital issue for using nanofluid in different applications. Figure 2-2 shows nanofluid samples, where one of them is visually stable while the second one visually separates the particles from the host fluid.

Sedimentation and aggregation are the two phenomena that cause the instability of nanofluids. Both phenomena are related to micro forces affect the nanoparticles. Due to

the density difference between the single nanoparticle and the base fluid, the gravity force pulls the nanoparticle down to cause sedimentation.
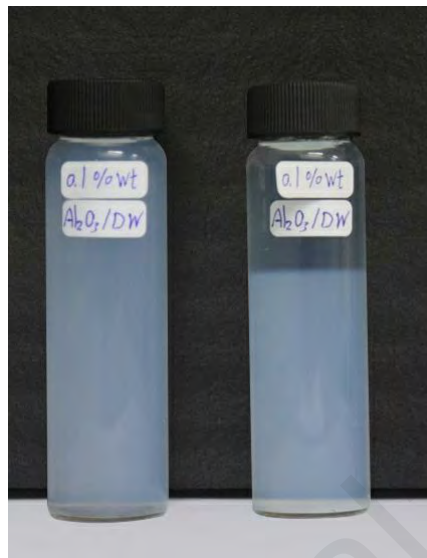
Figure 2-2: Stable (left) and unstable (right) nanofluids.

Equation (2-1) shows how to calculate sedimentation (settling) velocity according to Stokes's law.

$$U_s = \frac{d_p{}^2 (\rho_p - \rho_{bf})g}{18\mu_{nf}} \qquad (2\text{-}1)$$

where d_p is the diameter of nanoparticles, ρ_p and ρ_{bf} are the densities of nanoparticles and base fluid respectively, g is the acceleration gravity, and μ_{nf} is the dynamic viscosity of nanofluid.

The aggregation occurs due to the attractive interaction forces (such as Van der Waals force) between the neighboring nanoparticles. The distance between the adjacent nanoparticles strongly affects the interaction force. The closer nanoparticles, the higher the interaction force that can overcome the repulsive forces and form clusters of the aggregate nanoparticles. This aggregation or clustering of nanoparticles increases its size and speeds up the sedimentation process due to the significant difference in densities between nanoparticles and the base fluid, according to Equation (2-1). The nanoparticles

shape also influences the attractive force between the adjacent particles. As concluded by various studies presented by Fan Yu et al. (2017), the adjacent nanoparticles of plate or rod shape have a stronger attraction force than the spherical-shaped nanoparticles due to their larger contact area.

DLVO theory was developed to explain colloidal stability (Missana & Adell, 2000). DLVO theory states that the stability of a particle in solution is determined by the sum of Van der Waals attractive and electrical double layer repulsive forces between particles undergoing Brownian motion that led them to approach each other. Suppose the resistance to attraction exerted by electrical double layer repulsive forces is smaller than Van der Waals's attractive force. The two particles will aggregate together, and the suspension becomes unstable, and the opposite is true.

2.3.2 The ways of enhancing nanofluids stability

From the previous discussion, increasing the repulsive force between nanoparticles can enhance the nanofluid stability by counterbalancing the attractive van der Waals force. In general, the various mechanisms used to increase the repulsive force and improve the dispersing stability can be categorized under two main groups; the electrostatic stabilization mechanism and the steric stabilization mechanism.

2.3.2.1 Surfactant

Surfactants are defined as the chemical compounds added to reduce the surface tension of liquids and increase the suspension time of particles (Choudhary et al., 2017). As nanoparticles are usually hydrophobic, they cannot easily disperse and become stable in heat transfer fluid such as water and ethylene glycol (Chen & Xie, 2010). Adding surfactants (as an electrostatic repulsion technique) is convenient and straightforward and is thus attractive in practical applications. Due to hydrophilic and lipophilic groups that exists in the surfactants - long organic molecules-, the hydrophilic groups (once surfactant

is added to nanofluid) will adsorb on the solid, change the surface activity (Keblinski & Thomin, 2006; Kumar et al., 2004; Lee et al., 2006), change pH value (Xie et al., 2003), and reduce the surface energy of nanoparticles (Jiang et al., 2003). Surfactants or dispersants are classified according to Yu and Xie (2012) into four groups as follow:

1) Nonionic surfactants without charge groups in its head (include polyethylene oxide, alcohols, and other polar groups),

2) Anionic surfactants with negatively charged head groups (anionic head groups include long-chain fatty acids, sulfosuccinates, alkyl sulfates, phosphates, and sulfonates),

3) Cationic surfactants with positively charged head groups (cationic surfactants may be protonated long-chain amines and long-chain quaternary ammonium compounds),

Based on surfactants classification, the researchers cannot select the surfactant randomly. Generally, the water-soluble surfactants should be selected if the host fluid (base fluid of nanofluid) is polar solvent; otherwise, the oil-soluble ones should be. The vital key in evaluating solubility is the term hydrophilic/ lipophilic balance (HLB) value, where the higher HLB value indicates that the surfactant is water-soluble. In comparison, the lower HLB value indicates that the surfactant is oil-soluble (Yu & Xie, 2012). Ricardo et al. (2008) presented different ways and the considerations that should be taken to calculate HLB value.

Shanbedi et al. (2015) investigated the influence of different surfactant materials at various concentrations on the stability and thermophysical properties of aqua-based MWCNTs nanofluid. They used gum Arabic (GA), sodium dodecyl sulfate (SDS), and cetyl trimethylammonium bromide (CTAB) as surfactants in the ratios 0.5:1, 1:1, and 2:1 of surfactant: MWCNTs, respectively. They used the zeta potential test to evaluate the

dispersion stability of all nanofluids concentrations and surfactant in the range ± (20.5-32.0 mV). They found that the best surfactant: MWCNTs ratio is 1:1, and the SDS surfactant was the best surfactant type followed by GA and finally CTAB based on stability evaluation test.

Rastogi et al. (2008) studied the effect of using various surfactants such as Triton X-100, Tween 20, Tween 80, and sodium dodecyl sulfate (SDS) on the stability of aqua-based MWCNTs nanofluid. They found that the surfactants Triton X-100 and SDS provide the best and the worst nanofluid stability, respectively.

As reported by Chen et al. (2008), several problems resulted from using surfactants and listed them as follow:

1) the addition of surfactants may contaminate the heat transfer media,

2) Surfactants may produce foams when heating, while heating and cooling are routine processes in heat exchange systems,

3) Surfactant molecules attaching to the surfaces of nanoparticles may enlarge the thermal resistance between the nanoparticles and the base fluid, limiting the enhancement of the effective thermal conductivity.

2.3.2.2 Surfactant-Free method

The surface-free method is a surface modification technique (depends on steric repulsion mechanism) where the functionalization process takes place with nanoparticles to achieve long-term stability of nanofluid. Sadri et al. (2017) examined an environmentally friendly method with GNP suspended in distilled water. They used clove buds to functionalize GNP- water nanofluid with three particle concentrations (0.025, 0.075, and 0.1 wt.%). They concluded that the clove-treated graphene nanoplatelet (CGNP) gives remarkable stability even 63 days after preparation.

The same technique with cloves buds was also examined with multi-wall carbon nanotubes (MWCNTs) dispersed in distilled water by Sadri et al. (2017). They used Raman spectroscopy, X-ray photoelectron spectroscopy, and transmission electron microscopy to characterize the clove-functionalized MWCNTs (CMWCNTs). UV–vis spectroscopy was also used to examine the stability of the CMWCNTs nanofluid. They found that the CMWCNTs nanofluids have remarkable stability over 63 days after preparation.

The milling process with bead mill was used by Joni et al. (2009) to modify the surface of Titania nanoparticles with a primary particle size of 15 nm to easily disperse in an organic solvent of diethylene glycol dimethyl ether (diglyme). As introduced by Inkyo et al. (2008), the bead mill is composed of a 170-mL vessel, a pump, and a mixing tank. Nanoparticle suspensions were pumped into the vessel containing zirconia beads and a centrifugation rotor at the speed of 73.8 Hz (6095 rpm). The beads are agitated in the lower portion of the vessel (dispersing section), which drives the breakup of agglomerated particles. The suspension was pumped from the dispersing section to the upper region (centrifugation section), where centrifugal force separates the zirconia beads from the nanoparticle suspension. The nanoparticle suspension is then recycled back to the dispersing section. To prevent temperature increasing in the system, the vessel is housed in a cooling water jacket and is completely sealed from the outside environment. Using a bead mill to functionalize Titania nanoparticles dispersed in an organic solvent (diethylene glycol dimethyl ether) leads to producing a high zeta potential of a solution up to 80 mV and brought the solution into high dispersion stability (Joni et al., 2009).

Tang et al. (2006) modified Zinc oxide nanoparticles with polymethacrylic acid (PMAA) in an aqueous system. They got the benefit of carboxyl groups (COO–) in PMAA which interacted with the hydroxyl groups of nano-ZnO particle surface and

formed poly (zinc methacrylate) complex on the surface of nano-ZnO. They found that PMAA enhanced the dispersibility of nano-ZnO particles in water, and the stability of modified ZnO nanoparticles in the aqueous system was significantly improved.

2.3.3   Nanofluid stability evaluation method

2.3.3.1   Spectral analysis

Ultraviolet-visible (UV-vis) spectrometer is evaluating nanofluids' stability depending on spectral analysis techniques. In the spectral analysis technique, the intensity of light passing through a fluid sample or reflected from it is being evaluated by two methods. The first one is by comparing the intensity of light passing through the sample to its original intensity. The second method is by comparing the light reflected from the sample to the light reflected from the standard sample. To assess the dispersion stability of nanoparticles in the host fluid, the measured absorbance of the nanofluid sample is compared to the absorbance of base fluid, where the difference is associated with the concentration of nanoparticles. Measuring the absorbance should be done directly after preparation and considered a reference (Maximum value) as the sedimentation process has no effect due to small sedimentation velocity. So, if the sedimentation rate increases, the absorbance values will decrease, which indicates suspension stability. To evaluate the stability of nanofluids using UV–vis spectral analysis, the nanomaterials dispersed in the fluid should have absorption bands in the wavelength range between 190–1100 nm (Angayarkanni & Philip, 2015).

Abdolbaqi et al. (2016) used a UV-vis spectrometer to evaluate stability for a bioglycol-water mixture containing Al_2O_3 nanoparticles of different concentrations from 0.5-2.0%. They found that the peak wavelengths of absorbance for Al_2O_3 nanofluid were between 313-316 nm. Abdolbaqi et al. (2016) examined the stability of silica nanoparticles suspended in a mixture of bioglycol and water using a UV-vis spectrometer.

They found that SiO₂ nanofluid has absorption bands in the wavelength range between 200 and 400 nm and the peak absorbance occurs at the peak wavelength of 294 to 299 nm. They also concluded that the nanofluids with lower concentrations have more potential for agglomeration and faster sedimentation time. Mehrali et al. (2014) evaluated stability for graphene/DW nanofluid using a UV-vis spectrometer. They found that GNP-DW nanofluid of concentrations 0.025-0.1 wt.% has absorption bands in the wavelength range between 190 and 590 nm, and the peak absorbance occurs at the peak wavelength of 180 nm for all concentrations. They also studied the effect of using GNP with different specific surface areas for the same concentrations. They found that the absorption peak wavelength increased when increasing specific surface area, which indicates that a higher specific surface area gives better GNP dispersion.

2.3.3.2   Light scattering techniques

In nanofluids, the suspended particles continuously undergo random thermal motion due to their Brownian motion. The particle size directly affects particle movement speed, where the smaller particles move faster, and the larger particles move slowly. Therefore, when laser light is directed through a nanofluid sample, it will be scattered, and based on the intensity variations of the collected scattered laser light after passing the sample, the hydrodynamic diameter of particles can be measured. Thus, the Dynamic Light Scattering (DLS) method effectively measures the particle size over the larger sample volume. By using the DLS method, particle size can be calculated using the Stokes-Einstein equation as follow:

$$d_p = \frac{k_B T}{3\pi \mu_{nf} C_{df}}$$

(2-2)

where k_B is the Boltzmann Constant equals 1.328×10^{-23} J/K, T is the temperature, μ_{nf} is the nanofluid viscosity, and C_{df} is the diffusion coefficient (Angayarkanni & Philip, 2015) or particle diffusion constant (Keblinski et al., 2002).

Advantages of DLS for particle sizing are its ability to provide an ensemble-averaged estimate of particle size in suspensions, a widely accessible range of particle sizes in the submicron range, and fast data acquisition. DSL technique was being used to evaluate stability for different kinds of nanofluids; for example, a stability evaluation for iron oxide (Fe_3O_4) and copper oxide (CuO) was performed with the DLS technique by Shima et al. (2010). Fedele et al. (2011) used the DSL technique to study the stability of water-based dispersions containing different nanoparticles such as single-wall carbon nanohorns (SWCNHs), titanium dioxide (TiO_2), and copper oxide (CuO).

2.3.3.3 Zeta potential measurements

As the electro-kinetic properties of nanoparticles dispersed in aqueous solution playing a vital role in their stability, the dispersion behavior of nanofluids can be understood by studying the electrophoretic behavior through the measurement of zeta potential. Zeta potential is the potential difference between the bulk fluid (dispersion medium) and the stationary layer of fluid attached to nanoparticles. It indicates the degree of repulsion between adjacent, similarly charged particles in the dispersion. Ghadimi et al. (2011) presented that the stable suspension systems give high zeta potential values (either positive or negative), while the low zeta potential values indicate that the nanoparticles will settle down faster. Vandsburger (2009) concluded that the stability of nanofluids is expected to be moderate if zeta potential is near to ± 30 mV, while zeta potential of ± 45 mV indicates that the stability of nanofluids is supposed to be good. The excellent stability of nanofluid will be achieved if the zeta potential is above ± 60.

Table 2-1: Stability conditions according to zeta potential values (Vandsburger, 2009).

Zeta potential ($\hat{A} \pm mV$)	Stability
0	Little or no stability
15	Some stability but settling lightly
30	Moderate stability
45	Good stability
60	Very good stability

2.3.3.4   Sedimentation method

The sedimentation method is the simplest method to evaluate the stability of the nanofluids with the elapsed time. The only indication that nanofluid is stable in this method is the remaining suspended particles concentration constant with the elapsed time. In this method, nanofluid stability observation is done by taking the sedimentation photographs of nanofluids in test tubes using a camera for an extended period. Such method was used to evaluate the stability of aqueous copper nanosuspension as done by Li et al. (2007), CNT water-based nanofluid (Nasiri et al., 2012), and graphite nanopowder suspended in distilled water (Zhu et al., 2007). The disadvantage of this method is the long observation period to check the sedimentation of particles. Wozniak et al. (2013) presented an equation that can be used to calculate sedimentation rate as follow:

$$Sedimentation\ rate = 100\% - \left[\left(\frac{H_o - H_t}{H_o} \right) \times 100 \right]$$

(2-3)

where H_o is the initial height of the homogeneous suspension column in mm and H_t is the height of sediment in time. Figure 2-3 shows an illustration of the sedimentation process.
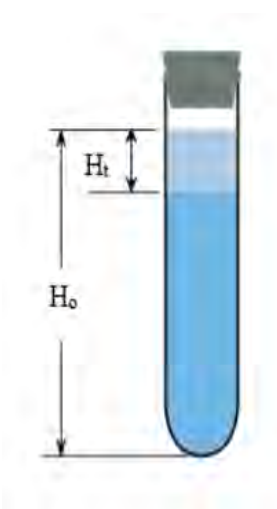
Figure 2-3: An illustration of terms of equation (2-3).

2.3.4   Effect of pH on nanofluids stability

In nanofluids, the pH values are related to the electrostatic charge on the nanoparticle surface. Thus, it is considered a critical parameter to control the stability of colloidal systems where the strong repulsive force increases the stability of nanofluids. Choudhary et al. (2017) studied the stability of Alumina/ water nanofluids. They concluded that the extreme values of pH on both sides (higher sides of acid and basic) of nanofluids gave nanofluids higher values for zeta potential. For highly acidic nanofluids (pH is less than 7), the number of H^+ ions becomes larger. Thus, the positive ions in the electric double layer around the nanoparticles increase, increasing positive zeta potential in magnitude.

On the other hand, for highly basicity nanofluids (pH is higher than 7), many OH ions are performed in the suspension, increasing the possibility of OH near nanoparticles. Thus, the negative ions are attracted to the stern layer's positive ions, which increase the negative magnitude of zeta potential. A second point that should be considered is the definition of the isoelectric point (IEP) where zeta potential equals zero. Thus, the pH value should be far from IEP to maintain the stability of the colloidal. Many researchers reported the value of IEP for their nanofluids. Choudhary et al. (2017) said that IEP is 8.6 pH value for all particles concentrations with sonication times of 120 and 180 minutes.

In contrast, it oscillates between 8 and 9.4 pH values for the sonication time of 60 minutes. Wamkam et al. (2011) obtained the IEP for TiO_2 / DW nanofluid (of concentration 3wt.%), which equals a 4.5 pH value. Zawrah et al. (2016) studied Al_2O_3 / DW nanofluid's stability and found that the IEP of their nanofluids was nearly 8. Diebold (2003) found that IEP equals 4.5 for TiO_2 / DW nanofluid.

2.4   Thermal and rheological properties of nanofluids.

2.4.1   Thermal conductivity

As a scientific concept, the thermal conductivity of metals in solid form has an order of magnitude higher than that of conventional fluids at room temperature (Das et al., 2008). Thus, since the first trial to make a nanofluid by Maxwell (1891), the various attempts to increase fluids' thermal conductivity by using such colloids failed until the rise of the nanofluids era started with the pioneering work of Masuda et al. (1993). Since that time, the curiosity and interest in scientific research focused on thermal conductivity enhancement of nanofluid (k_{nf}) and its effects on different modes of heat transfer. Various parameters had been considered in further studies to show their impact on the thermal conductivity of nanofluids (k_{nf}). For example, the type of nanoparticles, base fluid, the volume fraction of solid particles, particle shape/size, the nanofluids temperature, pH value, adding of surfactants, sonication time, and quantum effects are considered factors that affect the nanofluids thermal conductivity. Table 2-2 summarizes some experimental data of the thermal conductivity with different nanomaterials suspended in the most common heat transfer fluids.

Table 2-2: Summary of some experimental data of thermal conductivity with different nanomaterials.

Type of nanoparticles	Base fluids		Particle size (nm)	concentration	Max. enhancement
	D.W	E. G			
Alumina (Al$_2$O$_3$)	(Ho et al., 2010)		33	0.1-4 vol.%	14%
	(Heyhat, 2012)		40	0.1-2 vol. %	18%
	(Williams et al., 2008)		46	0.9-3.6 vol. %	
	(Wang et al., 1999)		28	3-5.5 vol.%	16%
		(Wang et al., 1999)	28	5-8 vol. %	41%
	(Li & Peterson, 2007)		36,47	0.5-6 vol. %	28%
	(Xie et al., 2002)		60.4	1.8-5 vol. %	21%
		(Xie et al., 2002)	15, 26, 60.4, 302	1.8-5 vol. %	30%
	(Das et al., 2003)		38.4	1-4 vol. %	9%
	(Lee et al., 2008)		30	0.01-0.3 vol.%	1.44%
	(Wen & Ding, 2004)		42	0.19-1.59 vol. %	10%
	(Li & Peterson, 2006)		36	2-10 vol. %	29%
	(Beck et al., 2009)		8, 12, 16, 46, 71, 245, 282	2-4 vol. %	17.67%
	(Masuda et al., 1993)		13	1.3-4.3 vol.%	29.6%
	(Chandrasekar et al., 2010)		43	0.33-5 vol.%	
	(Xia et al., 2014)		13, 20	0.1, 0.5, 1, 2.5 vol.%	
Silica (SiO$_2$)	(Masuda et al., 1993)		12	1.1-2.4 vol.%	1.1%
	(Mahian et al., 2016)		7	0.5, 1, 2 vol.%	4.5% (25 ˚C) 13% (60 ˚C)
TiO$_2$	(Jarahnejad et al., 2015)		30	3-9 wt.%	

Table 2-2 Continue.

TiO$_2$	(Silambarasan et al., 2012)		100-344	0.27-1.39 vol. %	8%
	(Fedele et al., 2012)		70	0.24-11.22 vol.%	21.3%
Zirconia (ZrO$_2$)	(Williams et al., 2008)		60	0.2-0.9 vol. %	
Fe$_3$O$_4$	(Philip et al., 2007)		6.7	6.3 vol.%	300%
	(Abareshi et al., 2010)		6.7	1, 3 vol.%	8.9 % (1 %) 15.1% (3%)
	(Sundar et al., 2013)		13	0.2-2 vol.%	48% (60 ˚C)
	(Parekh & Lee, 2010)		9.9	1.115-4.7 vol.%	17.25%
	(Gavili et al., 2012)		10	5 vol.%	200% (magnetic field only)
	(Razzaq et al., 2007)			10-40 vol.%	215%
	(Fertman et al., 1987)			0.01-0.2 vol.%	
Cu		(Eastman et al., 2001)	<10	0.3	40%
GNP	(Sadri et al., 2017)		2 (thick)	0.025, 0.075, 0.1 wt.%	22.92% (0.1%)
	(Kole & Dey, 2013)			0.041-0.395 vol.%	15%
	(Selvam et al., 2016)	(Selvam et al., 2016)	5-10 (thick)	0.001, 0.01, 0.1, 0.2, 0.3, 0.4, 0.5	21% (EG) 16% (DW)
	(Yarmand et al., 2016)		5 μm	0.02, 0.06, 0.1 wt.%	13.56% (20 ˚C) 15.87% (40 ˚C)
	(Sarsam et al., 2016)		2 (thick)	0.1 wt.%	8.36% (SDBS)
MWCNT	(Ding et al., 2006)			0.05-0.49 vol.%	10% (20 ˚C) 27% (25 ˚C) 79% (30 ˚C)
	(Liu et al., 2011)	(Liu et al., 2011)		1.5 vol.% (DW) 1 vol% (EG)	17% (DW) 12.4%(EG)
	(Sadri et al., 2017)			0.05, 0.08 vol.%	20% (0.08)

2.4.1.1 Modeling of thermal conductivity

(a) Theoretically investigated models

Many researchers considered the different parameters affecting the value of nanofluid thermal conductivity (k_{nf}) and expressed it into various mathematical models. The modeling of nanofluids' thermal conductivity is a complex problem due to the number of variables affecting its value. The first attempt to investigate the nanofluid thermal conductivity theoretically was introduced by Maxwell, the Maxwell or Maxwell-Garnett model (Khairul et al., 2016). It was developed to estimate the effective thermal conductivity for a dilute solid/ liquid colloid with micro and millimeter-sized particles as in equation (2-4).

$$k_{nf} = \left[\frac{(k_p + 2k_{bf} + 2\varphi(k_p - k_{bf}))}{(k_p + 2k_{bf} - \varphi(k_p - k_{bf}))} \right] k_{bf} \qquad \textbf{(2-4)}$$

where, φ is the percentage volumetric concentration (volume fraction) of suspended nanoparticles in the base fluid.

The Maxwell model is not accurate for mixtures at high concentrations. Therefore, the attempts continuously investigate more accurate models. Hamilton and Crosser (1962) presented a mathematical model to calculate the thermal conductivity of a homogeneous mixture of liquid and solid considering the particle shape of solid particles suspended in the liquid as shown in equation (2-5).

$$k_{nf} = \left[\frac{(k_p + (n-1)\, k_{bf} - \varphi(n-1)(k_{bf} - k_p))}{(k_p + (n-1)\, k_{bf} + \varphi(k_{bf} - k_p))} \right] k_{bf} \qquad \textbf{(2-5)}$$

where, $n = 3\,/\,(\psi)$ and ψ is the sphericity of solid particles.

The solid particle sphericity is expressed as the ratio of the sphere surface area (with the same volume of the particle) to the given particle surface area. Hence, if solid particles' sphericity equals unity, the model is similar to the Maxwell model. Xuan, Li, and Hu

developed a mathematical model to predict the thermal conductivity of nanofluids. They considered the effect of various parameters more than Hamilton and Crosser, such as temperature, particles density, and particle specific heat (Alawi et al., 2018). They expressed their model as shown in equation (2-6).

$$k_{nf} = \left[\frac{\left(k_p + 2k_{bf} - 2\varphi(k_{bf} - k_p) \right)}{\left(k_p + 2k_{bf} + \varphi(k_{bf} - k_p) \right)} + \frac{(\rho_p \varphi C_p)}{2k_{bf}} \sqrt{\frac{(k_B T)}{(3\pi r_c \mu)}} \right] k_{bf} \qquad \textbf{(2-6)}$$

To explain the reasons beyond enhancing nanofluid thermal conductivity, recent research changed the point of view from macroscopic to microscopic scale. They suggested various numbers of mechanisms which divided into two main categories. The first is the static mechanism, which assumes the particles are stationary while suspended in the base liquid. The second category is the dynamic mechanism that considers the particles in random motion as in the Brownian motion and micro convection to be responsible for k_{nf} enhancement (Akilu et al., 2016).

Yang et al. (2017) explained the effect of an interfacial layer between solid and liquid on enhancing k_{nf}. They introduced their model to calculate $k_{nf,}$ as shown in equation (2-7).

$$k_{nf} = \frac{(k_p - k_{Ir})\varphi_{Ir}k_{Ir}\left[2\lambda_I^3 - \lambda^3 + 1\right] + (k_p + 2k_{Ir})\lambda_I^3\left[\varphi_{Ir}\lambda^3(k_{Ir} - k_f) + k_f\right]}{\lambda_I^3(k_p + 2k_{Ir}) - (k_p - k_{Ir})\varphi_{Ir}\left[\lambda_I^3 - \lambda^3 - 1\right]} \qquad \textbf{(2-7)}$$

where, $\varphi_{Ir} = \varphi(\lambda^3 - 1)$, $\lambda = 1 + \frac{\delta}{r_p}$, δ is the shell (nanolayer) thickness around the nanoparticle, r_p is the radius of nanoparticle, and k_{Ir} is the interfacial thermal conductivity.

Chandrasekar et al. (2010) studied the effect of interfacial resistance on nanofluids' thermal conductivity. They concluded that enhancing nanofluids' thermal conductivity is strictly dependent on the aggregation of nanoparticles in the colloidal state and the connectivity between them. Hamzah et al. (2017) used a three-level homogenous model

to evaluate the effect of different parameters on enhancing nanofluids' thermal conductivity. They found that the aggregation and radius of gyration of the nanoparticles in the colloidal state have a noticeable effect on improving nanofluids' thermal conductivity. Based on the Maxwell model, Yu and Choi (2003) used the nanolayer concepts to develop their model by assuming that the nanolayer is the preferable thermal path between liquid and solid. Equation (2-8) shows Yu and Choi model.

$$k_{nf} = \left[\frac{k_{pe} + 2k_{bf} + 2\varphi(k_{pe} - k_{bf})(2 - \lambda)^3}{k_{pe} + 2k_{bf} - \varphi(k_{pe} - k_{bf})\lambda^3} \right] k_{bf} \qquad \textbf{(2-8)}$$

where, k_{pe} is the equivalent thermal conductivity of nanoparticles and can be calculated from equation (2-9).

$$k_{pe} = \left[\frac{[2(1 - \gamma) + \lambda^3(1 + 2\gamma)]\gamma}{-(1 - \gamma) + \lambda^3(1 + 2\gamma)} \right] k_p \qquad \textbf{(2-9)}$$

where, $\gamma = {k_{Ir}}/{k_p}$, and if $\gamma = 1$, the model is consistent with the Maxwell model.

Keblinski et al. (2002) studied the effect of Brownian motion (the particles move through the liquid and possibly colloids) on the enhancement of nanofluids' thermal conductivity. The Brownian motion can be described by diffusion rate coefficient or particle diffusion constant of equation (2-2).

Jang and Choi (2004) developed a theoretical model based on kinetic, Kapitza resistance (Interfacial thermal resistance), and micro convection. They considered four modes of microscopic heat transfer: thermal diffusion of nanoparticles, the collision between nanoparticles due to Brownian motion, thermal interaction between dynamic particles with fluid molecules, and collision between liquid molecules. Equation (2-10) shows their mathematical model.

$$k_{nf} = k_p \varphi + (1 - \varphi)k_{bf} + 3\varphi C_1 \frac{d_{bf}}{d_p} k_{bf} Pr_{bf} Re_p{}^2 \tag{2-10}$$

where, C_1 is a proportional constant, d_{bf} is the diameter of the base fluid molecule, and Re_p is the Reynolds number for nanoparticles, and it is calculated by the equation (2-11).

$$Re_p = \frac{\bar{C}_R d_p}{\nu_{bf}}, \qquad \bar{C}_R = {C_{df}}\big/{l_{bf}} \tag{2-11}$$

where, $\bar{C}_R$ is the random nanoparticle velocity and l_{bf} is the mean-free path.

(b) *Experimentally investigated correlations*

All the previous equations from (2-4) to (2-10) depend basically on a theoretical approach to enhancing nanofluids' thermal conductivity either with the macroscopic or microscopic study. Therefore, such equations have limited applicability concerning other experimental factors such as pH value, sonication time, preparation method, particle size, etc. Hence, there is no acceptable difference range when the data from such equations are compared with experimental results. The experimentally investigated correlations or semi-empirical models are derived using experimental data affected by various experimental parameters.

Khanafer and Vafai (2011) developed a general correlation for Al₂O₃-DW nanofluid using experimental data measured at various temperatures, nanoparticle diameters, and volume fractions. They validated their correlation shown in the equation (2-12) with different published experimental data and got a good agreement between the predicted data from their correlation and the published data.

$$k_{nf} = \left[0.9843 + 0.398\varphi^{0.7383} \left(\frac{1}{d_p} \right)^{0.2246} \left(\frac{\mu_{nf}(T)}{\mu_{bf}(T)} \right)^{0.0235} + 34.034 \, \frac{\varphi^2}{T^3} + \right. \tag{2-12}$$
$$\left. 32.509 \frac{\varphi}{T^2} - 3.9517 \frac{\varphi}{T} \right] k_{bf}$$

Equation (2-12) is valid for the ranges $0 \leq \varphi \leq 10\%$, $11\text{nm} \leq d_p \leq 150 \, nm$, and $20 \, ^\circ\text{C} \leq \text{T} \leq 70 \, ^\circ\text{C}$.

The equation developed by Khanafer and Vafai presented in Fedele et al. (2012) published work also demonstrated a general empirical correlation shown in equation (2-13) to evaluate the thermal conductivity of Al_2O_3-DW and CuO-DW nanofluids. Their correlation is estimated for the properties at the ambient temperature 25 °C and volumetric nanoparticles concentration of 4%.

$$k_{nf} = \left[1.0 + 1.0112\varphi + 2.4375\varphi \left(\frac{47}{d_p(nm)} \right) - 0.0248 \, \varphi \left(\frac{k_p}{0.613} \right) \right] \tag{2-13}$$

Sharma et al. (2012) developed an empirical correlation (2-14) to investigate the thermal conductivity for different nanofluids with oxide metals nanoparticles. they used the regression technique to establish the correlation based on much-measured data for Al_2O_3-DW, TiO_2-DW, Fe_3O_4-DW, ZrO_2-DW, CuO-DW, and ZnO-DW nanofluids of volumetric concentration less than 4%, the temperature range between 20 °C and 70 °C, and $20\text{nm} \leq d_p \leq 150 \, nm$.

$$k_{nf} = \left[0.8938 \left(1 + \frac{\varphi}{100} \right)^{1.37} \left(1 + \frac{T_{nf}}{70} \right)^{0.2777} \left(1 + \frac{d_p}{150} \right)^{-0.0336} \left(\frac{\alpha_p}{\alpha_{bf}} \right)^{0.01737} \right] \tag{2-14}$$

2.4.2 Viscosity

In forced convection heat transfer applications, the heat transfer acts as the benefit while pressure drop acts as the penalty. Therefore, the evaluation of nanofluids as a heat transfer medium should depend on the benefit vs. penalty evaluation. When the benefit is more prominent than the penalty, the nanofluid is commercially viable and vise verse. To

make such evaluation, the nanofluid viscosity should be measured or evaluated as the pressure drop or pumping power is depending on its value.

The viscosity of nanofluids not only affects the convection heat transfer but also influences the thermal conductivity. Tsai et al. (2008) studied the effect of base fluid viscosity for suspension of Fe_3O_4 nanoparticles with a volume concentration of 1 and 2% suspended in base fluid composed of diesel oil and polydimethylsiloxane. They controlled the viscosity of the base fluid by changing the volumetric fractions between both fluids. According to their study, the nanofluid thermal conductivity decreases with the increase of base fluid viscosity. The maximum values of thermal conductivity were obtained for viscosity values less than 100 cP.

2.4.2.1   Modeling of viscosity

(a) *Theoretically investigated models*

As done with the nanofluids' thermal conductivity, the dynamic viscosity of nanofluids had been investigated theoretically based on equations of analytical studies and empirical correlations. Einstein (1906) was the first scientist who derived an equation to investigate the dynamic viscosity of colloids composed of spherical solids dispersed in a base fluid with a volume fraction less than 5%. Einstein's equation for the dynamic viscosity is shown in equation (2-15).

$$\mu_{nf} = (1.0 + 2.5\varphi)\mu_{bf}$$

(2-15)

Based on Einstein's equation, several equations were developed to evaluate the dynamic viscosity of concentrated colloids of a high-volume fraction. Brinkman (1952) extent Einstein's equation to make it applicable for concentrated colloids as shown in equation (2-16).

$$\mu_{nf} = \left(\frac{1}{(1.0 - \varphi)^{2.5}}\right)\mu_{bf} = (1.0 + 2.5\varphi + 4.375\varphi^2 + \cdots)\mu_{bf} \tag{2-16}$$

Batchelor (2006) considered the effect of Brownian motion of the suspended solid particles and developed the equation (2-17) to evaluate the dynamic viscosity.

$$\mu_{nf} = (1.0 + 2.5\varphi + 6.2\varphi^2)\mu_{bf} \tag{2-17}$$

(b) ***Experimentally investigated correlations***

The work done by Masuda et al. (1993) was the first attempt to evaluate the dynamic viscosity of nanofluids experimentally. They measured the viscosity of several water-based nanofluids of metal oxides nanoparticles at different temperatures starting from room temperature to 67 ℃. Maiga et al. (2005) performed a curve fitting process using the least square method for the data measured by Masuda et al. (1993), Lee and Choi (1999), and Wang et al. (1999) to create an empirical correlation for the dynamic viscosity of silica nanoparticles dispersed in DW and EG as shown in equations (2-18) and (2-19), respectively.

$$\mu_{nf} = (1.0 + 7.3\varphi + 123\varphi^2)\mu_{bf} \tag{2-18}$$

$$\mu_{nf} = (1.0 - 0.19\varphi + 306\varphi^2)\mu_{bf} \tag{2-19}$$

Khanafer and Vafai (2011) used the least square method to make a curve fitting for the data measured by (Pak & Cho, 1998). They performed correlations to evaluate the viscosity of Al_2O_3-DW nanofluid with $d_p = 13$ nm and TiO_2-DW nanofluid with $d_p = 27$ nm as shown in equations (2-20) and (2-21), respectively.

$$\mu_{nf} = (1.0 + 23.09\varphi + 1525.3\varphi^2)\mu_{bf} \tag{2-20}$$

$$\mu_{nf} = (1.0 - 3.544\varphi + 169.46\varphi^2)\mu_{bf}$$

(2-21)

Equation (2-20) is accurate for the volume fraction range between 0 and 4%, and equation (2-21) is valid for the volume fraction range between 0 and 1%.

Vajjha and Das (2012) analyzed the measured data published by Namburu et al. (2007) and Sahoo et al. (2009) and established a general correlation to evaluate the viscosity of several water-based nanofluids with metal oxide nanopowder. Equation (2-22) shows Vajjha and Das correlation, and Table 2-3 shows the constant A1 and A2 values.

$$\mu_{nf} = (A_1 e^{A_2\varphi})\mu_{bf}$$

(2-22)

Table 2-3: Constant of equation (2-22) for different nanofluids (Vajjha & Das, 2012).

nanoparticles	A_1	A_2	d_p (nm)	φ
Al_2O_3	0.983	12.959	45	0-10%
CuO	0.9197	22.8539	29	0-6%
SiO_2	1.092	5.954	20	0-10%
SiO_2	0.9693	7.074	50	0-6%
SiO_2	1.005	4.669	100	0-6%

Data of equations (2-18) to (2-21) are evaluated at room temperature, while equation (2-22) considers the temperature dependency of viscosity where it is applicable for the temperature range of $0\ ^{\circ}\mathrm{C} \leq T \leq 90\ ^{\circ}\mathrm{C}$.

As the viscosity is very sensitive to the temperature variation, several correlations showed the temperature dependence of nanofluids viscosity. Khanafer and Vafai (2011)

conducted an empirical correlation showing the temperature dependence of Al₂O₃-DW nanofluid with nanoparticles diameter of 13 nm as shown in equation (2-23).

$$\mu_{nf} = \left(0.4444 - 0.254\varphi + 0.0368\varphi^2 + 26.333\frac{\varphi}{T} - 59.311\frac{\varphi}{T^2}^2\right)\mu_{bf} \qquad \textbf{(2-23)}$$

Khanafer and Vafai (2011) also performed a temperature dependence relation for the viscosity of Al₂O₃-DW nanofluid with a wide range of nanoparticles diameter from 13 to 131 nm and volume concentration range from 1% to 9%. Their correlation is shown in equation (2-24)

$$
\begin{aligned}
\mu_{nf} = \Bigl(&-0.4491 + \frac{28.837}{T} + 0.574\varphi - 0.1634\varphi^2 + 23.053\frac{\varphi^2}{T^2} \\
&+ 0.0132\varphi^3 - 2354.7358\frac{\varphi}{T^3} + 23.498\frac{\varphi^2}{d_p{}^2} \\
&- 3.0185\frac{\varphi^3}{d_p{}^2}\Bigr)\mu_{bf}
\end{aligned}
\qquad \textbf{(2-24)}
$$

Sharma et al. (2012) investigated an empirical model to calculate the viscosity of different water-based nanofluids with metal oxide nanoparticles. Their model considers the viscosity dependence on temperature, nanoparticle size, and nanoparticles volume fraction as shown in equation (2-25).

$$\mu_{nf} = \left[(1 + \varphi)^{11.3}\left(1 + \frac{T_{nf}}{70}\right)^{-0.038}\left(1 + \frac{d_p}{170}\right)^{-0.061}\right]\mu_{bf} \qquad \textbf{(2-25)}$$

As discussed in this literature, the nanoparticle type does not affect the nanofluid viscosity. Therefore, once the volume concentration, nanoparticle size, base fluid, and temperature are the same, the viscosity of nanofluid will be the same, whatever the nanoparticle type.

2.4.3 Density

As the density of metals is more incredible than liquid, the addition of metal nanoparticles to water or any other fluid will increase its density. The density of nanofluid can be obtained analytically based on the mass balance principle of the mixture, where the mass of the mixture equals the masses of its compounds. Equation (2-26) shows how to calculate the density of nanofluid.

$$\rho_{nf} = \frac{m_{bf} + m_p}{V_{nf}} = \frac{\rho_{bf}V_{bf} + \rho_p V_p}{V_{nf}} = (1 - \varphi)\rho_{bf} + \varphi\rho_p \tag{2-26}$$

Many researchers, such as (Pak & Cho, 1998; Ho et al., 2010), examined the validity of equation (2-26) by conducting an experimental work to measure the densities of Al_2O_3-DW and TiO2-DW nanofluids with volume fraction from 0 to 4%. They found an excellent agreement between the experimental data and the data that had been calculated by equation (2-26). Based on the published data by (Ho et al., 2010), which indicated the temperature dependence for nanofluid viscosity, Khanafer and Vafai (2011) developed an empirical correlation to evaluate the viscosity of Al_2O_3-DW nanofluid as a function of temperature where their correlation had given the data is completely matched with the published one.

$$\rho_{nf} = 1001.064 + 2738.6191\varphi - 0.2095\,T;\ 0 \le \varphi \le 0.04, 5 \le T\ °C \le 40. \tag{2-27}$$

2.4.4 Specific heat

Based on the assumption which considers the base fluid and nanoparticles in thermal equilibrium, Xuan and Roetzel (2000) developed the equation (2-28) to evaluate the specific heat of nanofluids.

$$C_{p,nf} = \frac{(1 - \varphi)\rho_{bf}C_{p,bf} + \varphi\rho_p C_{p,p}}{\rho_{nf}} \tag{2-28}$$

Zhou and Ni (2008) conducted experimental work to evaluate the specific heat of Al_2O_3-DW at several volume concentrations from 0-21.7%. Their results showed a good agreement with equation (2-28) and indicated that specific heat decreases when volume

concentration increases. Sekhar and Sharma (2015) developed an empirical correlation where they considered the effects of temperature, volume fraction, and nanoparticle size on the specific heat of nanofluids. They conducted their study on metal oxides/ water-based nanofluids such as Al₂O₃, CuO, SiO₂, and TiO₂ with particle size range from 15-50 nm. Equation (2-29) shows their correlation valid for the temperature range between 20 ℃ and 50℃ and volume fraction from 0 - 4%.

$$C_{p,nf} = 0.8429 \left(1 + \frac{T_{nf}}{50}\right)^{-0.3037} \left(1 + \frac{d_p}{50}\right)^{0.4167} \left(1 + \frac{\varphi}{100}\right)^{2.272} \tag{2-29}$$

2.5 Studies of the forced turbulent convection using nanofluids

Attention to nanofluids as a heat transfer medium was initially upon the fact that increasing fluid thermal conductivity by adding solid nanoparticles will enhance its ability to transfer the heat. But for forced convection heat transfer application, the efficiency of fluids does not depend on the fluid thermal conductivity as a unique parameter. Therefore, parameters such as convection heat transfer coefficient and pressure drop become more critical than nanofluid thermal conductivity (Timofeeva, 2011). Various studies were performed, either experimentally or numerically, to evaluate the use of nanofluids in the different applications of convection heat transfer since Pak and Choi (1998) started the first experimental of convection heat transfer using nanofluids. The enhancement of convection heat transfer had been reported by many researchers when they used nanofluids as a heat transfer medium in different flow passages.

2.5.1 Experimental studies of pipe flow

An experimental study was conducted by Yarmand et al. (2017) to investigate the performance of heat transfer and friction loss of the GNP-PT/DW hybrid nanofluid under turbulent flow in a square duct with uniform heat flux on its outer surface. The nano fluid

with a concentration range of 0.02-0.1 wt.% was prepared using the two-step method. All the experiments were performed under turbulent fully developed flow with Reynolds number range of 5000-17500, and the test section was stainless-steel tube with 1.4 m long and 10 mm aside. Their work showed a percentage enhancement in Nu number up to 28.48% compared to the DW in the highest nanofluid concentration. Their results also showed the enhancement of the Nu number depends on the Reynolds number as well. It was 4.58% at the lowest Reynolds number and 6.35% at the highest Reynolds number for the concentration of 0.02 wt.%. The enhancement was in the range between 14.63% and 28.48% for the 0.1 wt.% concentration. The convection heat transfer coefficient was enhanced and showed a percentage enhancement of 49.16% at the Reynolds number of 17500 and 0.1 wt.% concentration. Evaluation of friction factor and pumping power were also investigated to calculate the performance index and the energy efficiency of the whole system. They calculated the thermal performance based on the positive enhancement in the convection heat transfer coefficient divided by the negative enhancement or the pressure drop increment. They found that all the concentrations have a thermal performance above unity even at a low Reynolds number, which indicates that their nanofluid is energy efficient and has promising features as a convective medium.

In another study, the same researcher, Yarmand et al. (2016), conducted experimental work to evaluate the performance of functionalized GNP in a square duct under the same previous conditions. They tested the GNP/DW nanofluid with weight concentrations of 0.02%, 0.06%, and 0.1%. They got an enhancement of 3.3% up to 26.5% in the Nusselt number for 0.02 wt.% at Re 5000 and 0.1 wt.% at Re 17500, respectively. Based on the equation (2-30), they evaluated the performance index. They got a net positive enhancement because the enhancement in the heat transfer is higher than the penalty due to pressure drop increment. The performance index for all the nanofluid concentrations was higher than unity except for 0.02 wt.% at Re 5000.

$$\varepsilon = \frac{h_{nf}\big/h_{bf}}{\Delta P_{nf}\big/\Delta P_{bf}} \tag{2-30}$$

Aliabadi et al. (2016) conducted experimental work to evaluate the performance of Cu/DW, Fe/DW, and Ag/DW nanofluids of 0.1 wt.% concentration on heat transfer characteristics inside rectangular duct equipped with different cylindrical pins shown in Figure 2-4. They prepared all nanofluid samples using the one-step technique and investigated their performance in comparison with the DW. They run their experiments under constant surface temperature using a film of condensed water vapor on the outer surface of the test section. They validated their test rig by comparing Nu number, and friction factor obtained experimentally with those calculated from published correlations for the test section without pins under fully developed turbulent flow. Then they evaluated the convection heat transfer coefficient and pressure drop for all pin arrays using DW at volume flow rates from 4.0 to 10.0 L/min. According to their results, the convection heat transfer and pressure drop were directly proportional with the pin diameter and pin number (i.e., they were decreased when the pin diameter increases for the same pin diameter array). So, the pin array of diameter 6.0 mm and pitch 20.0 mm produced the highest heat transfer coefficient and the highest pressure drop in the water run experiment.
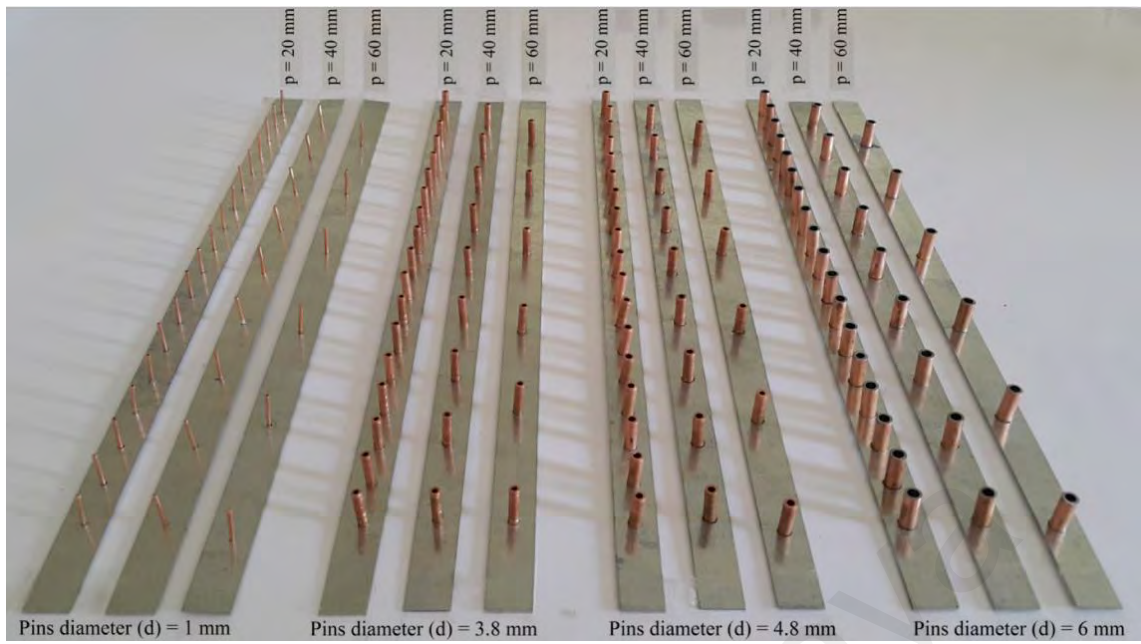
Figure 2-4: A picture showing the design of pin arrays used to build the pin-channel (Aliabadi et al., 2016).

The average enhancements in heat transfer coefficient for DW run were about 5.7%, 10.7%, 15.3%, and 25.6% for the channel with a pin diameter of 1.0, 3.8, 4.8, and 6.0, respectively. The pressure drop increments for the same pin channel were 2, 3, 3.9, and 6.8 times higher than the empty ducts, respectively. Due to the increase in heat transfer and pressure drop, they used the thermal-hydraulic performance or performance index as an evaluation criterion, as shown in equation (2-31).

$$\varepsilon = \frac{Nu_m/Nu_{nm}}{\left(f_m/f_{nm}\right)^{1/3}} \qquad (2\text{-}31)$$

where, subscripts *m* and *nm* refer to modified and non-modified duct, respectively.

They evaluated the thermal-hydraulic performance for both the DW and nanofluids and assessed the percentage of ε_{nf} to ε_{bf}. According to the results of Aliabadi et al. (2016), the Ag/DW nanofluid was the best for all the study cases based on the percentage

enhancement of convection heat transfer coefficient and the percentage of both the performance indices, which were more significant than unity for all the pin arrays.

The circular pipe heat exchanger is the most common application in convection heat transfer studies using nanofluids under laminar or turbulent flow conditions. Ranjbarzadeh et al. (2017) conducted an experimental study to investigate the heat transfer and friction loss performance through an isothermal circular cupper tube of 10 mm outer diameter using Graphene oxide/DW nanofluid with 0.025, 0.075, and 0.1 vol.% concentrations. The flow condition was turbulent flow with a Reynolds number range of 5250 and 36500. The outer surface temperature of the test section was kept constant at the evaporation temperature of the water inside a heating chamber. The nanofluid was prepared by the two-step method, and its thermophysical properties were measured at room temperature. According to their results, they got a maximum thermal conductivity enhancement for the highest concentration of 28% compared to the DW at room temperature. Their results also showed that heat transfer enhancement and pressure drop increase when the nanofluid concentration increases and Reynolds number. The maximum increase in the friction coefficient was 16%, while the Nusselt number showed a maximum enhancement of 17.6% compared to the base fluid. They used equation (2-31) to evaluate the thermal performance of the nanofluid of their study. They found the thermal performance increases when the nanofluid concentration increases, and all the thermal performance values were higher than unity.

Sadri et al. (2017) conducted experimental work to investigate the characterization of an environmentally friendly covalent GNP/DW nanofluid and its heat transfer performance in a circular tube heat exchanger. Three concentrations, 0.025, 0.075, and 0.1 wt.%, were prepared. All the thermophysical properties were measured experimentally, where the thermal conductivity measurements showed a maximum

enhancement percentage of 22.92% for the 0.1 wt.% concentration compared to the base fluid at 45°C. The dynamic viscosity measurements showed that all the nanofluid concentrations are Newtonian fluids with a slight increment in comparison with the viscosity of the base fluid. The specific heat of nanofluid was reduced by 0.43–1.52% due to the low specific heat capacity of the GNP nanoparticles. Also, a maximum increase of 0.045% in the nanofluid density was recorded at 20 °C for the 0.1 wt.% concentration compared to that of the DI water. The heat transfer experiment was conducted under fully developed turbulent flow with the Re range of 6371 to 15927, and uniform heat flux at the outer surface of the pipe with a fixed inlet flow temperature of 30 °C. According to their results, the average enhancement of the convective heat transfer coefficient approximately was 9.26, 26.59, and 37.54% for the nanofluid concentrations of 0.025, 0.075 and 0.1 wt.%, respectively, and the maximum Nusselt number enhancement was obtained at the highest Re number with the average percentages of 4.96, 13.58 and 18.69% for particle concentrations of 0.05, 0.075 and 0.1 wt.%, respectively. They evaluated the performance index based on equation (2-31). They found that all the nanofluid concentrations have a positive potential where the performance index is higher than unity for all the concentrations.

Sadeghinezhad et al. (2014) conducted an experimental study to evaluate the heat transfer characteristics and pressure drop of Graphene nanoplatelet (GNP) dispersed in DW through horizontal stainless-steel pipe. The pipe was 10 mm diameter and 1.4 m in length, with uniform heat flux on the outer surface. A fully developed turbulent flow conditions were employed in their experimental work. Nanofluids with four concentrations of 0.025, 0.05, 0.075, and 0.1 wt.% were prepared using the two-step method. They measured all the thermophysical properties experimentally and studied the effect of nanoparticle concentration, flow velocity, and heat flux on heat transfer and pressure drop. Their measurements showed that base fluid thermal conductivity

enhancement was between 7.96% and 25% for the low and high concentrations, respectively. Compared with the base fluid, the nanofluid of 0.1 wt.% concentration showed a maximum enhancement of the convective heat transfer coefficients equals 131%, 146%, and 160%, and a maximum enhancement of Nu number equals 75%, 79%, and 83% for the heat fluxes of 8231, 10351, and 12320 W/m^2, respectively. The pressure drop increased by 0.4% at the lowest velocity of 0.3 m/s for 0.025 wt.% and reached 14.6% at the highest flow velocity of 1.3 m/s for 0.1 wt.%. The researchers evaluated the thermal performance of all the nanofluids based on equation (2-31). They showed that the thermal performance increased when the nanofluid concentration increased, and the thermal performance values were higher than unity. From their results, there are two points to stand on: the first one is the heat flux effect on the Nu number for the same fluid, while the Nu number is heat flux independent. The second point is evaluating Nu numbers at different velocities but not at different Reynolds numbers. Because the number differs from one fluid to another at the same velocity, which gives wrong indications about the enhancement of Nu number as it mainly depends on Re and Prandtl numbers.

Esfe et al. (2014) conducted an experimental study to evaluate the performance of the heat transfer and pressure drop inside the circular pipe with constant hot surface temperature using Mg/DW nanofluid of volume fractions 0.0625%, 0.125%, 0.25%, 0.5%, and 1%, under fully developed turbulent flow with Reynolds number range between 3200 and 19000. Evaluation of thermophysical properties such as thermal conductivity and viscosity was done experimentally. At the same time, the specific heat and density of the nanofluid were evaluated using equations of the thermal equilibrium model and the mixing theory, respectively. Their results showed a significant enhancement of Nusselt number up to 1.32 of the base fluid Nu number and a considerable enhancement of the heat transfer coefficient up to 1.36 of the base fluid at 1% concentration. The pressure drop measurements through the test section showed that:

the pressure drop of nanofluid was increased slightly compared to those of the DW. They did not explain why the pressure drop of the highest nanofluid concentration is lower than those of the lower concentration. They also calculate the thermal performance factor for all nanofluids based on Nu number and friction factor, and they got a trend over than unity for all the nanofluids.

Heyhat et al. (2012) studied the effects of using Al_2O_3 – DW nanofluid of volumetric concentrations of 0.1, 0.5, 1.0, 1.5, and 2 % on the convection heat transfer and pressure drop under turbulent flow regime with Re number range of 3000 - 16000 inside a circular pipe. The test section used in their experiments was a copper tube of 5 mm diameter and 2 m length. They kept the outer surface of the test section at constant temperature by using steam evaporated from a water path where the test section passes through it. They found that the convection heat transfer coefficient had a 23% enhancement than distilled water at a maximum of 2 vol.%. At the same time, the measured Nusselt number did not match the same trend of enhancement as the convection heat transfer coefficient due to the effects of the nanofluids Prandtl number. They also found that the pressure drop through the test section increased gradually with the increasing volumetric concentrations of nanofluids.

Williams et al. (2008) used horizontal stainless-steel pipe as a test section of 9.4 mm inside diameter and 3 m length to evaluate the heat transfer performance and pressure drop for Al_2O_3 - DW and ZrO_2 - DW nanofluids. They exposed the outer surface of the test section to constant heat flux from the resistant heater rapped over the test section. The Reynolds number for their experiments was in the range of 9000-63000. The volumetric concentrations of Alumina/ water nanofluid were 0.9%, 1.8%, and 3.6%, and the volumetric concentrations of Zirconia/ water nanofluid were 0.2%, 0.5%, and 0.9%. They concluded that the nanofluids could be treated as a single-phase as their heat transfer and

pressure drop results perfectly matched the traditional empirical correlations of Dittus-Boelter and Blasius for Nusselt number and pressure drop, respectively.

Pak and Choi (1998) conducted experimental work to study the convection heat transfer and friction behavior of aqua-based nanofluids with Al_2O_3 and TiO_2 nanoparticles of diameter 13 nm and 27 nm, respectively. They prepared the nanofluids with volume concentrations varied from 1% to 10% using a mechanical stirrer of 10000 rpm. They studied the viscosities at different concentrations and got two and three times the water viscosity for Al_2O_3-DW and TiO_2-DW nanofluids, respectively. They got the maximum enhancement of thermal conductivity of 32% and 11% for Al_2O_3-DW and TiO_2-DW nanofluid, respectively, at a volume concentration of 4.3%. Their test rig contained a 0.2 m^3 reservoir tank for nanofluid and stainless-steel tube as a test section with dimensions of 10.66 mm and 0.480 m for inside diameter and length, respectively. The test section was electrically heated with a maximum heating capacity of 15 kW. They found that the Nu number increased when the volume concentration increased as well as the Reynolds number. When they conducted their experiments under constant average velocity, they found that the convective heat transfer coefficient decreased by 12% more than the DW.

Studying the thermal and flow performance of the nanofluids through different pipe configurations with the same thermal boundaries and flow conditions was done along with optimization of the various designs of heat exchangers when using nanofluid as a convective medium. Jafarimoghaddam and Aberoumand (2017) presented an experimental study to compare the performance of the Ag/DW nanofluid as a convective medium in rectangular and semicircular pipes with the same length and hydraulic diameter of 0.5 m and 9.4 mm, respectively. The test sections were exposed to a uniform heat flux at their outer surfaces. Seven volume concentrations from 0.03% up to 2% were

used in their study under laminar flow conditions with relatively low Reynolds numbers from 301 to 740. They prepared the nanofluid by applying the one-step method using the electrical explosion wire. Referring to their results, the convection heat transfer coefficient increased by increasing the volumetric concentration in both the geometries. They found that the enhancement percentage in the semicircular pipe was higher than that of registered within the rectangular one. Although the friction factor in the semicircular tube was higher than that of the rectangular one for the same nanofluid concentration and Reynolds number, the highest friction factor of nanofluids did not exceed 1.04 times the DW. Therefore, the extra pump power can be neglected in the performance evaluation of the nanofluid as a convective medium.

2.5.2   Numerical studies of pipe flow

Senay et al. (2019) presented a numerical study to evaluate the heat transfer and friction loss of Al_2O_3/DW and TiO_2/DW nanofluids in a square duct exposed to uniform heat flux on its outer surfaces under constant flow velocity conditions. They built a turbulent flow model using the ANSYS-FLUENT package with a Reynolds number range equivalent to the velocity range of 1 - 8 m/s. They validated their model by comparing the Nu number obtained numerically with the Dittus & Boelter correlation for DW. All nanofluid concentrations were treated as a homogenous single-phase fluid. The thermophysical properties of different nanofluid concentrations from 0.01-0.04 vol.% were evaluated theoretically. According to their results, the TiO_2/DW nanofluid showed a higher enhancement in the heat transfer and pressure drop in comparison with the Al_2O_3/DW nanofluid for the same Reynolds number. The enhancement of heat transfer with TiO_2/DW was higher than those obtained with Al_2O_3/DW for all the velocities, reaching about 29% higher values at the highest concentration at Re number 20000. The negative point in their work is conducting their study under constant velocity, which gave a different Reynolds numbers range for each nanofluid concentration.

Abdolbaqi et al. (2014) presented a CFD analysis study to evaluate the heat transfer and pressure drop performance of CuO, TiO$_2$, and Al$_2$O$_3$ aqua-based nanofluids with volume concentrations of 1-4% inside a square pipe with a hydraulic diameter of 0.02 m and 1.6 m length under uniform heat flux boundaries and Re number range of 10^4-10^6. They evaluated all nanofluid thermophysical properties theoretically using published empirical correlations. They validated their model by comparing the friction factor Blasius equation and Nu number with those calculated by Dittus & Boelter equations. Based on their results, the CuO/DW nanofluid showed the highest Nu number and the convection heat transfer coefficient for each concentration. They attributed the reason to the higher thermal conductivity and Prandtl number of the CuO/DW nanofluid. The CuO/DW nanofluid also showed the highest increasing percentage of the friction factor compared with the DW and the other nanofluids.

Rostamani et al. (2010) studied the heat transfer characteristics and friction loss of CuO/DW, TiO$_2$/DW, and Al$_2$O$_3$/DW nanofluids numerically using a 2-D model for rectangular duct under fully developed turbulent flow with Re number range of 20000-100000, and a uniform heat flux along the outer surfaces. Their model was built by a commercial CFD package, and the nanofluids' volume concentrations were varied from 1 to 6% and were treated as single-phase fluids. All the thermophysical properties were evaluated theoretically at the flow inlet temperature. Their results showed that the CuO/DW nanofluid has the highest heat transfer enhancement over TiO$_2$/DW and Al$_2$O$_3$/DW nanofluids. Both the Nusselt numbers and convection heat transfer coefficient were increased with the increasing nanoparticles concentration and Reynolds number. The wall shear stress evaluation showed that the CuO/DW nanofluid and TiO$_2$/DW nanofluid have the highest and lowest shear stress values, respectively.

Sadri et al. (2018) conducted a numerical CFD study to investigate the thermal and hydrodynamic performance of aqua-based clove-treated graphene nanoplatelets nanofluids flowing inside a circular horizontal tube. The pipe surface was subjected to uniform heat flux, and the flow conditions were adjusted as a forced turbulent flow of Re number range of 6371 - 15927, and the inlet flow temperature was fixed at 30 °C. They created the mesh and solved the governing equations of their 3-D model using a commercial CFD package and the thermophysical properties of all nanofluid concentrations (0.0, 0.025, 0.075, and 0.1 wt.%) were measured experimentally. They treated all nanofluids in their study as a single-phase fluid. They got an acceptable deviation from the experimental data that was evaluated at the same conditions for the average convection heat transfer coefficient and pressure drop.

Boertz et al. (2018) conducted a 2-D numerical study to evaluate the performance of heat transfer and friction loss of nanofluid flowing inside a circular tube with constant heat flux boundary under fully developed turbulent flow with a Re number range of 6000-12000. They prepared the nanofluids from silica nanoparticles (from 0 vol.% to 10 vol.%) in a mixture of DW/EG with a mass ratio of 60:40 as a base fluid. They modeled the nanofluid as a single-phase fluid and calculated all the thermophysical properties theoretically. They applied the finite volume approach to solve the governing equations using the computational fluid dynamics code Open FOAM (Open-source Field Operation And Manipulation) and PCG (Preconditioned Conjugate Gradient) solver with the DIC (Diagonal Incomplete-Cholesky) preconditioner for symmetric matrices to solve the system equations and calculating the pressure field. According to their results, the average Nu number showed a max enhancement of 13.2% compared to the base fluid at Re of 12000 and 10% vol.% concentration. The pumping power also increased with the increase of the Reynolds number and nanoparticles concentrations. It reached up to 1.8 of the total

pumping power consumed by the base fluid at the Re number of 8000 and concentration of 6%.

Saha and Paul (2014) performed a numerical study to evaluate the heat transfer performance of water-based metal oxide nanofluids flowing inside a horizontal circular tube of 1 m length and 0.013 m diameter and exposed to uniform heat flux on its outer wall. The flow conditions that employed were a forced turbulent flow of Re number range 1000-100000. The nanoparticles of Al_2O_3 and TiO_2 with different particle sizes ($dp)$ of 10, 20, 30, 40 nm were chosen to prepare a nanofluid's of 4 vol.% and 6 vol.% concentrations. They theoretically calculated the nanofluids' thermophysical properties and used a commercial CFD package to solve the governing equations using the single-phase fluid approach. They validated their model by comparing the resulted Nu number and friction factor for DW with those obtained mathematically using Gnielinski and Blasius equations, respectively. Referring to their results, the impact of nanofluids' kinematic viscosity on the velocity profile was noticeable as the maximum velocity increased for the same Re with the decreasing of particles diameter and increasing of the nanoparticle concentration. The Al_2O_3/DW nanofluid showed a higher thermal performance than the TiO_2/ DW nanofluid for the same nanoparticle size. The nanofluid prepared from the smallest nanoparticle size (10nm) showed the highest thermal performance than those prepared with the larger nanoparticle size. They evaluated the thermal performance based on equation (2-31), which was higher than unity for both concentrations.

Hejazian and Moraveji (2013) presented a comparative numerical study to evaluate single-phase and multi-phase approaches in the heat transfer studies of nanofluids. The heat transfer performance of TiO_2/DW nanofluid of volumetric concentrations between 0.05% and 0.25% was evaluated under forced turbulent flow conditions using a 2-D

model for a circular horizontal tube of 1.2 m length and 0.05 m diameter, with constant wall temperature boundary condition. They used a commercial CFD package to create the mesh and solve the governing equations of their model. They validated their model with a published experimental data from the same authors. According to their results, the mixture model (multi-phase) gave a more accurate prediction of the experimental data than the single-phase model. The average errors percentages for Nu's experimental data numbers are 10.85% and 9.36% at the same Re number range for the single-phase and mixture model, respectively. Also, the deviation from the experimental data can improve the single-phase model by altering the solution scheme, improving its error percentage, and saving the run time.

Lotfi et al. (2010) conducted a numerical study to investigate the thermal performance of Al_2O_3/DW nanofluid of various volumetric concentrations (1-7 vol.%) in a forced turbulent flow through a horizontal circular pipe. A Single-phase, two-phase mixture model and the two-phase Eulerian models were applied to study the flow field with nanofluid as a convective medium. Their numerical study was validated using the traditional expressions for Nusselt number given by Dittus–Boelter and Gnielinski formulas and some published experimental works. According to their results, the mixture model was the most precise one compared to the single-phase and the two-phase Eulerian models; they found that: the rate of thermal enhancement decreased when the volume concentration increased.

Space limitations and economic considerations of the fabrication process have a prominent role in selecting heat exchanger configuration. Therefore, it is essential to evaluate the performance of different designs and geometries to make the selection decision more established. Mohanrajhu et al. (2015) conducted a comparative numerical study to assess the performance of automotive radiator with flat and circular tube design

using Alumina nanofluid with the base fluid containing 60% vol.% of EG and 40 vol.% of DW. Their work was carried out under a turbulent regime with a Re number range 5000-14000 and nanoparticles volume concentrations of 1-5 vol.%. Both the flat and circular pipes have the same hydraulic diameter and thermal boundary conditions as well. The inlet flow temperature for both tubes was 90 °C, and the nanofluids' thermophysical properties were estimated at this temperature. The thermal radiation losses from the outer surfaces were negligible where the convection heat transfer coefficient at the air side of the tube was fixed at 50 W/m^2.K with a free stream outside temperature at 30 °C. Their results showed that:

- Both the Nusselt number and the convection heat transfer coefficient were increased when Reynolds number and nanofluid concentration increased for both configurations.

- The enhancement of Nusselt number and convection heat transfer coefficient in the flat tube was higher than those of the circular tube at the same Re and nanofluid concentration.

- A similar trend of the Nusselt number was observed for the pressure drop along with both the configurations.

- For a constant pumping power per unit length of 5W/m, the average convection heat transfer coefficient decreased with the increase in nanofluid concentration.

- The convection heat transfer coefficient for the two vol.% and five vol.% nanofluids were lower than those of the base fluid by 6% and 23.8%, respectively.

- Nanofluid with 1 vol.% concentration showed a 1.2% improvement in the convection heat transfer coefficient than the base fluid.

The pressure drop results obtained by Mohanrajhu et al. (2015) conflicted with those obtained numerically by Hussein et al. (2013). They found that the pressure drop obtained from the flat tube is lower than those obtained from the Blasius equation for the circular pipe at the same turbulent flow conditions. Hussein et al. (2013) obtained another essential point, as they found the enhancement of Nusselt number was the highest with SiO_2 followed by Al_2O_3/DW and TiO_2/DW while the enhancement arrangement was reversed in the thermal conductivity evaluation for the same nanofluids.

2.5.3   Studies of annular flow

The heat exchangers of cylindrical annular geometry are found in many engineering and industrial applications such as thermal power plants, solar collectors, thermal storage systems, and even in cooling devices of electronic components. Therefore, a lot of research work were done on the heat transfer mechanisms inside the annulus either for concentric annuli such as (Davis, 1943; Gnielinski, 2015; McAdams, 1954; Wiegand et al., 1945), or eccentric one such as (Cantab, 1963; Deissler & Taylor, 1955; Kenjereš & Hanjalić, 1995; Nikitin et al., 2009; Ogino et al., 1987; Usui & Tsuruta, 1980). All the works that have been done for eccentric cases concluded that: the heat transfer rate in the concentric annuli is higher than those in the eccentric annulus due to the non-uniform temperature distribution created along the eccentric annulus. Various studies were performed either experimentally or numerically to evaluate the thermal and hydraulic performances of different types of nanofluids in the annular-shaped heat exchanger.

Bahmani et al. (2018) presented a numerical solution using the finite volume method to evaluate the heat transfer and the pressure drop through a double pipe heat exchanger using Alumina/DW nanofluid. Their model was solved using the FORTRAN code for parallel, and counter flow conditions with Reynolds numbers range from 10000 to 100000. They considered the nanofluid as a single-phase Newtonian fluid with constant

thermophysical properties evaluated at 258 K. They found that the maximum thermal efficiency enhancement was achieved at the 5 vol.% concentration, and a reduction in the enhancement was recorded for the volumetric concentrations greater than 5%.

Arzani et al. (2015) conducted a numerical study to evaluate the effect of using two types of GNP-DW on the heat transfer and the pressure drop through an annular heat exchanger with a concentric cross-section. The inner pipe of their model was subjected to uniform heat flux, and the outer one was insulated entirely. GNP-SDBS/DW and GNP-COOH/DW nanofluids were used with concentrations of 0.25 wt.%, 0.05 wt.%, and 0.1 wt.% under turbulent flow conditions with Reynolds number range from 5000 to 17000. Their 2-D model was solved by ANSYS Fluent, considering the nanofluid as a two-phase mixture model with constant thermophysical properties evaluated at the flow inlet temperature. The highest enhancement in the convection heat transfer was 22% for the 0.1 wt.% concentration compared to the DW at the Reynolds number of 17000. The highest pressure drop increment was obtained for the same concentration and Reynolds number as well.

Nasiri et al. (2011) evaluated the heat transfer performance experimentally for the Alumina/DW and the Titania/DW nanofluids of 0.1vol.%, 0.5 vol.%, 1 vol.%, and 1.5 vol.% concentrations through a concentric double pipe heat exchanger of 2.2 diameter ratio. The design of their test section consisted of three concentric pipes: the inner one was a metallic rod. The nanofluids flowed in the annulus between the inner rod and the middle pipe, while the annular space between the middle pipe and the outer shell was filled with the flowing hot water for heating purposes. The outer surface of the shell was insulated. They ran their experiments under fully developed turbulent flow conditions in the nanofluid side at Reynolds number range from 4000 to 13000 and put nine baffles in the waterside to create strong turbulence. The thermophysical properties of their

nanofluids were evaluated theoretically based on the nanoparticle's properties and the DW. The Nusselt number and heat transfer coefficient were obtained versus the Peclet number to show the effect of the Prandtl number on the heat transfer performance. According to their results, both the nanofluids tend to give the same enhancement in heat transfer for the same Pe number range and volumetric concentration. Based on a comparison with a published experimental data of cylindrical pipe flow, they found that the enhancement of the Nusselt number seems to be higher in the circular pipe for the material and Pe number range.

Sonawane et al. (2013) conducted an experimental study to evaluate the Al_2O_3-DW nanofluid as a coolant in a concentric double pipe heat exchanger of 2.0 diameter ratio. Volume concentrations of 2.0% and 3.0% were used with volume flow rates 1-3 l/min and 0.1-1 l/min for the hot and the cold fluid, respectively. They obtained maximum enhancement of the overall heat transfer coefficient equals 14% and 47.3% for the volume concentrations of 2.0% and 3.0%, respectively.

Darzi et al. (2013) studied the effect of using Al_2O_3-DW nanofluid with volumetric concentrations of 0.25%, 0.5%, and 1% in a concentric double pipe heat exchanger experimentally; under turbulent flow conditions with the Reynolds number range 5000 to 19000. The inner tube of their test section was made from copper while the outer was from stainless steel, and the diameter ratio of 15.67, and they concluded that the nanofluid has a good enhancement only at a high Reynolds number.

The performance evaluation of nanofluids as a convective medium through heat exchangers of eccentric annulus had been done by many researchers (El-Maghlany & Elazm, 2016; Matin & Pop, 2013; Hu, 2017; Matin & Pop, 2014; Mirzaee & Lakzian, 2017; Shahzadi & Nadeem, 2017; Sheikholeslami et al., 2014; Teimouri, 2017). They

considered only the natural convection either with the stationary inner tube or the rotating one (El-Maghlany & Elazm, 2016; Teimouri, 2017).

2.5.4   Purpose of study

According to the current literature, the enhancement of convection heat transfer occurring by nanofluids stills a matter of debate. Some work proved that enhancing thermal conductivity is the vital key to improving the convection heat transfer. In contrast, some others showed an inversed relationship between thermal conductivity and convection heat transfer enhancement. Therefore, the current study will investigate the effect of the properties such as thermal and momentum diffusivities side by side with the thermal conductivity because dispersing of the nanoparticles in the base fluids affects the thermal conductivity and affects the properties such as specific heat and kinematic viscosity.

Despite the importance of the nanofluids performance evaluation in the different geometries to guide the engineers to select the best heat exchanger configurations with nanofluids applications, there is a lack in the research focus on the comparative studies between the different pipe geometries, especially between square and circular pipe geometries under the same turbulent flow conditions. Therefore, a part of the current work will focus on the nanofluid performance evaluation in square and circular conduits of the same hydraulic diameter and have the same flow and boundary conditions.

The annular geometry heat exchangers are widely used in the heat transfer equipment and the nano heat transfer studies focused mainly on the concentric types. A lack of studies focused on the annular heat exchanger with an eccentric annulus, especially under turbulent flow conditions, was found. Therefore, the current study will investigate the thermal and hydraulic performance of different types of nanofluids in the annular heat exchanger with various vertical eccentricities.

The nanofluids that will be used in the current study are two types of metal oxide nanoparticles and hybrid nanocomposite of metal oxide and carbon-based nanoparticles. Preparation of stable nanofluids using the two-step method and investigation of their thermal performance in the different pipe geometries are also highly considered.

CHAPTER 3: METHODOLOGY

3.1   Introduction

In this chapter, the preparation methods, characterization, and thermophysical properties evaluation of all the nanofluids used in the current study will be discussed. The components of the experimental test rig and the analysis method of the data collected will be shown. The numerical study, including governing equations, physical models, solution method, and validation of all the physical models, will be discussed.

3.2   Nanofluids characterization and preparation methods

In the current study, two metal oxide nanopowder and a composite of functionalized multi-walled carbon nanotubes f-MWCNTs plus Alumina were used to prepare all the nanofluid samples of the concentrations 0.1 wt.%, 0.075 wt.%, and 0.05 wt.% using the two-step method. The silica (SiO_2) and Alumina (Al_2O_3) nanopowders of 13 nm diameter were purchased commercially from Sigma-Aldrich to prepare two metal oxide nanofluids with the indicated concentrations. The f-MWCNTs nanopowder was prepared experimentally and then mixed with the commercial Alumina with different weight percentages to prepare the hybrid nanofluid. All nanofluids were firstly prepared at the highest concentration wt.% and then diluted according to the dilution equation of the solutions (3-1).

$$C_1V_1 = C_2V_2$$

$$(3\text{-}1)$$

where, C_1 is the concentration in volume V_1, and C_2 is the concentration in volume V_2.

The amount of nanomaterial needed to prepare nanofluids according to the predefined mass or weight concentration can be calculated as follows:

For hybrid nanofluids with n nanopowders, the nanopowders are added to the base fluid according to a certain percentage λ that calculated by equation (3-2):

$$\lambda_i = \frac{m_{p_i}}{m_{p_T}} , \qquad \sum_{i=1}^{n} \lambda_i = 1 \qquad\qquad \textbf{(3-2)}$$

where, m_{p_T} is the total mass of nanoparticles and can be calculated by equation (3-3)

$$m_{p_T} = \sum_{i=1}^{n} m_{p_i} = \frac{C}{1-C} m_{bf} \qquad\qquad \textbf{(3-3)}$$

where, C is the total mass concentration and C_i is the mass concentration for a single nanoparticle in the hybrid nanofluid, $C_i = \lambda_i C$, and the weight concentration percentage ω (wt.%) equals $100 \times C$.

3.2.1 Covalent Functionalization of Multi-Walled Carbon Nanotube (MWCNTs-OH)

The MWCNTs are hydrophobic. Therefore, it cannot be dispersed in any polar base-fluid like distilled water to perform a stable colloid. Treating the MWCNTs to be hydrophilic and become a well-dispersed nanoparticle can be done by several functionalization approaches. The acid method is one of those approaches which assists in introducing functional groups such as carboxyl and hydroxyl groups on the surface of MWCNTs, and it will be used in the current study.

Figure 3-1 shows the step order of the functionalized MWCNTs preparation using the acid treatment method. In this method, a strong acidic medium is prepared by mixing Nitric acid (HNO_3) and sulfuric acid (H_2SO_4) in a container at the ratio of (1:3). The first step is dispersing the pristine MWCNTs in the H_2SO_4 and shaking the solution well, where the MWCNTs will mix with the sulfuric acid. Next, the container is relocated into an ice bath, and the nitric acid drops were added to the solution mixture. The ratio of sulfuric to nitric (3:1) was adopted due to its preference as an acid treatment (Kanakia, 2013; Sarsam et al., 2016). Next, the solution was stirred for 30 min at room temperature

and then sonicated for 3 hrs. After the sonication probe process, the sample mixture was refluxed for 30 min at room temperature with constant stirring.

After stirring, the washing process takes place, where the MWCNTs were washed several times using DW until the pH reached (4-5). Then, the MWCNTs were centrifuged at 6000 rpm for 15 min to exclude the excess acid and finally dried inside the drying oven for 24 hrs at 80 °C. After finishing the drying process, the functionalized MWCNTs were ready in a very fine powder to be mixed with the Alumina nanoparticles according to the designed weight percentages in the DW to prepare the highest nanofluid concentration.
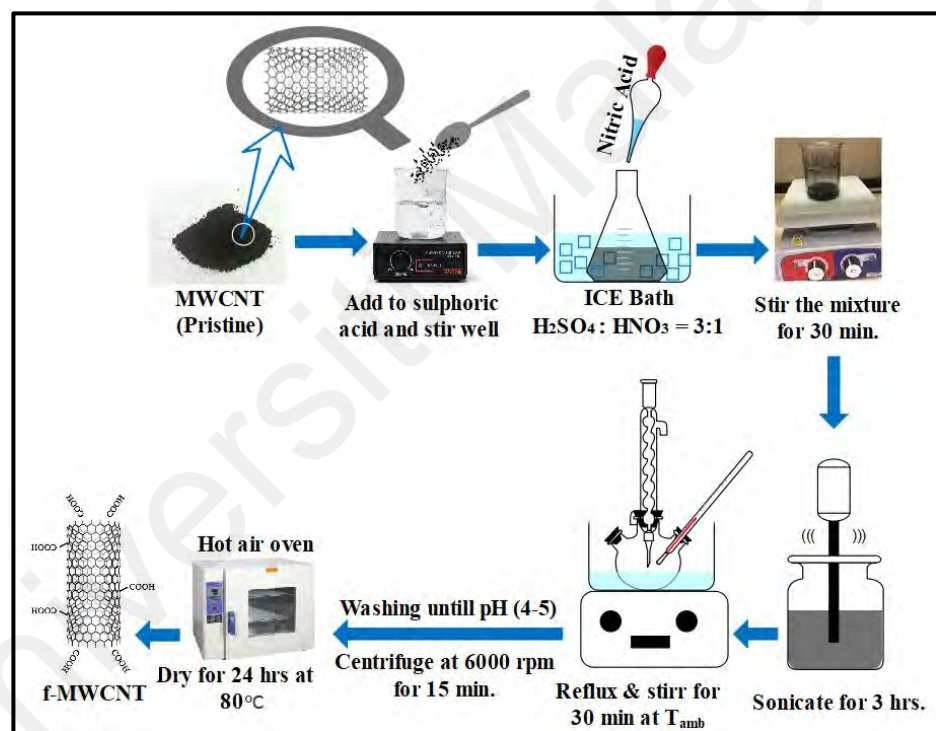
Figure 3-1: Steps of f-MWCNT preparation

3.2.2   Preparation of f-MWCNTs–Al$_2$O$_3$ Nanocomposite

The total mass of all the nanoparticles (m_{p_T}) was firstly calculated based on the designed nanofluid concentration then, the mass of each nanoparticle type (m_{p_i}) was calculated based on equation (3-2). After weighing, both the nanoparticle types were dispersed in the DW with the required quantity of the surfactant (Triton X-100). The

mixture was then sonicated for 3 hrs in the ultrasonic bath sonicator at 60 °C. Then, it was sonicated for one hr in the prob-sonicator to make it ready for use after completion of the sonication process.

In the current study, a hybrid nanocomposite of f-MWCNTs: Al_2O_3 of concentrations 20:80, 30:70, and 40:60 was selected to prepare the hybrid nanofluid, and the Triton X-100 was used as a surfactant with a mass ratio of (1:1) to the f-MWCNTs based on the studies conducted by Rastogi et al. (2008) and Shanbedi et al. (2015). All the hybrid nanocomposite ratios were tested using Spectroscopy to select the optimum mixing ratio for the heat transfer experiment.

3.2.3   Hybrid Nanofluid Characterization

3.2.3.1   FTIR spectroscopy

The Fourier transform infrared spectroscopy (FT-IR) test identifies or characterizes any unknown material and any contaminant on or in its surface. This analysis can identify the material depending on the unique spectral fingerprint of its molecules or chemical structure. The FTIR spectrometer uses the infrared lights to scan the test sample by sending infrared radiation of wavenumber range 10000 to 100 cm^{-1} through the sample, where some of the irradiated beams will be absorbed, and the rest may be transmitted or/and reflected. The absorbed radiation by the test sample molecules is converted into vibrational or/and rotational energy, and the spectrometer can present it as a spectrum (after a mathematical process using Fourier transform) of wavenumber range 4000 to 400 cm^{-1}.

In the current study, FTIR analysis was employed to analyze the surface of the hybrid nanocomposites. Figure 3-2 shows the representative FT-IR spectra of the hybrids. The broadband at 1670 cm^{-1} was attributed to the bending mode of adsorbed water (Nasiri et al., 2011). The intense band at 1230 cm^{-1} was assigned to the symmetric bending

vibrations in the Al–O–H group. The two strong bands at 760 and 460 cm^{-1} were ascribed to the vibration of AlO$_6$, and the peak at 810 cm^{-1} could be due to an Al–O stretching vibration (Zhu et al., 2008). These results confirm the formation of g-Al$_2$O$_3$ in calcined nanohybrid powders. The bands at 2311 cm^{-1} correspond to the C–H stretch and bending vibration, which originates from the pre-treatment of the MWCNTs. The detectable transmission bands approximately 1530cm^{-1} are strongly linked to the C=O stretching vibrations of carboxylic acid groups (–COOH), and new peaks around 760 cm^{-1} be assigned to the stretching vibration of C–O–C groups (Chen et al., 2008; Ho et al., 2010). The FT-IR results clearly show that hydrophilic groups, such as hydroxyls and carboxylic acid moieties, have been introduced onto the treated MWCNTs surfaces.
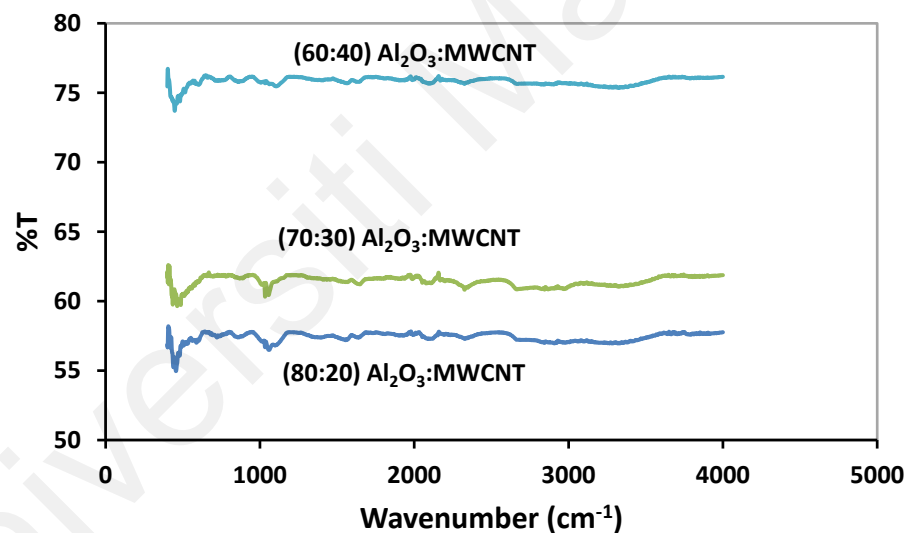
Figure 3-2: FT-IR spectrum for Al$_2$O$_3$: f-MWCNTs hybrid nanofluids at different ratios.

3.2.3.2   Raman spectroscopy

Raman spectroscopy is a nondestructive chemical analysis technique that can distinguish the structural fingerprint and by which the different molecules can be identified. The Raman analysis is a light scattering technique, where the incident laser beam on the molecule should be scattered at the same wavelength (or color) of the source. There are tiny amounts (typically 1×10^{-7} %) scattered at a different wavelength (or color),

which is called Raman Scatter and gives helpful information about the chemical structure of the test sample. This shifted energy (Raman Scatter) appears in the number of peaks, showing the intensity and the wavelength position of the Raman scattered beam. Each peak corresponds to the system's vibration, rotation, and/or other low-frequency modes for a specific molecular bond.

Raman spectroscopy revealed necessary information on the evolution of hybrid after chemical or physical treatment (Niyogi et al., 2002). Figure 3-3 illustrates the Raman spectra of the hybrid nanofluids with a sonication time of 3 h. The D band intensity/G band intensity (ID/IG) ratio represents the defect density in graphitic structures. As shown in Figure 3-3, there are three peaks at $\approx$ 1290 cm^{-1} (D band: usually use to evaluate the defects, impurities, and the quality of MWCNTs), at $\approx$ 1630 cm^{-1} (G band helps to identify the following: metallic or a semiconductor of MWCNTs, chirality, and MWCNTs diameter) and at $\approx$ 2650 cm^{-1} (G′ band). The relative intensity of the D-band to the G-band (ID/IG) is representative of the crystallinity and the quality of the MWCNTs. The ratio of hybrid (40:60) has a higher ID/IG ratio than a hybrid (30:70) and hybrid (20:80), which indicates the intense formation of defects or functional groups on the treated MWCNTs (Cho et al., 2012). By comparison of the ID/IG ratios of these spectra, it could be seen that this ratio was varied as sonication time increased. Hybrid (20:80) had the lowest ID/IG ratios of 0.811. The ID/IG ratios gradually increased to 0.832 and 0.851 of (30:70) and (40:60), respectively, under the sonication process at three h. The number of defects increased in the MWCNTs after the functionalization process, especially after three hrs of sonication treatment.
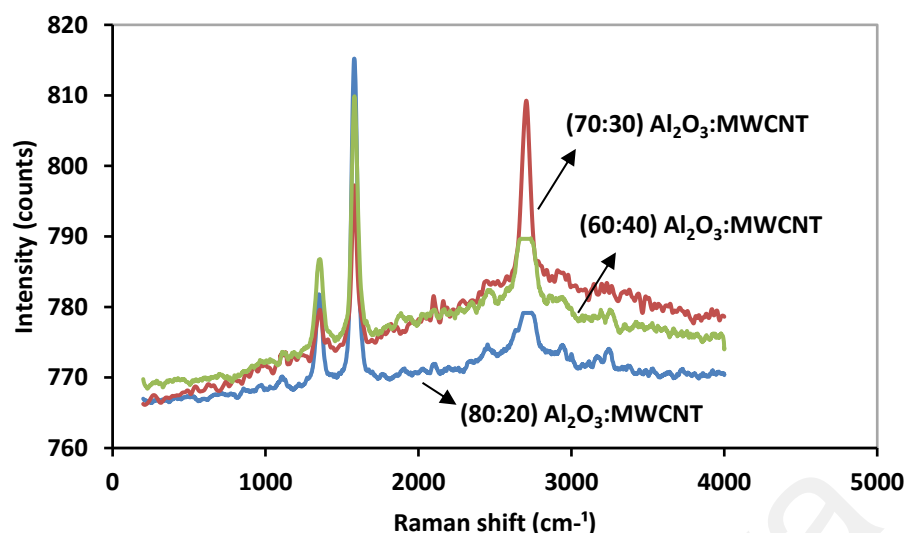
Figure 3-3: Raman spectra for Al₂O₃: MWCNTs hybrid nanofluids at different ratios.

3.2.3.3 FE-SEM analysis

THE Field emission scanning electron microscopy (FE-SEM) analysis is used to inspect the topographical and the elemental information of the test sample at very high magnification using the scanning electron microscope.

The results of FE-SEM characterization are shown in Figure 3-4, which includes four FE-SEM images for (a) Al₂O₃, (b) the pristine MWCNTs, (c) acid-treated MWCNTs (functionalized MWCNTs), and (d) Al₂O₃-coated MWCNTs. However, no clear difference can be seen in the structure of MWCNTs, but more apparent changes are found from the samples that have undergone ultrasonication for three hrs. At three hrs, the MWCNTs are severely shortened and dispersed, with the risk of the MWCNTs being damaged under prolonged acid treatment. The morphologies of the MWCNTs and the synthesized MWCNTs/alumina adsorbent were shown in Figure 3-4 (c) and (d), respectively. It is well known that after the acidification of MWCNTs, their surface presents polar groups, such as hydroxyl or carboxyl groups which can interact by hydrogen bonding with the Al₂O₃ surface. It was observed that alumina nanoparticles

were successfully coated on the surface of MWCNTs to form multi-wall carbon nanotube alumina composites, as depicted in Figure 3-4 (d).

(a) Al$_2$O$_3$

(b) Pristine MWCNTs

(c) MWCNTs@OH
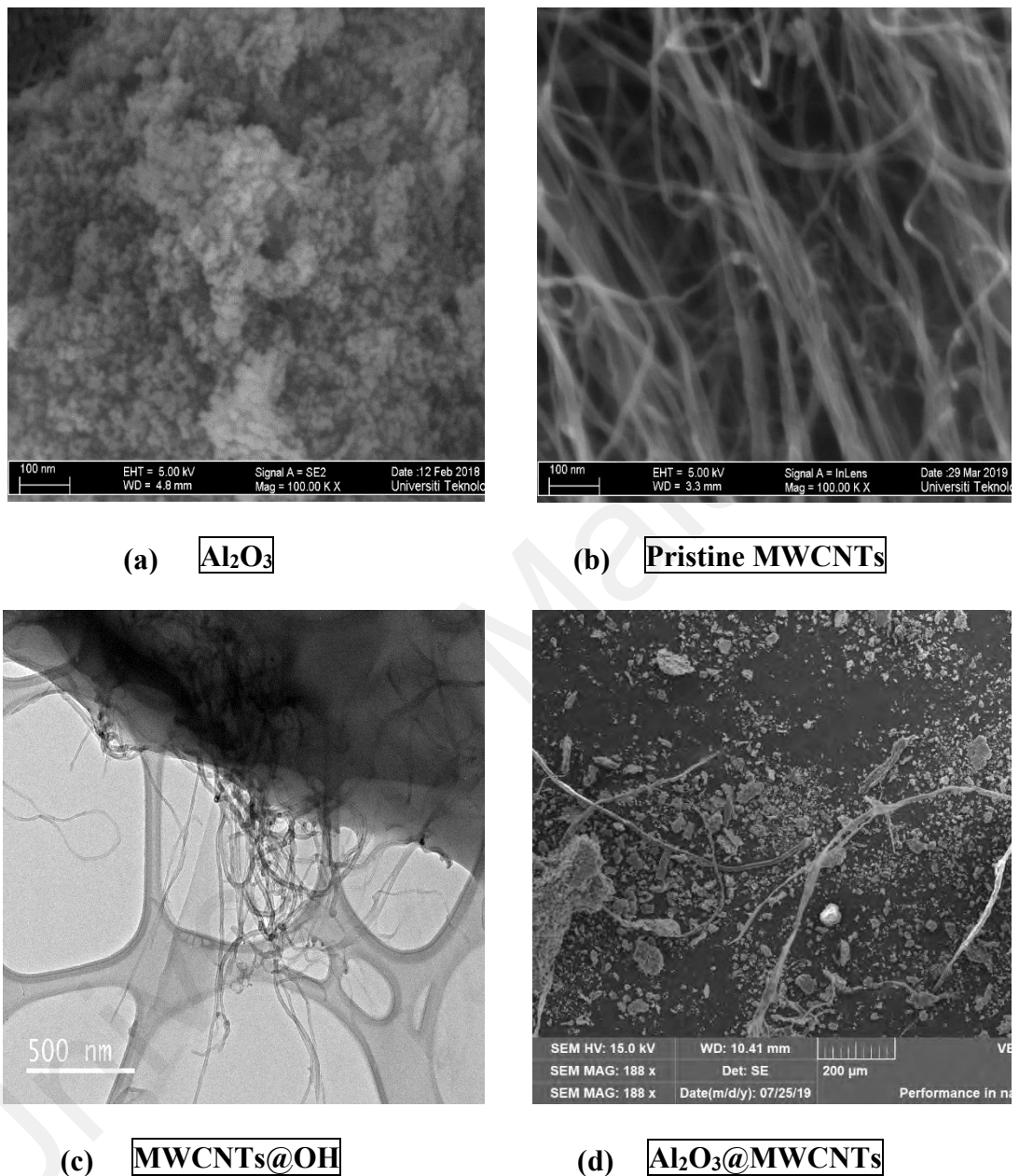
(d) Al$_2$O$_3$@MWCNTs

Figure 3-4: The structural modifications of (a) Al$_2$O$_3$, (b) the pristine MWCNTs, (c) MWCNTs @ OH, (d) Al$_2$O$_3$-coated MWCNTs.

3.2.3.4 Dispersion Stability of nanofluid samples

The sedimentation method (static position method) was used to evaluate the dispersion stability, where the observation of the nanofluid samples was continued for 30 days. Figure 3-5 shows the photo taken for the Al$_2$O$_3$/DW and SiO$_2$/DW nanofluids for 30 days. The dispersion for both the nanofluids was so good, with sedimentation rate equals 93%

during the first 15 days, which emphasized that both the samples were fit to run the experiments.

Figure 3-5: Dispersion of metal oxides nanofluids over 30 days.

Although the sedimentation method seems to be effective in evaluating the dispersion stability of some metal oxides nanofluids such as Al_2O_3/DW and SiO_2/DW due to their transparency, it should not be in the case of dark nanofluids like carbon-based nanofluids. Therefore, the Shimadzu UV spectrometer (UV-1800) with a wavelength range of 190 - 1100 nm was used to evaluate the dispersion stability of the hybrid nanofluid and the two metal-oxide nanofluids as well. The (UV-vis) spectrum method was applied to all concentrations of the three types of nanofluid in the current study over 15 days, where the absorbance of each concentration was evaluated on the first day of preparation and after 15 days which meets the same period of the experimental run. The stability was evaluated based on Beer-Lambert law which states that the absorbance of a solution is directly proportional to the concentration of species in any solution for the same path length (Mayerhöfer & Popp, 2019). Therefore, the percentage difference between the average absorbance value in the same wavelength range on the first day and the 15th day was

calculated using equation (3-4) to evaluate the dispersion stability of the different nanofluid samples.

$$\% \ Absorbance \ reduction \ = \frac{Abs_i - Abs_f}{Abs_i} \times 100 \qquad (3\text{-}4)$$

where, the Abs_i and Abs_f are the average absorbance on the first day and the 15th day, respectively.

The hybrid nanofluid samples were diluted with a ratio of 1:10 in a distilled water to increase their transparency and avoid spectrometer saturation. In contrast, the Al_2O_3/DW and SiO_2/DW samples were used without dilution unless compared with the hybrid sample.

Figure 3-6 shows the absorbance versus the wavelength for the Al_2O_3/DW nanofluid concentrations on the first day and after 15 days of the preparation. The absorbance profiles show the effect of the Al_2O_3/DW nanofluid concentration, where the highest concentration shows the highest beak while the lowest concentration shows the lowest beak. All concentrations show maximum beak at 285 nm and then decayed gradually to the near-IR wavelengths, which may be attributed to the scattering. Based on equation (3-4), the percentages absorbance reduction for 15 days was 5.5 %, 6.4%, and 7.9 for the concentrations 0.1 wt.%, 0.075 wt.%, and 0.05 wt.%, respectively.

The SiO_2/DW nanofluid showed a similar attitude to the alumina one, where the beak occurred at 285 nm but with lower values than the Al_2O_3/DW nanofluid, as shown in Figure 3-7. The absorbance reduction percentages for the SiO_2/DW nanofluid over 15 days were 4.32 %, 4.4%, and 5.8 % for the concentrations 0.1 wt.%, 0.075 wt.%, and 0.05 wt.%, respectively.
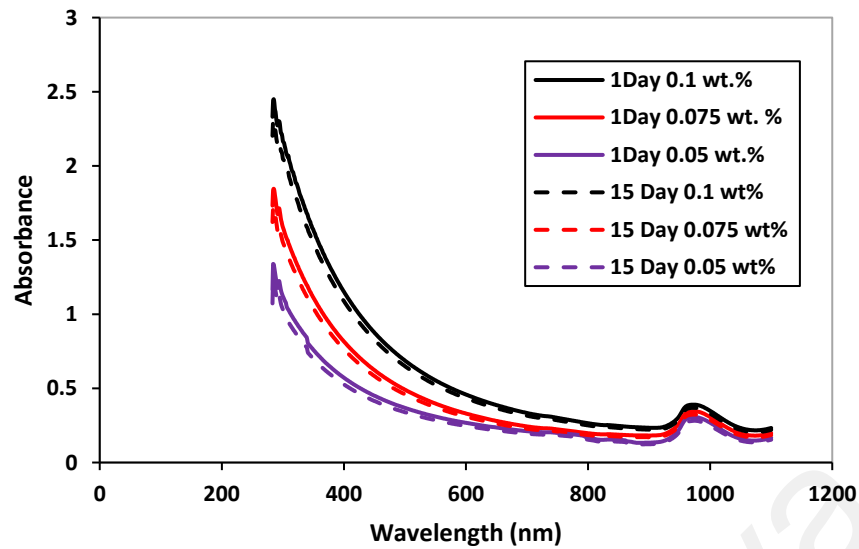
Figure 3-6: Absorption profiles of the Al$_2$O$_3$/DW nanofluid at different concentrations.
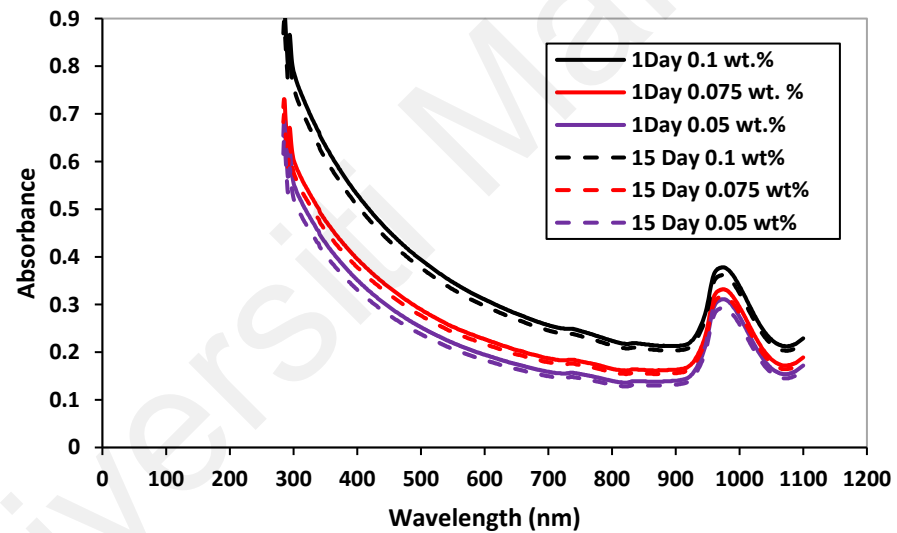
Figure 3-7: Absorption profiles of the SiO$_2$/DW nanofluid at different concentrations.

Figure 3-8 shows the comparison between the Alumina, f-MWCNTs, and Alumina/ f-MWCNTs hybrid nanofluids of 0.1 wt.% concentration diluted in a DW at ratio of 1:10. The profiles of the thee absorbance curves in Figure 3-8 shows that the hybrid sample has the highest beak while the Alumina one has the lowest beak, and there is no beak shifting in the case of the hybrid sample in comparison with the Alumina and the f-MWCNTs which means there is no chemical interaction on the nanoparticle surface due to the mixing of the two nanoparticle types.

Figure 3-9 shows the absorbance profiles of the different concentrations of the f-MWCNTs-Al$_2$O$_3$ nanofluid on the first day and after 15 days of the preparation. The absorbance profiles of the hybrid samples confirmed the effect of the nanofluid concentration on the UV absorbance as in the previous two cases. The absorbance reduction percentages for the f-MWCNTs-Al$_2$O$_3$/DW nanofluid over 15 days were 5.24 %, 6.61 %, and 6.03 % for the concentrations 0.1 wt.%, 0.075 wt.%, and 0.05 wt.%, respectively.

As the absorbance reduction percentages over 15 days for all nanofluid samples were less than 10%, all samples were suitable to conduct the experiments and Confidence in the results.
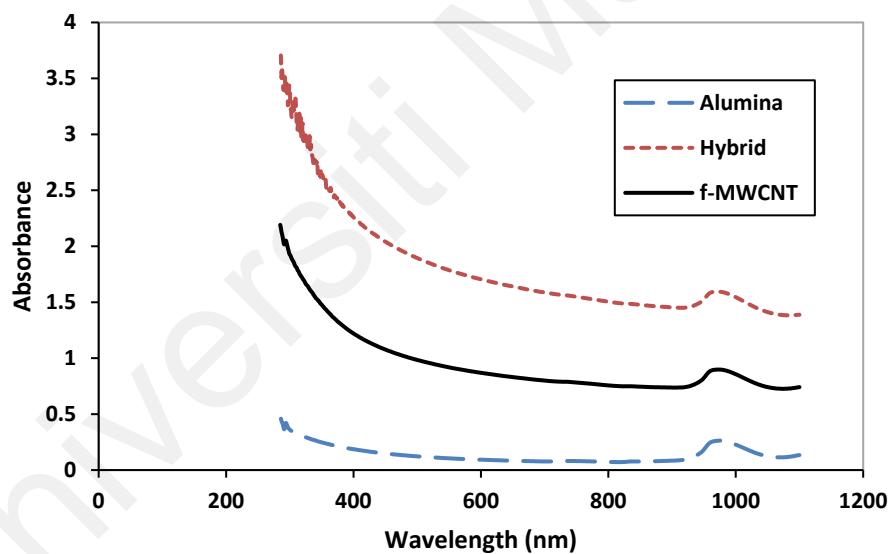
Figure 3-8: Absorption profiles of f-MWCNTs, Al$_2$O$_3$, and hybrid nanofluids of 0.1 wt.% concentration diluted with 10:1.
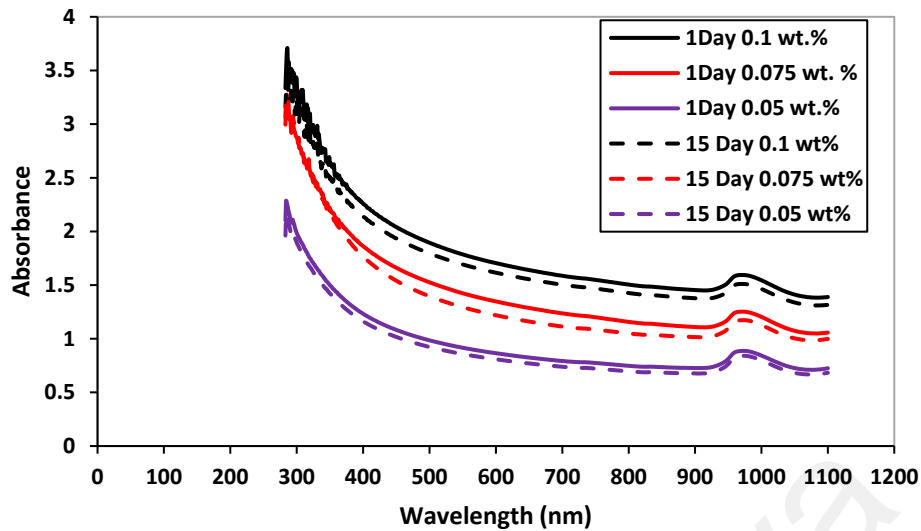
Figure 3-9: Absorption profiles the hybrid nanofluid at different concentration diluted with 10:1.

3.3   Thermophysical properties of nanofluids

3.3.1   Thermal conductivity

Evaluation of thermal conductivity for all the samples was done experimentally using the Decagon Devices KD2 thermal properties analyzer (KD2 Pro, Decagon Devices, Inc., USA) which depends on the transient hot-wire technique. The KD2 pro probe is very sensitive to any convective current in the measurement of medium and the positioning of the probe, where it must be vertical without any deviation to give accurate readings. The vertical alignment and the temperature of the samples were adjusted by a simple setup built for that purpose. A jacketed beaker was connected to a chilled water bath to control the temperature and provide an isothermal environment to the sample. The vertical alignment of the probe was adjusted by using a rubber stopper for the jacketed beaker, as shown in Figure 3-10 (a), and the fixation of the sample tube with the rubber stopper is shown in Figure 3-10 (b).

(a)   (b)
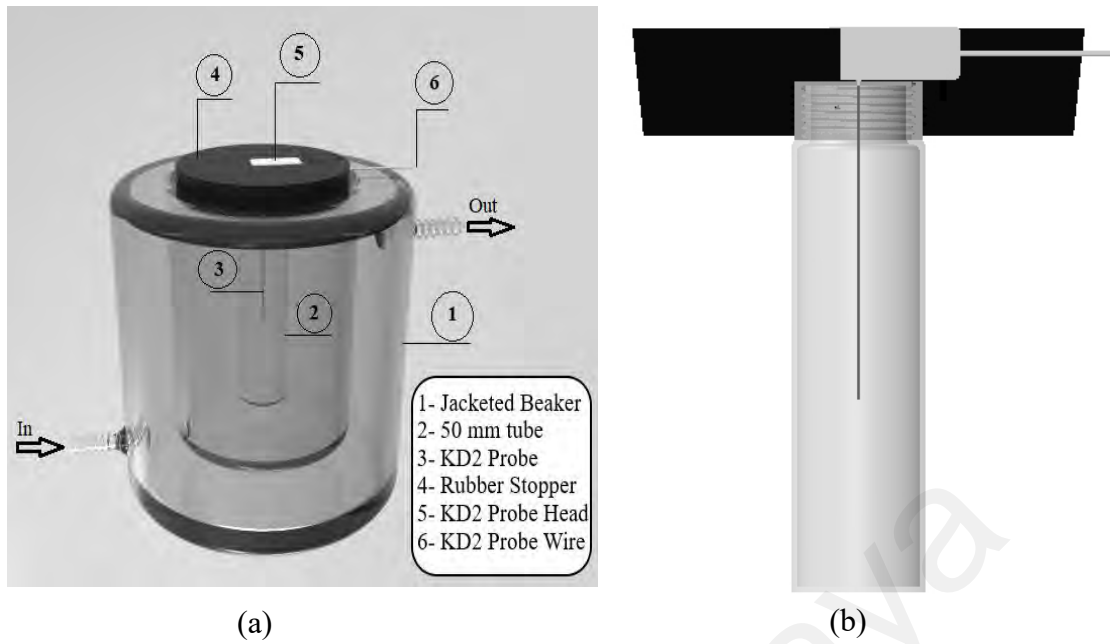
Figure 3-10: 3-D drawing of the setup components used with the KD2 thermal properties analyzer: (a) the whole jacketed backer setup, (b) the 50 mm sample tube, and the KD2 probe head with the rubber stopper.

Evaluation of thermal conductivity for different samples was conducted at a temperature range between 20 °C and 40 °C, where the KD2 accuracy has the highest value in this range according to the manufacturer guidelines and as recorded by Mehrali et al. (2014). Measurement of thermal conductivity was done by adjusting the temperature of the chilled water bath at a specific value. A thirty min at least should be passed to reach the steady-state conditions and ensured that the sample temperature was the same as its environment, and the data recorded were taken as the average value of four measurements evaluated at each temperature.

3.3.2   Density

The samples' density was evaluated experimentally using the Anton Paar density meter (DMA™ 1001, Serial number: 82542702, Software version: 1.0.0). The data taken by the density meter was validated by comparing the DW density with those recorded in the standard tables of the thermophysical properties of water offered by NIST at the same temperatures of the density meter readings.

3.3.3   Specific heat

In the current study, the specific heats for all the samples were calculated theoretically based on the energy balance equation of the nanofluid components. All the nanofluids were considered ideal solutions, where the nanofluid volume equals the sum of its components. Therefore, the energy balance equation was applied as stated by equations (3-5) to (3-7).

$$m_{nf}C_{p,nf} = \sum_{i=1}^{n} m_{Pi} Cp_i + m_{bf}Cp_{bf}, m_b = m_{nf} - m_{p_T} \tag{3-5}$$

$$C_{p,nf} = \sum_{i=1}^{n} C_i Cp_i + (1 - C)Cp_{bf} \tag{3-6}$$

$$\therefore C_{p,nf} = C \sum_{i=1}^{n} \lambda_i Cp_i + (1 - C)Cp_{bf} \tag{3-7}$$

Equation (3-7) was applied to calculate the specific heat of a single nanofluid used in the current study such as Al_2O_3/DW and SiO_2/DW and for the hybrid nanofluid Al_2O_3-fMWCNTs/DW where, λ_i equals 0.6 and 0.4 for Al_2O_3 and f-MWCNTs, respectively.

3.3.4   Viscosity

Fluid viscosity refers to the resistance of fluid flow, which means the higher viscosity, the higher force of flow, and the shearing stress, which increases the pressure drop and fluid pumping power. Figure 3-11 shows the main differences between the Newtonian and the non-Newtonian fluids. The Newtonian fluids are ideal fluids, where the shearing stress is directly proportional to the rate of shearing strain, and the constant slope value of the straight line represents the viscosity. The second type is the shear-thinning fluids, where the viscosity decreases when shearing stress increases. Moreover, the shear thickening fluids, where the viscosity increases when shearing stress increases. As most of the colloids are non-Newtonian fluids, it is essential to investigate if the nanofluids are

Newtonian or not because Newtonian fluids are more suitable for heat transfer applications and can be treated as a single-phase fluid.
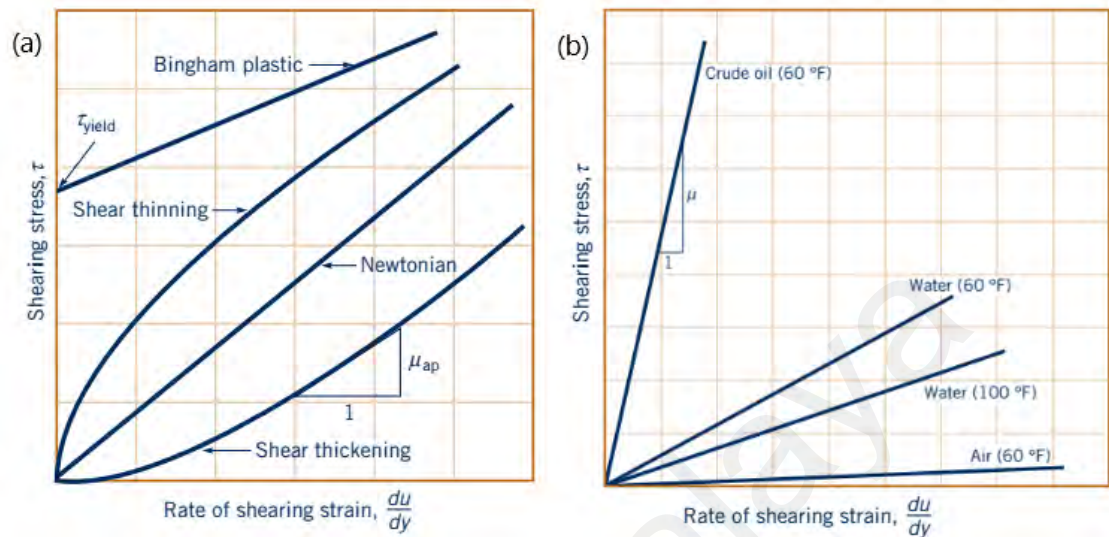
Figure 3-11: A picture showing the viscosity profile (a) of Newtonian and non-Newtonian fluids, (b) different Newtonian fluids (Munson, 2013).

The viscosity of all the samples in the current study was evaluated experimentally using Anton Paar rotational rheometer (Physica MCR 301) within a temperature range of 20-60 °C. The Rheometer was validated by comparing the measured viscosity of the DW with those recorded in the standard table of NIST for the same temperature range.

3.4   Experimental setup and the flow loop description

Figure 3-12 shows the schematic drawing of the test rig used in the current study demonstrated in Figure 3-14. The experimental test rig consists of the main flow loop with the bypass line. It contains flow controlling valves, Araki EX-70R magnetic pump of maximum capacity 14 L/min and zero discharge head of 6.8 m, pressure gage, Bürkert Contromatic SE 32 inline paddle wheel flowmeter, 10 L capacity jacketed reservoir tank, drain line, two parallel test sections with different geometries, and a set of hand-operated gate valves that used to switch the flow between test sections. A 2.2 kW capacity chiller or refrigerated bath circulator (DAIHAN-brand, WCR- P30) was used to control the temperature of the water flowing through the jacketed space of the nanofluid tank. A

pressure transducer (PX154-025DI made by OMEGA) of accuracy ±0.75% was used to measure the pressure drop through the test section. A digital data logger (GRAPHTECH midi logger GL 220) was connected to five k-type thermocouples of accuracy ± 0.1 º C in each test section. The thermocouples were inserted into thermocouple sleeves to measure the surface temperature of both test sections.
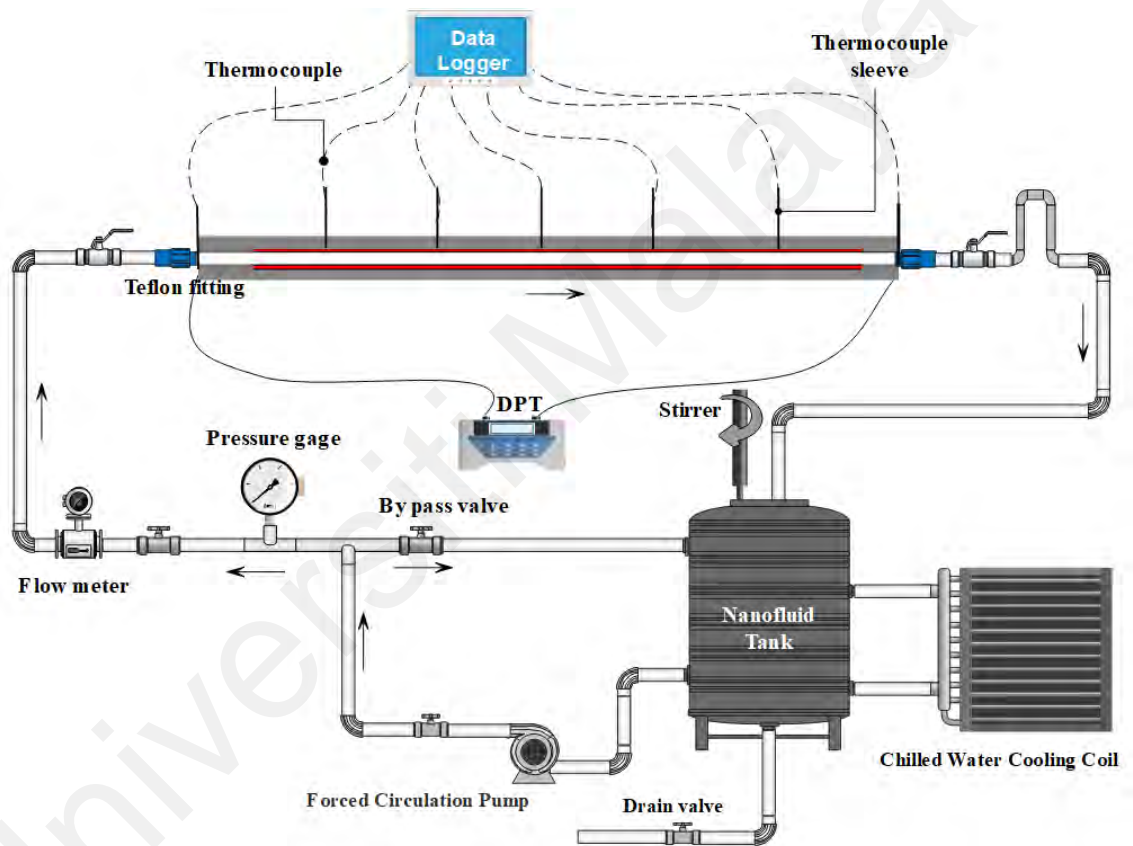
Figure 3-12: Schematic drawing for the experimental test rig with horizontal straight pipe for nanofluid performance studies.
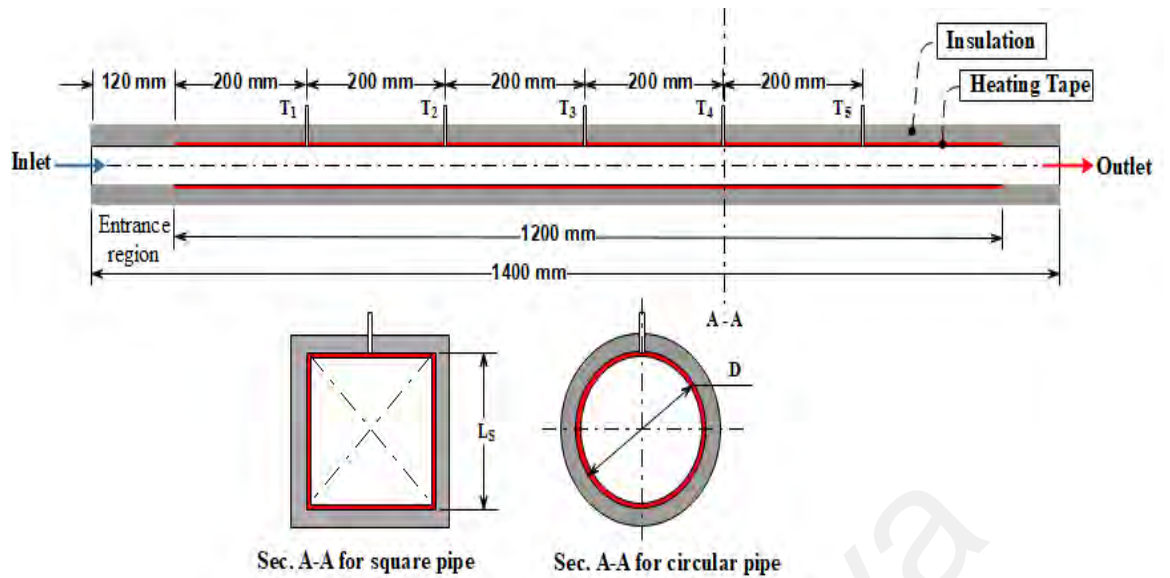
Figure 3-13: Sectional view for the test sections of circular and square cross sections.

Figure 3-14: A photo showing the test rig in the laboratory.

Figure 3-13 shows the detailed drawing and the different sectional views of both test

sections fixed parallel in the test rig, as shown in Figure 3-14. The test sections' entrance

region was 120 mm long to confirm a fully developed flow through the heated section. Both pipes were straight stainless-steel of outer diameter 12 ± 0.1 mm and had the same inside hydraulic diameter of 10 mm. One pipe with a circular cross-section and the second with a square cross-section, and both the test sections were 1400 mm in length. Each pipe has five equally spaced thermocouples on its surface and two RTD sensors (PT 100) to measure the bulk temperatures of the flow at the inlet and outlet.

The heated section was wrapped carefully with an electrical tape heating element of 900 W maximum power capacity to give a uniform heat flux along the circumferential area. The input electrical power was controlled by QPS VT2-1 variable voltage transformer. A bright aluminum foil-covered glass wool of thick layer was used as an insulation to minimize the heat loss from the heater to the surrounding either by convection or radiation. The test sections were specially built to retard the axial heat flow along the axial flow direction by introducing Teflon fittings at both ends.

The test rig power was controlled by the central power unit, which contained all the power switches for the heater, the paddle, the flowmeter, the DPT, and the pump. It also has a data logger system connected to the RTD sensors at the inlet, the outlet, and the nanofluid tank. In addition, a speed regulating inverter to control the pump speed helped to get different pump flow rates.

3.5   Experimental procedure and data analysis

Before starting the experimental run, the fluid velocity was calculated based on the designed value of Re numbers and hence the volume flow rate based on the test section geometry. The valve sets were first adjusted according to the selected test section. The main power switch was turned on to connect the power to all the test rig components. Then, the pump was turned on to circulate the fluid through the test loop starting from the nanofluid tank. After a while, the heater was switched on. Its power was controlled by

adjusting the input voltage using the voltage transformer. The heat added to both the test sections was adjusted at 435 W for all the experimental runs. The inlet temperature was adjusted at the designed value by controlling the chilled water temperature. The flow rate was adjusted by controlling the gate valve before the flowmeter. After reaching steady-state conditions, the temperature and pressure readings were registered and analyzed in a spread sheet. For each flow rate, the temperature readings were taken at least four times with 10 min intervals after reaching the steady-state conditions, and then the average value of all readings was considered for each thermocouple. The Wilson plot method was then applied to calibrate the thermocouple readings and calculate the inner wall temperature of the test sections, as discussed in detail in Appendix A.

After completion of each run, all the fluid was drained completely. Then, the test rig was flushed nicely by flowing water that contains some chemicals (Decon 90) to ensure no nanoparticles remaining inside the test rig.

3.6 Numerical study

In this part, a numerical evaluation for heat transfer and pressure drop performance of all nanofluids was conducted to compare with and verify the experimental results obtained under the same flow conditions. The numerical investigation was conducted for three different pipe geometries of the same hydraulic diameter and same flow conditions. In addition to the circular and square cross-sectional pipes studied experimentally, a circular annular pipe with various vertical eccentricities was considered in this numerical study. The purposes of the numerical study are:

1. To create an experimentally validated model that can help in saving time and effort for any future work.

2. To investigate the thermal performance of nanofluids in different tube geometries that are not available for experimental investigation.

3. To validate the single-phase approach of nanofluids modeling with the experimental results.

3.6.1 Governing equations of numerical models

The single-phase approach was accepted in modeling nanofluid flow, and this conclusion was mentioned by many researchers (Pak & Cho, 1998; Xuan & Roetzel, 2000). Therefore, the temperature and velocity field for the nanoparticles was considered the same as the base fluid, and the effective properties of the nanofluids were used to solve the continuity, momentum, and energy equations.

As all nanofluids in the current study were considered as single-phase fluids of constant thermos-physical properties evaluated at the inlet temperature, the conservation equations of the forced turbulent flow under steady-state conditions for a 3-D physical domain are as follows:

Continuity equation:

$$\nabla . \vec{V} = 0.0$$

(3-8)

Momentum equation:

$$\vec{V}(\nabla . \vec{V}) = \frac{1}{\rho}\left[-\nabla P + \mu \nabla^2 \vec{V} + \rho \vec{g}\right]$$

(3-9)

Energy equation:

$$(\nabla . \vec{V})T = \alpha_{th} \nabla^2 T$$

(3-10)

3.6.2 Computational domains and meshing

The physical model and meshing of 3-D thin-walled horizontal pipes of circular cross-sections and square cross-sections are shown in Figure 3-15 and Figure 3-16, respectively. The hydraulic diameter of both the pipes was 10 mm, and the outer surfaces of both the pipes were considered as heated surfaces of the same length as in the experimental test

section. In the modeling process, both pipes were considered solid pipes with uniform constant heat flux on their walls, and the heat transferred to the fluid flowing inside the pipes in the directions shown in Figure 3-15 and Figure 3-16.

Figure 3-17 shows the physical model and the computational domain of 3-D horizontal annulus of length L formed between two eccentric pipes of circular cross-sections. The inner and outer radii were Ri and Ro, respectively. The distance "e" represents the vertical shifting between the centers of the inner and the outer pipes, while the non-dimensional eccentricity "e*" was calculated by dividing "e" by the difference between the outer and the inner radius. In the current model, the inner pipe was considered a solid pipe with a uniform constant heat flux on its surface, while the outer surface of the outer pipe was insulated entirely. Therefore, the heat was transferred only from the inner pipe wall to the fluid flowing in the annular space as shown in Figure 3-17. The annular pipe has a hydraulic diameter of 10 mm, where the inner pipe diameter was 10 mm, and the diameter ratio between the outer and inner pipe was 2. Its length was 1.2 m to ensure the fully developed turbulent flow at the outlet. The eccentricities considered in the current study were 0.1, 0.2, 0.3, 0.4, 0.5, and 0.6 plus the concentric case of 0.0 eccentricity.

To solve the governing equations within the physical model, a hexahedral mesh was generated for the three physical models, the circular, square, and annular, using the meshing tool in ANSYS-Fluent software. Figure 3-18 shows the generated mesh for the physical domain of the annular pipe with the nonuniform distribution. The finest cells were adjacent to the wall, and the larger cells were nearer to the centers as in the circular and square mesh because the boundary layers near the walls have sharp characteristics changes due to the turbulence effect.
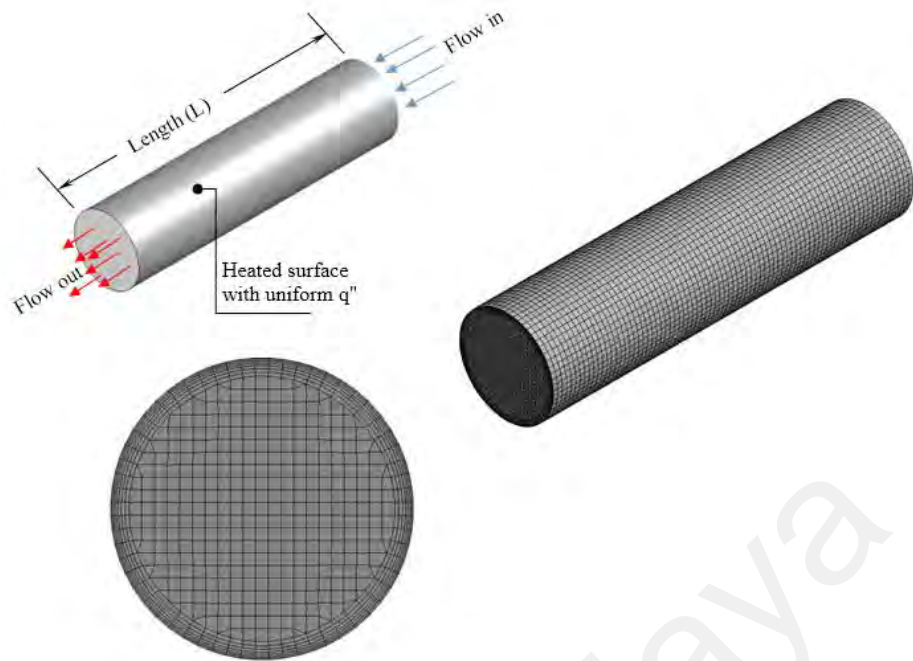
Figure 3-15: Physical model and meshing of the circular tube.
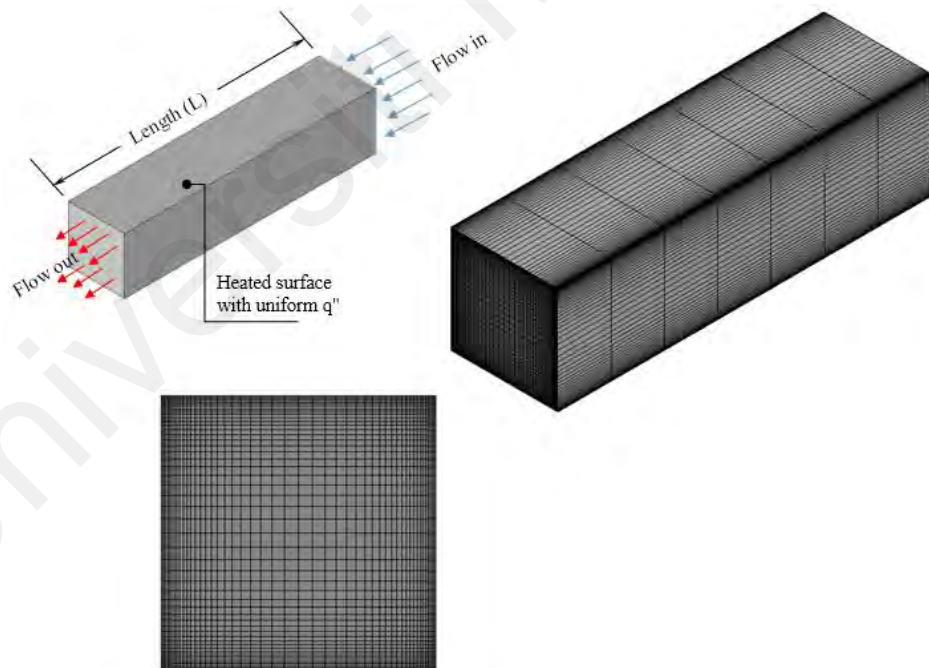

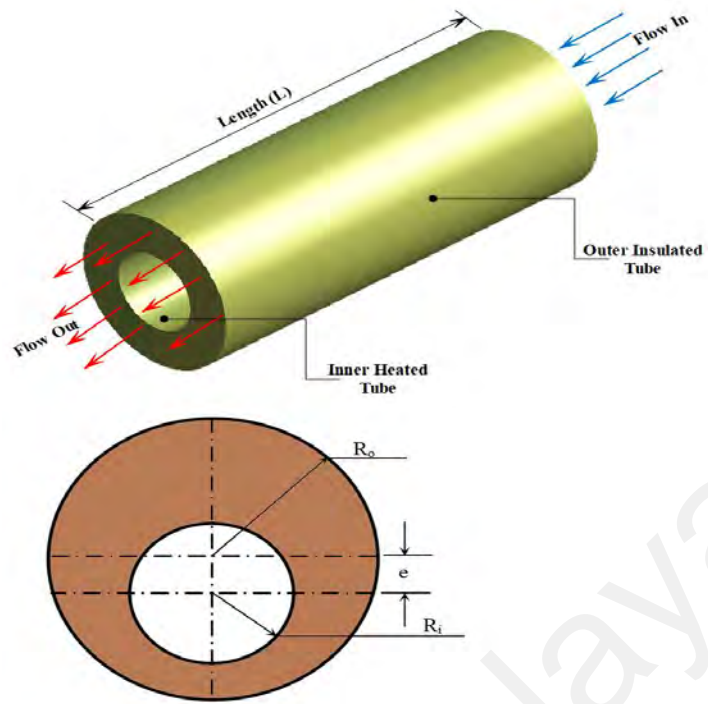
Figure 3-16: Physical model and meshing of the square tube.

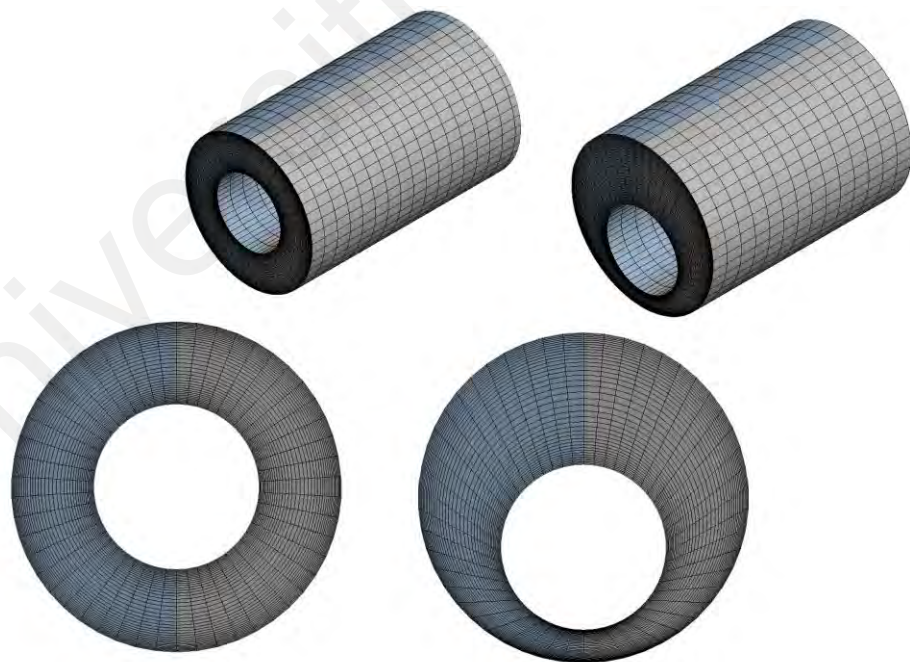**Figure 3-17: Physical model of the annular heat exchanger.**

Figure 3-18: The meshing profile for the concentric and eccentric heat exchanger.

3.6.3 Numerical solution

The turbulent model employed to solve the conservation equations for the three physical models was the slandered (k-ε) turbulent model, and it is available in the ANSYS-Fluent software. It depends on the finite volume approach to convert the governing equations from the partial differential form to a system of discrete algebraic equations. The enhanced wall treatment model was chosen for the near-wall treatment, and the Simple scheme was applied for the pressure velocity coupling. The inlet was defined as a velocity inlet criterion. The outlet type was a pressure outlet with zero gauge pressure. The specification of turbulence for both the inlet and the outlet was selected as "Intensity and hydraulic diameter." The discretization method applied the second-order upwind scheme for momentum, turbulent kinetic energy, turbulent dissipation rate, and energy. The residuals of the numerical solution were taken as $1e^{-6}$ for all the solution parameters. The equations of the (k-ε) turbulent model presented by Launder and Spalding (1972) and their constants are given by equation (3-11).

$$\nabla.(\rho k V) = \nabla.\left[\left(\frac{\mu_t}{\sigma_k}\right)\nabla(k)\right] + G_k - \rho\varepsilon \tag{3-11}$$

The G_k represents the generation of turbulence kinetic energy due to mean velocity gradient and $\mu_t = \rho\,C_\mu{k^2}/{\epsilon}$ is the turbulence viscosity. The Specific Rate of dissipation for kinetic energy, ε, for (k-ε) model is presented by equation (3-12).

$$\nabla.(\rho\varepsilon V) = \nabla.\left[\left(\frac{\mu_t}{\sigma_\varepsilon}\right)\nabla\varepsilon\right] + \frac{\varepsilon}{k}(\,C_{1\varepsilon}G_k + \varepsilon\,C_{2\varepsilon}\rho) \tag{3-12}$$

where, the values of constants C_μ, $C_{1\varepsilon}$, $C_{2\varepsilon}$, σ_k, and σ_ε are 0.09, 1.44, 1.92, 1.0, and 1.3, respectively.

3.6.4   Boundary conditions

The inlet temperature was kept constant at 30 °C for all the nanofluids as in the experimental run. All the thermophysical properties were assumed to be constant through the flow passages and evaluated at the inlet flow temperature as recorded in Table 4-1. The comparison between different flow passage configurations based on the thermal performance should be calculated at the same heat rate since each configuration has a different surface area. The heat flux added to its wall should be calculated according to equation (3-13) to give the same heat rate for all the pipes.

$$q = q''A_s = q_c^{''} (\pi DL) = q_s^{''} (4L_sL) \tag{3-13}$$

The heat fluxes added to the tube walls in the numerical solution are higher than those of the experimental run to enhance the outlet temperature significantly. Therefore, a uniform constant heat flux of 50000 W/m^2 was applied at the wall of the square duct, and according to equation (3-13), a 63661.98 W/m^2 was applied to the wall of the circular. The inner tube of the annular heat exchanger had the dimensions, and the outer tube surface of the annular heat exchanger was considered a completely insulated wall with no heat generation. The range of Reynolds number was selected for all the numerical models as in the experimental work from 6000 to 11000.

3.7   Formulation of pressure drop and heat transfer

The value of the mean velocity through all the cross-sectional pipes was determined based on the Re number value as in equation (3-14):

$$V = \frac{Re\ \mu}{\rho D_h} \tag{3-14}$$

This means that the inlet flow velocity could be different for each nanofluid concentration and could have the same value for the same fluid in all the flow passages

in the current study at different Reynolds numbers. Equation (3-15) shows how to calculate the velocity of nanofluid.

$$V_{nf} = \frac{\rho_{bf}}{\rho_{nf}} \frac{\mu_{nf}}{\mu_{bf}} V_{bf}$$

(3-15)

The pumping power and pressure drop are considered as two essential factors in comparison between the three geometries. The hydraulic pumping power was calculated from equation (3-16), and the volume flow rate was calculated from equation (3-17). Therefore, the volume flow rate could be different and according to the values cross the sectional areas.

$$\dot{W} = \dot{V} \Delta P$$

(3-16)

where, $\dot{W}$ is the hydraulic pumping power in W, $\dot{V}$ is the total volume flow rate in m^3/s, and ΔP is the total pressure drop across the pipe length in Pa.

$$\dot{V} = A_c V$$

(3-17)

$A_c = \frac{\pi D^2}{4}$ for the circular cross-section and $A_c = \pi(R_o^2 - R_i^2)$ for the annular heat exchanger while, for the square cross-section $A_c = L_S^2$.

The pressure drop across the tube length can be evaluated experimentally using the differential pressure transducer (DPT) and numerically by calculating the difference between the average outlet and inlet pressure using the CFD Post module ANSYS-Fluent package. Equation (3-18) shows the factors that affect the pressure drop through any closed conduit (Bergman et al., 2011).

$$\frac{\Delta P}{L} = 2C_f \left(\frac{\rho V^2}{D_h} \right)$$

(3-18)

where, C_f is the friction coefficient or "fanning friction factor," and calculated from equation (3-19)

$$C_f = \frac{\tau_s}{\rho V^2/2} \qquad\qquad (3\text{-}19)$$

where, τ_s is the wall shear stress, V is the average flow velocity, and the friction coefficient $C_f = f/4$ where, f is the friction factor.

Therefore, equation (3-18) can be used to determine the friction coefficient and friction factor of different nanofluids used in the current study where, it depends mainly on the Reynolds number and relative pipe roughness in case of turbulent flow as stated by Petukhov (1970) and Munson (Munson, 2013). If V from equation (3-14) was added to equation (3-18), the pressure drops per unit length in all the conduits can be represented by equation (3-20).

$$\frac{\Delta P}{L} = \frac{Re^2 f}{2 D_h^3}\, \nu.\,\mu \qquad\qquad (3\text{-}20)$$

Equations (3-21) and (3-22) show how to calculate the average convection heat transfer and average Nusselt number, respectively, where, q'' is the total heat flux, T_w is the average temperature of inner wall surface, and T_b is the average bulk temperature of the fluid and it is equal to the mean value of inlet and outlet temperatures.

$$h = \frac{q''}{(T_w - T_b)} = \frac{Nu\, K}{D_h} \qquad\qquad (3\text{-}21)$$

$$Nu = \frac{D_h}{K}\, \frac{q''}{(T_w - T_b)} \qquad\qquad (3\text{-}22)$$

Referring to equation (3-20), the pressure drop per unit length through any pipes could be increased due to using of nanofluids because the increases raise the penalty value of nanofluids in heat transfer applications. So, nanofluid is a mixed blessing weapon as it has one positive face when it enhances the convection heat transfer and a negative face due to pressure drop increases. Therefore, it is crucial to evaluate the performance index of the nanofluid being studied to know if it is economical or not. The performance index is defined as the ratio of positive enhancement (Heat transfer enhancement) to the negative enhancement (pressure drop increment), as shown in equation (3-23).

$$I.P = \frac{h_{nf}/h_{bf}}{\Delta P_{nf}/\Delta P_{bf}} \tag{3-23}$$

As volume flow rate changes due to using nanofluids and hence the pumping power, it will be more accurate in the performance index evaluation if the pumping power is included. Equation (3-24) shows pumping power as a penalty in the performance index evaluation instead of pressure drop.

$$I.P = \frac{h_{nf}/h_{bf}}{\dot{W}_{nf}/\dot{W}_{bf}} \tag{3-24}$$

3.8 Results validation

To validate the results of the current study, the experimental data from the test rig for water run in the circular and square test sections were compared with the numerical results, which validated the experimentally obtained data. The numerical solution of the annular heat exchanger was validated by comparing the data obtained from the models with those obtained from the published empirical correlations at the same range of Reynolds numbers.

3.8.1 Validation of circular and square test sections

One of the most accurate empirical correlations was presented by Gnielinski (1975) to calculate the Nusselt number for the flow through the smooth pipe as given by equation (3-25).

$$Nu = \frac{\left(\frac{f}{8}\right)\left(Re_{D_h}-1000\right)Pr}{1+12.7\sqrt{f/8}\left(Pr^{2/3}-1\right)} \tag{3-25}$$

where, f is calculated according to the correlation of Petukhov (1970) and Blasius' correlation stated by Taler (2016) as shown in the equations (3-26) and (3-27), respectively.

$$f = (0.790 \ln Re_{Dh} - 1.64)^{-2} \tag{3-26}$$

$$f = 0.3164 \, Re_{Dh}^{-0.25} \tag{3-27}$$

Duan et al. (2012) showed that the friction factor f calculated by Blasius correlation should be modified for non-circular cross-section tubes to include the effect of the characteristic geometric parameter. They modified the Blasius friction factor for tubes with square cross-sections to be calculated as in equation (3-28).

$$f = 0.3068 \, Re_{Dh}^{-0.25} \tag{3-28}$$

In the current study, the friction factor in equation (3-25) will be calculated according to equations (3-27) and (3-28) for circular and square pipes, respectively, because the Blasius correlation was more accurate in the Re range of this study.

Dittus and Boelter presented one more empirical correlation introduced in the (Bergman et al., 2011) textbook as in equation (3-29). They can be used to validate the Nusselt number in pipe flow.

$$Nu = 0.023 \, Re^{0.8} Pr^{n} \tag{3-29}$$

where, $n = 0.4$ or 0.3 in the case of heating or cooling, respectively.

The measured pressure drop was validated by comparing it with those obtained by calculation from the equation (3-18), where the friction factor was calculated by Petukhov or Blasius correlation (Taler, 2016).

3.8.2 Validation of annular pipe model

The numerical model of the annular pipe was validated for the concentric case by comparing the Nusselt number and the friction factor for the water run case with those determined from empirical correlations. For the annular pipe geometry, different correlations were used to calculate the Nusselt number and pressure drop for different

ranges of the Reynolds number under the fully developed turbulent flow conditions. Table 3-1 shows the other empirical correlations used to calculate the Nusselt number for annular flow based on the hydraulic diameter of the annulus. At the same time, pressure drop was evaluated by equation (3-18) based on the correlations of the friction factor. In Gnielinski correlation for the Nusselt number, the friction factor f_{ann} *was* calculated as shown in equations (3-30) and (3-31).

$$f_{ann} = (1.8 \log_{10} Re^* - 1.5)^{-2} \tag{3-30}$$

$$Re^* = Re \frac{\left(1 + a^{*2}\right) \ln a^* + \left(1 - a^{*2}\right)}{\left(1 - a^{*2}\right) \ln a^*} \tag{3-31}$$

The factors k_1 and F_{ann} in the Gnielinski correlation were calculated using the equations (3-32) and (3-33), respectively. The parameter a^* is the inner to outer diameter ratio of the annular heat exchanger.

$$k_1 = 1.07 + \frac{900}{Re} - \frac{0.63}{(1 + 10Pr)} \tag{3-32}$$

$$F_{ann} = 0.75 \, a^{*-0.17} \tag{3-33}$$

Table 3-1: Nusselt number correlations for the fully developed turbulent flow through smooth annuli.

Author	Nu_{D_h}	Re range
Gnielinski (2015)	$\dfrac{(f_{ann}/8)Re\,Pr}{k_1 + 12.7\sqrt{f_{ann}/8}(Pr^{2/3}-1)}\left[1 + \left(\dfrac{D_h}{L}\right)^{2/3}\right]F_{ann}\left(\dfrac{Pr}{Pr_w}\right)^{0.11}$	10^4-10^6
Davis (Dirker & Meyer, 2004)	$0.038a^{0.15}(a-1)^{0.2}Re^{0.8}Pr^{1/3}\left(\dfrac{\mu}{\mu_w}\right)^{0.14}$	Not specified
McAdams (1954)	$0.03105a^{0.15}(a-1)^{0.2}Re^{0.8}Pr^{1/3}\left(\dfrac{\mu}{\mu_w}\right)^{0.14}$	Not specified
Weigand et al. (1945)	$0.023a^{0.45}Re^{0.8}Pr^{0.4}\left(\dfrac{\mu}{\mu_w}\right)^{0.14}$	Not specified
Dittuse& Boelter (Bergman et al., 2011)	$0.023Re^{0.8}Pr^{0.4}$	Not specified

CHAPTER 4: RESULTS AND DISCUSSION

4.1　Thermophysical properties of nanofluids

4.1.1　Thermal conductivity

Validation of the data measured by the KD2 thermal properties analyzer was made by comparing the data measured for the water and the standard data recorded in the NIST (National Institute of Standard and Technology) Table for a distilled water which gave an average percentage error of 0.3719 % as shown in Figure 4-1.
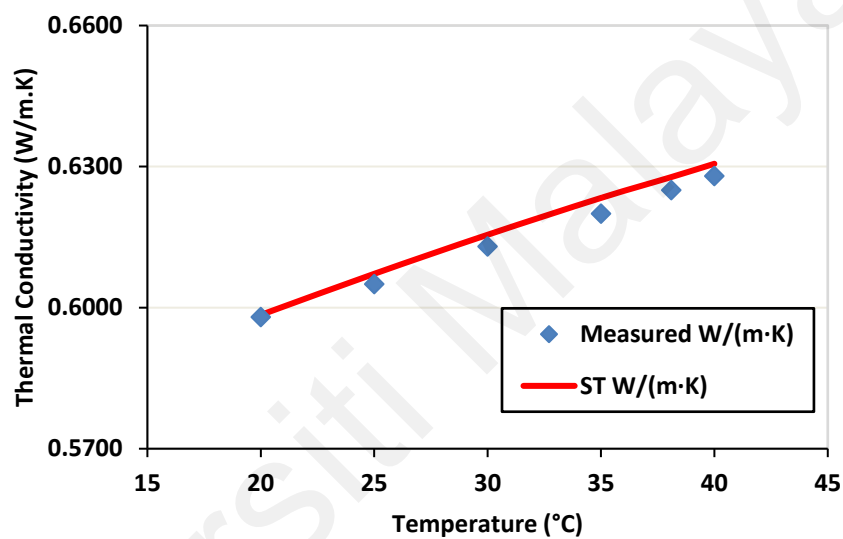

Figure 4-1: Comparing the measured data of DW and the standard data recorded by the NIST.

The variation of thermal conductivity with the temperature of all the samples is shown in Figure 4-2 where, all the nanofluids concentrations showed a significant enhancement comparing to the DW, which can be attributed to the Brownian motion of the nanoparticles as recorded by many researchers (Alawi et al., 2018; Jabbari et al., 2017; Shahsavar & Bahiraei, 2017; Tawfik, 2017). As shown in Figure 4-2, all the nanofluids concentrations in this study show a nonlinear increment when temperature increases, and the thermal conductivity increases when the concentration increases. The thermal conductivity of nanofluids also has the same order as the nanoparticles used to prepare it, which confirms the effect of the suspended solid particles on the thermal conductivity of

nanofluids. The SiO$_2$/DW nanofluid showed the lowest average enhancement for all the nanofluids in the current study, where the concentration 0.05 wt.%, 0.075 wt.%, and 0.1 wt.% showed the average enhancement percentages of 0.788 %, 0.717 %, and 1.075 %, respectively. For Al$_2$O$_3$/DW nanofluid, the concentration of 0.05 wt.%, 0.075 wt.%, and 0.1 wt.% showed the average enhancement percentages of 0.879 %, 1.337 %, and 1.696 %, respectively. The hybrid/DW nanofluid showed the average percentage enhancement of 3.102%, 1.829 %, and 1.158 % for the concentration of 0.1 wt.%, 0.075 wt.%, and 0.05 wt.%, respectively.
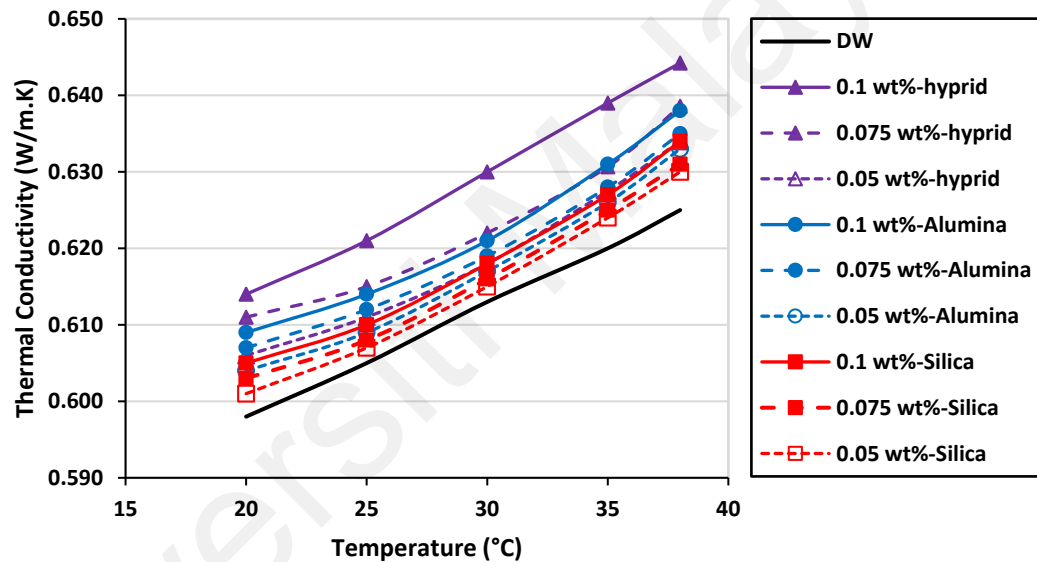

Figure 4-2: Thermal conductivity for all the samples at different temperatures.

4.1.2 Density

Figure 4-3(a) shows the comparison between the measured density of DW by Anton Paar density meter and the standard values in a temperature range from 20 °C to 45 °C, where the average error is 0.056% which means the data collected by that meter is correct for this temperature range. Figure 4-3(b), (c), and (d) show the density profile for Al$_2$O$_3$/DW nanofluid, SiO$_2$/DW nanofluid, and hybrid nanofluid, respectively. The effect of solid particles density on nanofluids density is noticeable. For the same nanofluid concentration, the higher the nanoparticle density, the higher the nanofluid density. The

maximum increment was observed for the Al_2O_3/DW nanofluid density, where the average percentage increments were 0.095%, 0.062%, and 0.031% for the concentrations of 0.1 wt.%, 0.075 wt.%, and 0.05 wt.%, respectively. Then, the hybrid nanofluid density showing an average percentage increment of 0.084%, 0.042%, and 0.018% for the concentrations 0.1 wt.%, 0.075 wt.%, and 0.05 wt.%, respectively. Finally, the SiO_2/DW nanofluid with an average percentage increment of 0.061%, 0.036%, and 0.014% for the concentrations of 0.1 wt.%, 0.075 wt.%, and 0.05 wt.%, respectively.
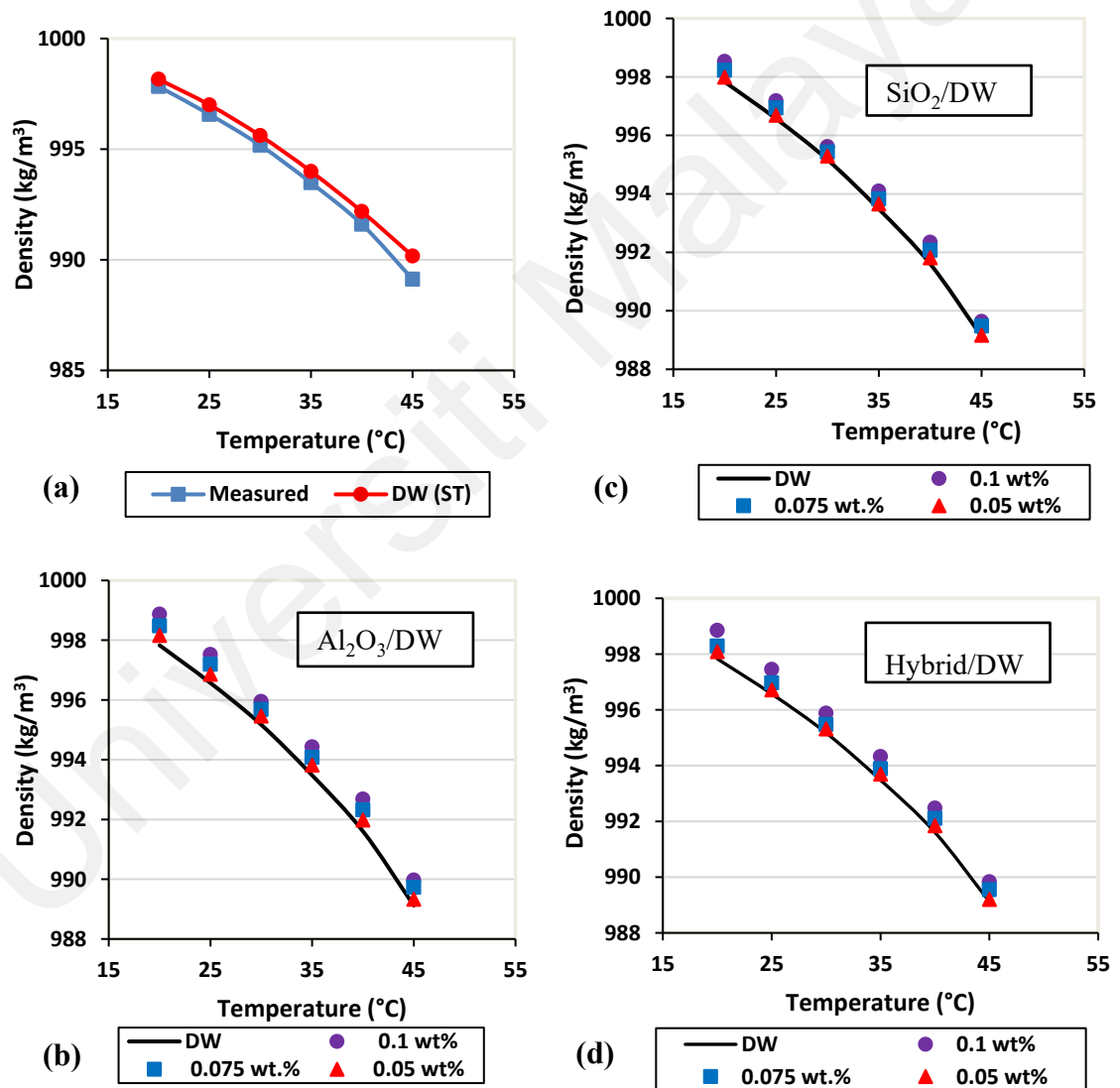

Figure 4-3: The density profile of the DW and different nanofluid concentrations: (a) The measured and the standard values for DW, (b) DW and Al_2O_3 nanofluid, (c) DW and SiO_2 nanofluid, and (d) DW and hybrid nanofluid.

4.1.3   Specific heat

Figures 4-4, 4-5, and 4-6 show the effect of temperature on the specific heat of the DW comparing to the data of the Al_2O_3/DW, SiO_2/DW, and the hybrid nanofluid Al_2O_3-fMWCNT/DW, respectively. The specific heat results show that increasing the nanofluid concentration reduced the specific heat of the base fluid, and the order of nanofluids specific heat for the same concentration is the same as the specific heat of the solid particle. So, Al_2O_3/DW shows the highest specific heat than SiO_2/DW and Al_2O_3-fMWCNT/DW.
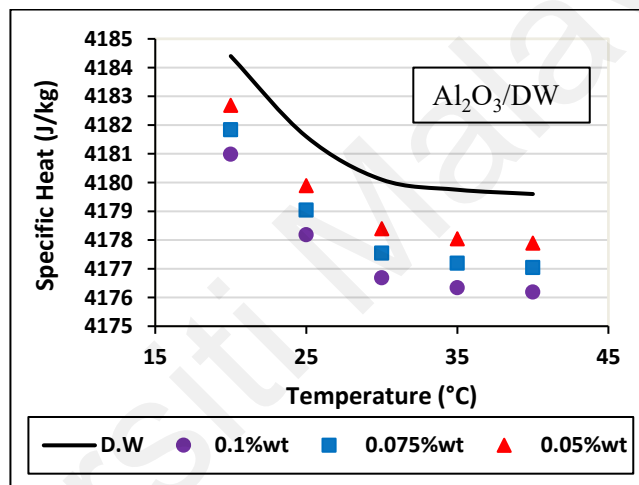

Figure 4-4: Specific Heat of different Alumina nanofluid concentrations compared to DW.
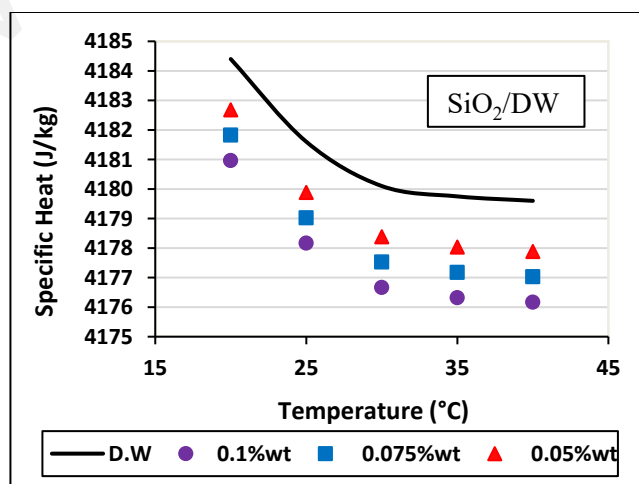

Figure 4-5: Specific Heat of different Silica nanofluid concentrations compared to DW.
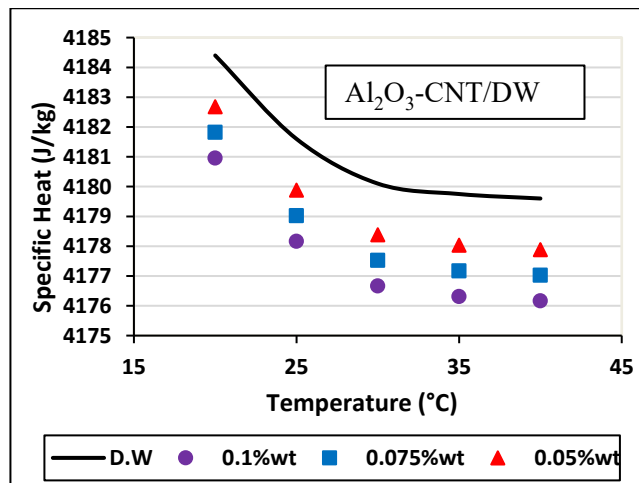
Figure 4-6: Specific heat of different hybrid nanofluid concentrations compared to DW.

The average percentage reduction in specific heat of Al_2O_3/DW nanofluid are 0.0817%, 0.0612%, and 0.0408% for the concentrations of 0.1 wt.%, 0.075 wt.%, and 0.05 wt.%, respectively. The average percentage reduction in the specific heat of Al_2O_3-f-MWCNT/DW nanofluid are 0.0823%, 0.0617%, and 0.0411% for the concentrations of 0.1 wt.%, 0.075 wt.%, and 0.05 wt.%, respectively. These results indicate that the specific heat of fMWCNT decreases when mixing it with Al_2O_3 compared to Al_2O_3 at the same temperature. The average percentage reduction in specific heat of SiO_2/DW nanofluid are 0.0822%, 0.0616%, and 0.0410% for the concentrations of 0.1 wt.%, 0.075 wt.%, and 0.05 wt.%, respectively.

4.1.4 Viscosity

Figure 4-7 shows that the measured viscosity of DW by the Anton Paar rheometer is in good agreement with the standard values in the temperature range 20-60 °C, where the average percentage error is 3.806%.
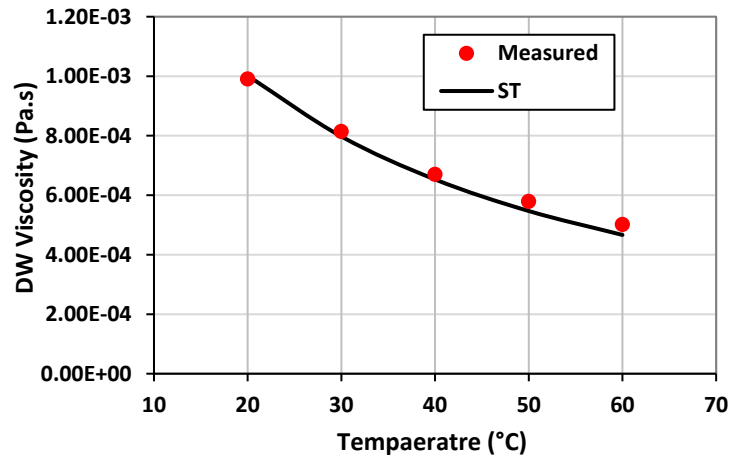
Figure 4-7: The measured viscosity of DW in comparison with the standard values.

The relation between shear stress and shear strain rate for all the nanofluid samples at different temperatures in the current study is represented in Figures 4-8 to 4-16. A curve fitting process was made to know the linearization data for each curve, where the R squared parameter for each straight line nearly equals unity. Therefore, the stress-strain relation for all nanofluid samples is linear and passes through the origin, confirming that all nanofluid samples are Newtonian fluids. The stress-strain curves for all nanofluid samples in Figures 4-8 to 4-16 showing that the temperature affects the nanofluid viscosity, where the line slope (viscosity) decreases when the temperature increases.

Figure 4-8: Shear stress variation with the shear strain rate at different temperatures for 0.05 wt.% Al$_2$O$_3$/DW nanofluid.

Figure 4-9: Shear stress variation with the shear strain rate at different temperatures for 0.075 wt.% Al$_2$O$_3$/DW nanofluid.

Figure 4-10: Shear stress variation with the shear strain rate at different temperatures for 0.1 wt.% Al$_2$O$_3$/DW nanofluid.

Figure 4-11: Shear stress variation with the shear strain rate at different temperatures for 0.05 wt.% SiO$_2$/DW nanofluid.
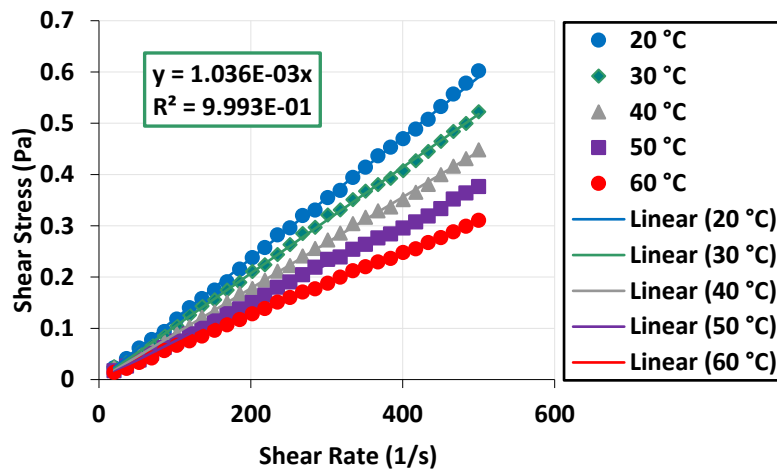
Figure 4-12: Shear stress variation with the shear strain rate at different temperatures for 0.075 wt.% SiO₂/DW nanofluid.
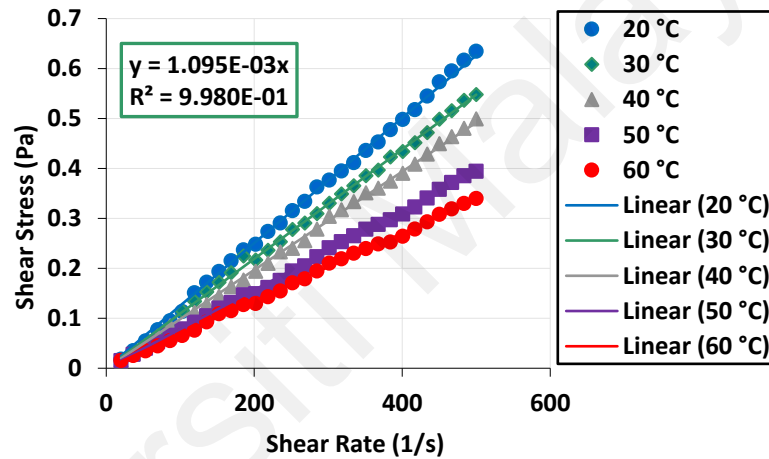
Figure 4-13: Shear stress variation with the shear strain rate at different temperatures for 0.1 wt.% SiO₂/DW nanofluid.
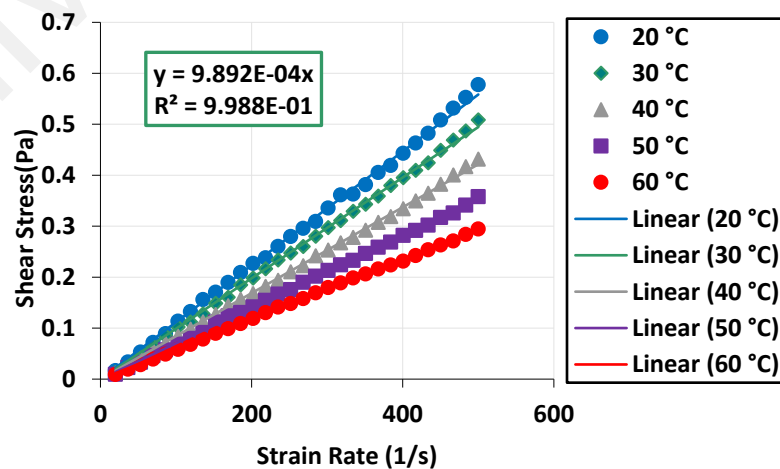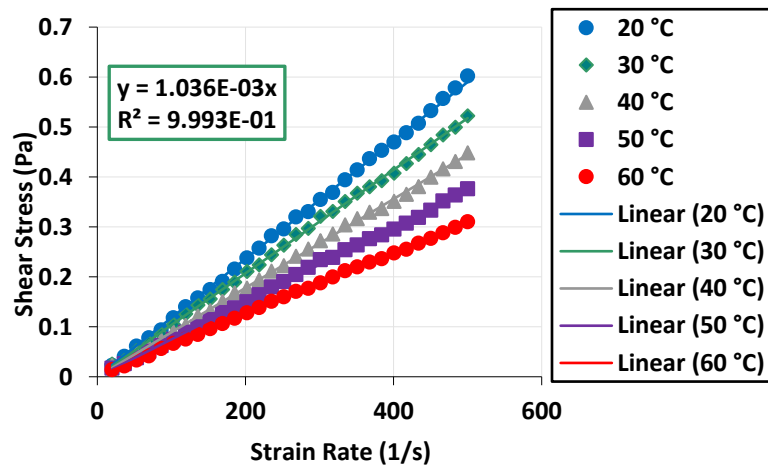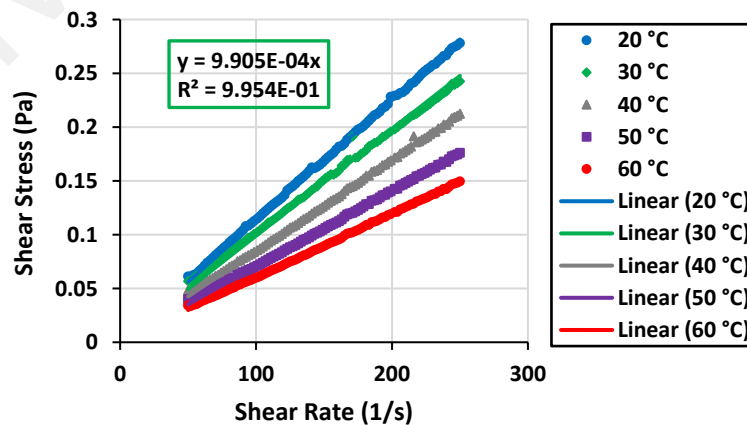

Figure 4-14: Shear stress variation with the shear strain rate at different temperatures for 0.05 wt.% hybrid nanofluid.
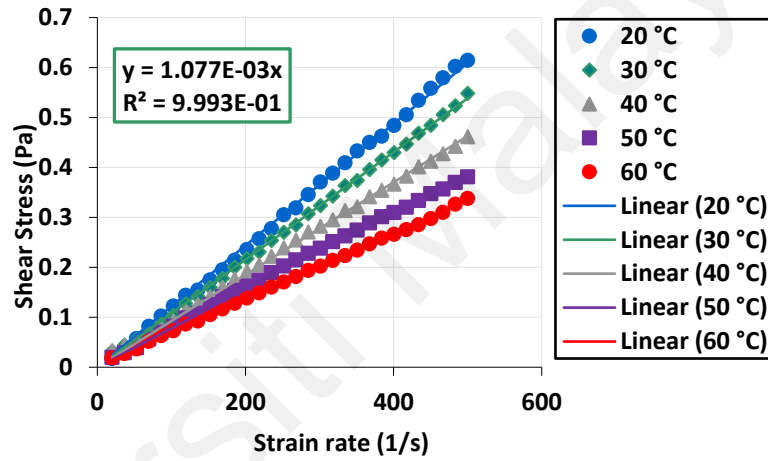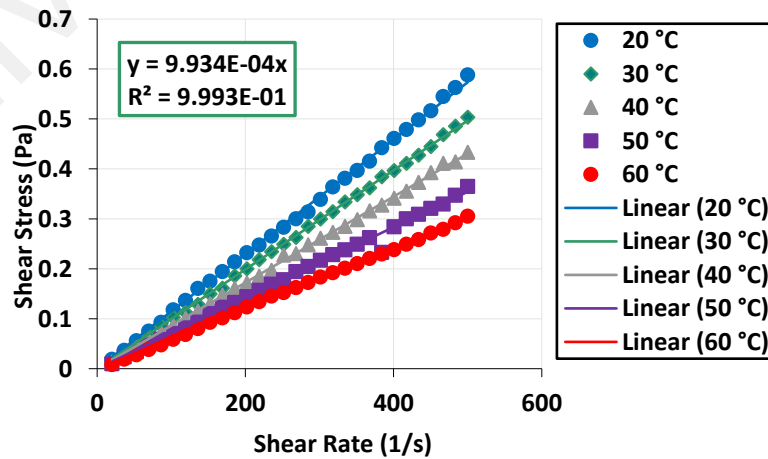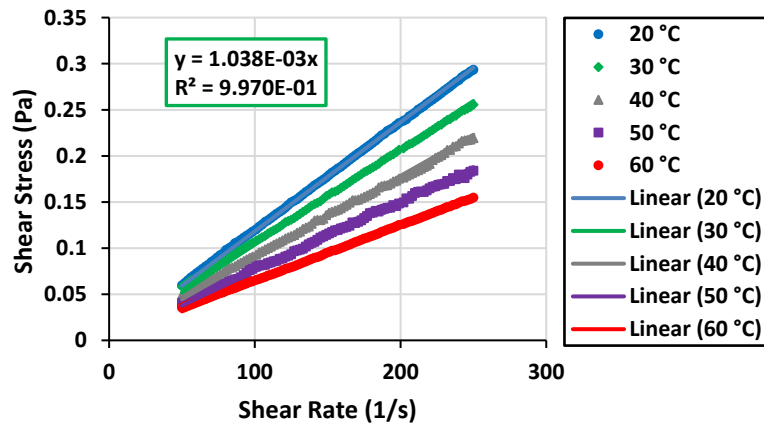
Figure 4-15: Shear stress variation with the shear strain rate at different temperatures for 0.075 wt.% hybrid nanofluid.
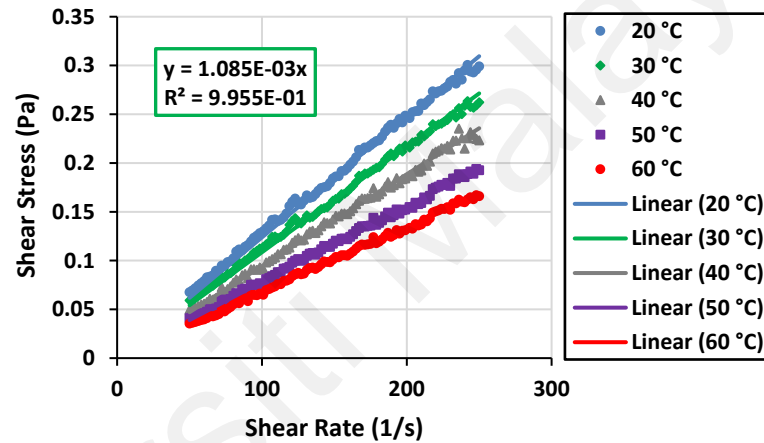
Figure 4-16: Shear stress variation with the shear strain rate at different temperatures for 0.1 wt.% hybrid nanofluid.

It can be seen that viscosity depends on the nanofluid concentration, temperature, and nanoparticle type. For nanofluid concentration, the viscosity increases at a higher concentration, where it can be attributed to the increase of nanoparticles agglomeration within the suspension when the concentration increases. Consequently, the internal shear stress in the nanofluid will be increased due to the higher force needed to dissipate the solid particles in the suspension, leading to increased viscosity.

The viscosity is a nanoparticle-dependent phenomenon at the same wt.% concentration, where the viscosity of SiO_2/DW is higher than that of hybrid and Al_2O_3/DW, respectively. Thess results can be attributed to the difference in nanoparticles

density, where the low density gives a high volume for the same mass. Therefore, for lower density nanoparticles and hence nanofluid, the suspended nanoparticles have a higher volume and higher agglomeration within the suspension, leading to the similar results of the nanofluid concentration-effect mentioned in the previous paragraph.

Comparing to DW, the average percentage increasing in viscosity of Al_2O_3/DW nanofluid are 32.35%, 26.54%, and 19.63% for the concentrations of 0.1 wt.%, 0.075 wt.%, and 0.05 wt.%, respectively. The average percentage increasing in viscosity of Al_2O_3-fMWCNT/DW nanofluid are 33.62%, 27.06%, and 20.75% for the concentrations of 0.1 wt.%, 0.075 wt.%, and 0.05 wt.%, respectively. The average percentage increasing in viscosity of SiO_2/DW nanofluid are 34.54%, 28.05%, and 21.77% for the concentrations 0.1 wt.%, 0.075 wt.%, and 0.05 wt.%, respectively.

Table 4-1 shows the thermophysical properties of all the nanofluids in the current study at a bulk temperature of 30 °C, which is designed to be the inlet flow temperature in the present study for the experimental and the numerical work.

Table 4-1: Thermophysical properties of all the nanofluids at 30 °C.

Nanofluid	$\mu \times 10^4$ (Pa.s)	ρ (kg/m³)	K (W/m.K)	C_P (J/kg.K)	Pr	$\alpha_{th} \times 10^7$ (m²/s)	$\nu \times 10^7$ (m²/s)
D.W	8.141	995.173	0.613	4180.100	5.551	1.474	8.180
Al_2O_3 (0.1%)	10.77	995.950	0.621	4176.685	7.241	1.493	10.81
Al_2O_3 (0.075%)	10.36	995.680	0.619	4177.539	6.989	1.488	10.40
Al_2O_3 (0.05%)	9.89	995.460	0.617	4178.392	6.699	1.483	9.937
SiO_2 (0.1%)	10.95	995.611	0.618	4176.665	7.4	1.486	11.00
SiO_2 (0.075%)	10.36	995.426	0.616	4177.524	7.071	1.481	10.47
SiO_2 (0.05%)	9.93	995.291	0.615	4178.382	6.749	1.479	9.98
Al_2O_3-CNT (0.1%)	10.85	995.876	0.630	4176.662	7.194	1.515	10.90
Al_2O_3-CNT (0.075%)	10.38	995.475	0.622	4177.521	6.972	1.496	10.43
Al_2O_3-CNT (0.05%)	9.91	995.315	0.618	4178.381	6.697	1.486	9.951

4.2 Validation of the experimental test rig

The validation curves of the experimental results for the circular test sections based on the DW experimental run are shown in Figure 4-17 and Figure 4-18. Figure 4-17 compares the Nusselt number obtained experimentally with those obtained from the empirical correlations of Dittus & Boelter and Gnielinski. The experimental Nu number shows an average error of 5.78% and 8.27% compared to the empirical correlations of Dittus & Boelter and Gnielinski, respectively. Figure 4-18 shows the measured $\Delta P/L$ in good agreement with the values obtained from the equations of Petukhov and Blasius with average errors of 3.81% and 9.63%, respectively.

Figure 4-19 and Figure 4-20 show the validation of the square test section based on Nu number and pressure drop per unit length, respectively. The data obtained from the square test section shows the experimental Nusselt number in good agreement with those obtained from the Gnielinski and Dittus & Boelter correlations, where the average errors are 7.28% and 9.75% in comparison with the data from Gnielinski and Dittus & Boelter correlations, respectively. The measured $\Delta P/L$ in the square test section shows average errors of 6.01% and 9.59% compared to the Petukhov and Blasius equation, respectively.

A comparative assessment was made between the input and output energy at different values of Re number to ensure that the percentage of heat loss to the surroundings from both the circular and square pipes has no significant effects on the heat transfer calculations. The conventional energy balance equation $(q = I \Delta V = \rho \dot{V} C_p (T_o - T_{in}))$ showed reasonable average losses of 3.76% and 4.23% for the circular and square pipe, respectively, which would not affect the calculation of heat transfer parameters.
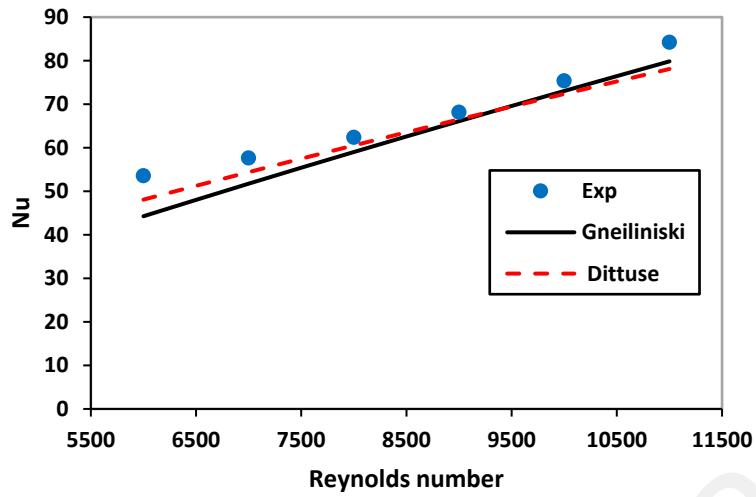
Figure 4-17: Average Nusselt number of DW for the circular pipe.
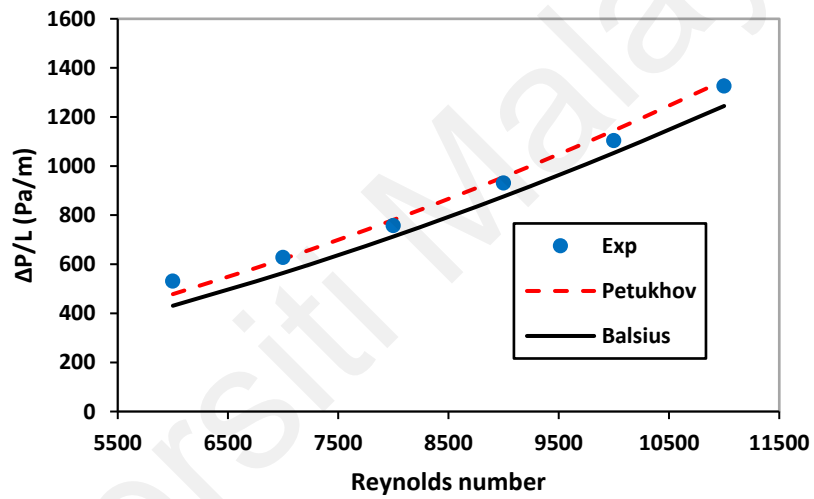
Figure 4-18: Pressure drop per unit length of DW for the circular pipe.
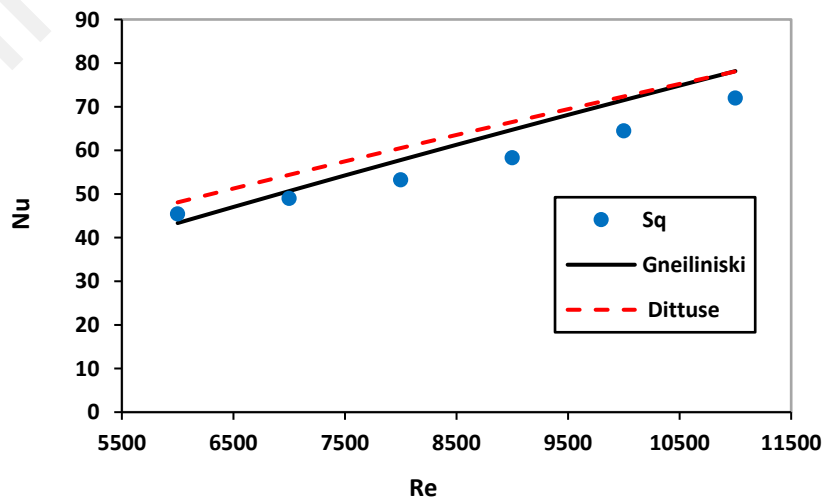
Figure 4-19: Average Nusselt Number of DW for the square pipe.
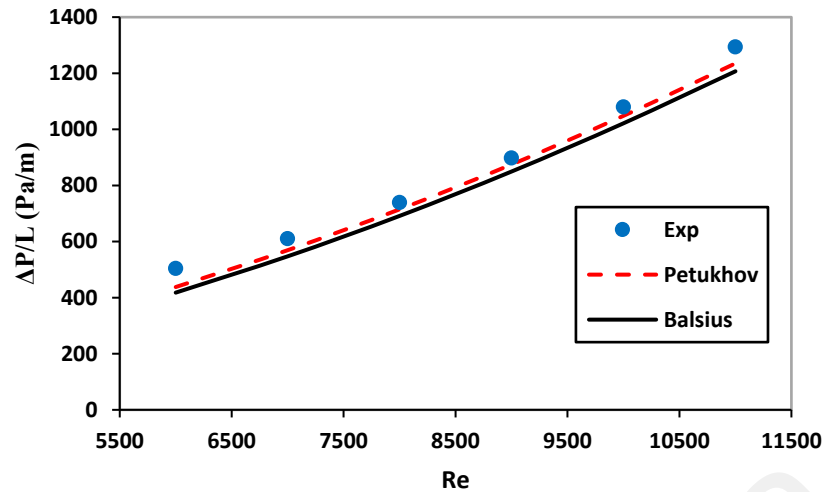
Figure 4-20: Pressure drop per unit length of DW for the square pipe.

One more comparison between the Nusselt number and friction factor obtained experimentally from both the test sections was applied to validate the test rig. In the fully developed forced turbulent flow, the average convection heat transfer coefficient should be lower in a square cross-section pipe than the circular one. This difference can be attributed to the nonuniformity of the convection heat transfer coefficient around the periphery, approaching zero along with the corners of the square pipe (Bergman et al., 2011; Deissler, 1959). Moreover, the friction factor obtained from the data of the square test section is a little bit lower than those of the circular tube, which is consistent with the results obtained by other researchers (Bisht et al., 2014; Deissler, 1959).

Referring to Figure 4-21 and Figure 4-22, the data obtained by the current study are compatible with the basic knowledge of heat transfer and friction loss, where the Nu number and friction factor are higher in the case of the circular test section than those of the square one at the same Reynolds number.
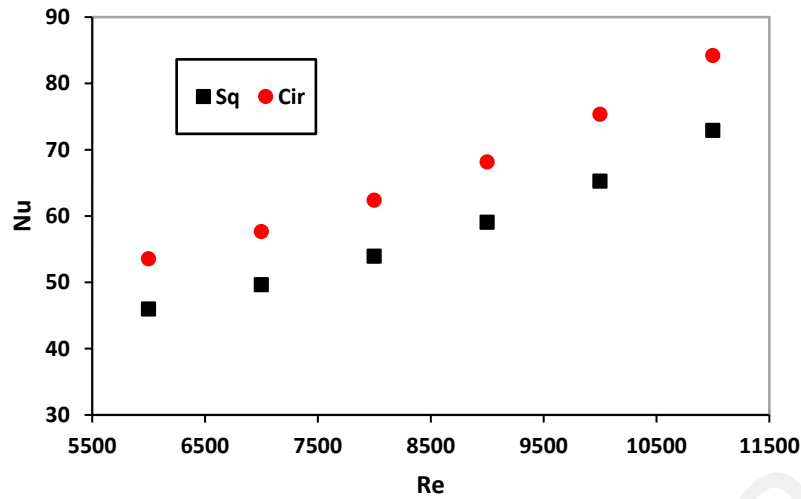
Figure 4-21: Average Nusselt number of DW for square and circular pipes.
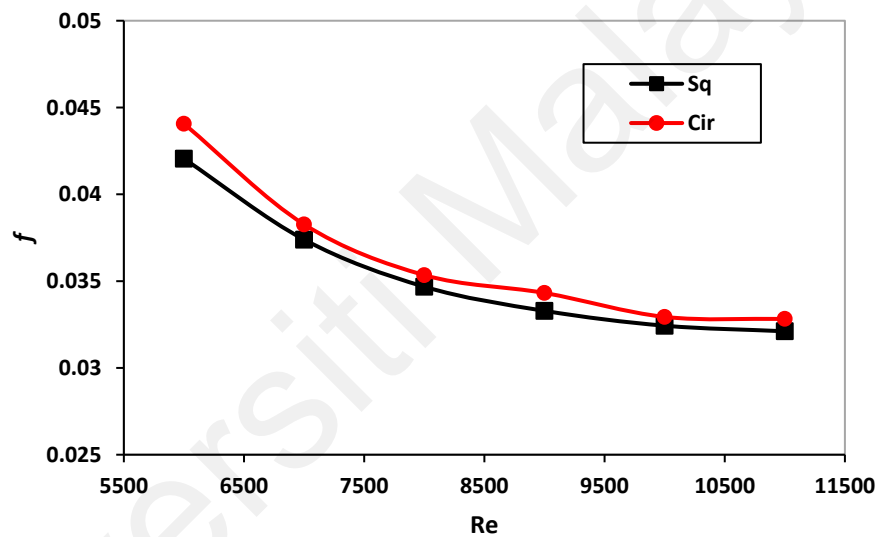
Figure 4-22: Friction factor profile of DW for the square and circular pipes.

4.3   Experimental evaluation of heat transfer and pressure drop

4.3.1   Circular pipe

Figure 4-23 displays the profile of the average Nusselt number vs. the designed Reynolds number range of the current study, where there is a significant Nu number enhancement when using nanofluids in comparison with the DW. As shown in Figure 4-23, the enhancement of the Nusselt number for each nanofluid is directly proportional to its concentration and with the Reynolds number. The SiO_2/DW nanofluid of 0.1 wt.% concentration shows the highest average enhancement of 7.46%, followed by the Al_2O_3/DW of 0.1 wt.% concentration with 6.32 %, then the hybrid nanofluid of 0.1 wt.%,

where it shows an average enhancement of 6.08%. For 0.075 wt.% concentration, the SiO2/DW nanofluid shows the highest average enhancement of 5.83%, followed by Al2O3/DW with 3.79%, and finally, the hybrid nanofluid with 3.73%. For 0.05 wt.% concentration, the SiO2/DW nanofluid shows the highest average enhancement of 3.29%, followed by the hybrid nanofluid with 2.32% and finally the Al2O3/DW with 1.38%.

These results confirm that: at the same Reynolds number, the highest Prandtl number the highest Nusselt number regardless of the order of nanofluid's thermal conductivity, where the order of the average enhancement of Nusselt number is the same as the order of the Prandtl number shown in Table 4-1.
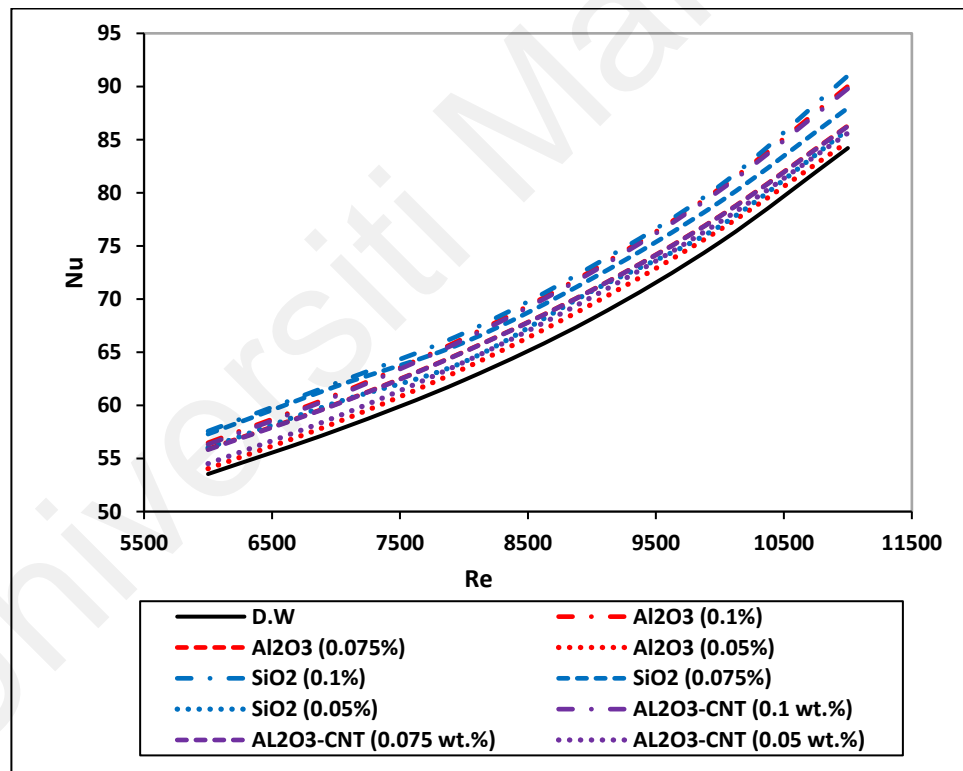
Figure 4-23: Average Nusselt number of DW and nanofluids in the circular pipe.

The order of convection heat transfer enhancement is slightly different from that of the Nusselt number enhancement. The thermal conductivity influences the convection heat transfer coefficient according to the equation (3-21). For the convection heat transfer coefficient, the hybrid nanofluid of 0.1 wt.% concentration gives the highest average

enhancement of 9.02%, followed by the SiO$_2$/DW of 0.1 wt.% concentration with 8.83 %, then the Al$_2$O$_3$/DW nanofluid of 0.1 wt.% with an average enhancement of 7.72%. For 0.075 wt.% concentration, the SiO$_2$/DW nanofluid shows the highest average enhancement of 6.35%, followed by hybrid with 5.25% and finally the Al$_2$O$_3$/DW nanofluid with 4.81%. For 0.05 wt.% concentration, the SiO$_2$/DW nanofluid shows the highest average enhancement of 3.63%, followed by the hybrid nanofluid with 3.16% and finally the Al$_2$O$_3$/DW with 2.04%.
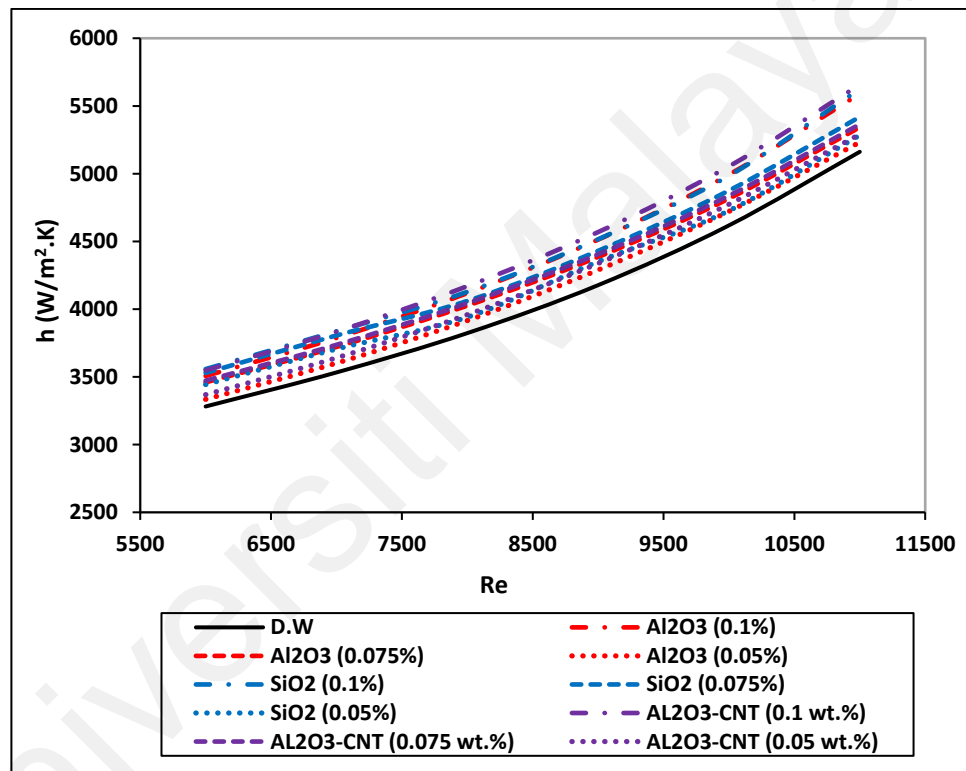
Figure 4-24: profile of the average convection heat transfer coefficient in the circular pipe.

By comparing the nanofluids order based on thermal conductivity values with that obtained based on average Nu number values, the experimental results of the circular pipe showed the impact of Pr Number over the thermal conductivity in convection heat transfer performance. Therefore, the thermal conductivity of nanoparticles not only the parameter affects the convection heat transfer, but also the other thermophysical properties such as

specific heat and viscosity have significant effects on the convection heat transfer and may overrule the thermal conductivity enhancement.

The pressure drop evaluation should be deeply considered side-by-side with nanofluids' heat transfer characteristics if used for practical purposes. Figure 4-25 shows the pressure drop per unit length for all the nanofluids used in the current study within the Reynolds number range of 6000-11000. The main features of Figure 4-25 show that the pressure drop increases when the nanofluid concentration increases and the Reynolds number. The average increment differs from one nanofluid to another one, where the effect of dynamic and kinematic viscosity (momentum diffusivity) plays a vital role in this increment. For 0.05 wt.% concentration, the SiO_2/DW, hybrid, and Al_2O_3/DW have the average increment of 13.24%, 11.83%, and 11.26%, respectively. The average increments are 22.67%, 20.29%, and 20.1% for the nanofluids SiO_2/DW, hybrid, and Al_2O_3/DW, respectively, at 0.075 wt.% concentration. For the highest concentration, 0.1 wt.%, the nanofluids SiO_2/DW, hybrid, and Al_2O_3/DW have the average increments of 32.91%, 31.22%, and 29.71%, respectively.

The order of pressure drop increment of nanofluids compared with that of DW is the same as the order of the product of both the dynamic and kinematic viscosity, which matches the relation in equation (3-20).
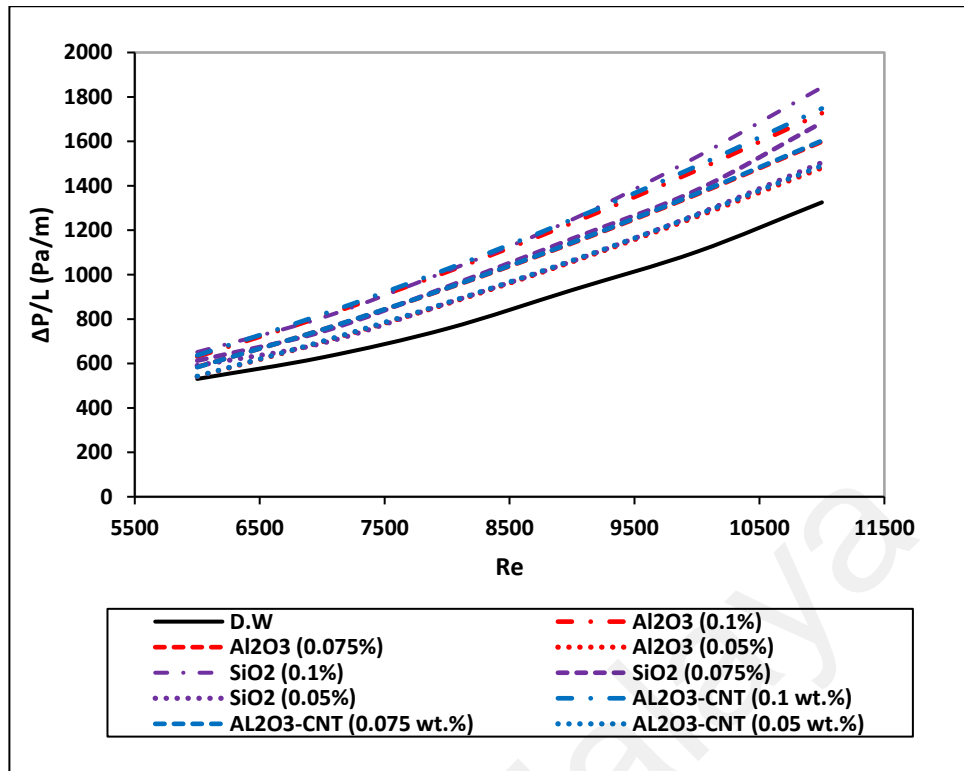
Figure 4-25: Pressure drop of DW and nanofluids in the circular pipe.

Figure 4-26 and Figure 4-27 show the performance index profile at different Reynolds numbers for the circular test section based on the evaluation of pressure drop and pumping power, respectively, as a penalty. Both figures show that the DW appears as the most efficient convective medium compared to other nanofluid concentrations. The lowest concentration of each nanofluid has the highest performance comparing with the higher concentration. The Al_2O_3/DW shows the highest thermal performance compared with other nanofluids' data based on both evaluations. The Al_2O_3/DW thermal performance is followed by the hybrid nanofluid and the SiO_2/DW, reflecting the significant effect of nanofluids' penalty over its benefit. Moreover, evaluation of performance index depending on the pumping power as a penalty reduces the average performance for each nanofluid concentration compared to the performance evaluation based on the pressure drop. The effect of pumping power on the performance index reflects the impact of increasing the volume flow rate and the pressure drop increment when using nanofluids instead of DW. Therefore, consideration of the heat transfer enhancement compared to

the pressure drop or pumping power consumption could be a weighted factor to select the nanofluid type instead of the distilled water in different heat transfer applications. In case of enhanced heat transfer requirement, the user should overrule the pressure loss compensation of the nanofluids; otherwise, it would not be economical.
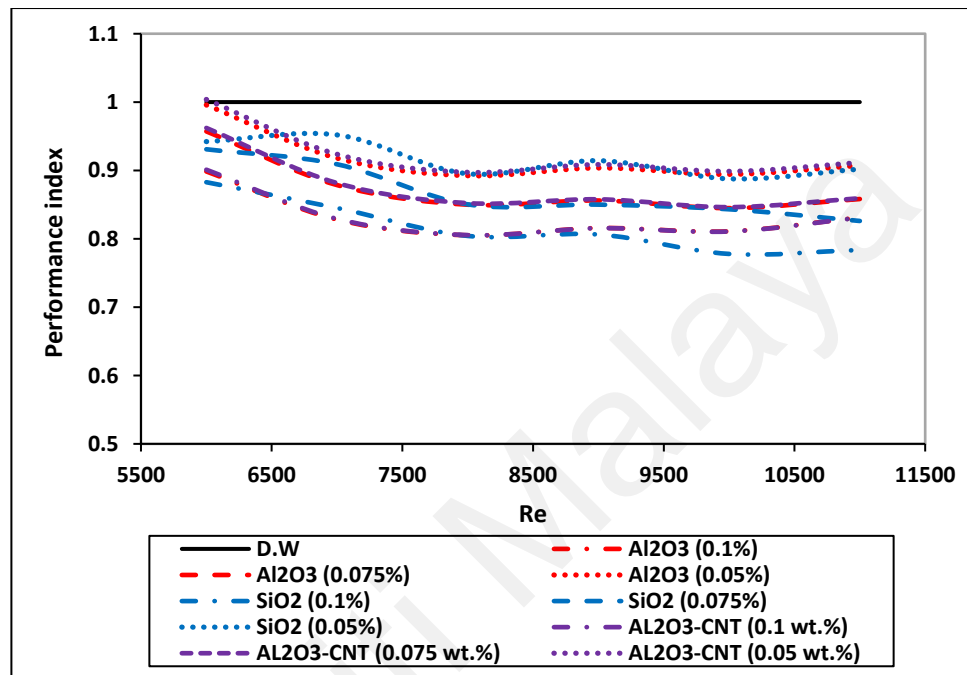
Figure 4-26: Performance index based on the pressure drop for the circular pipe.
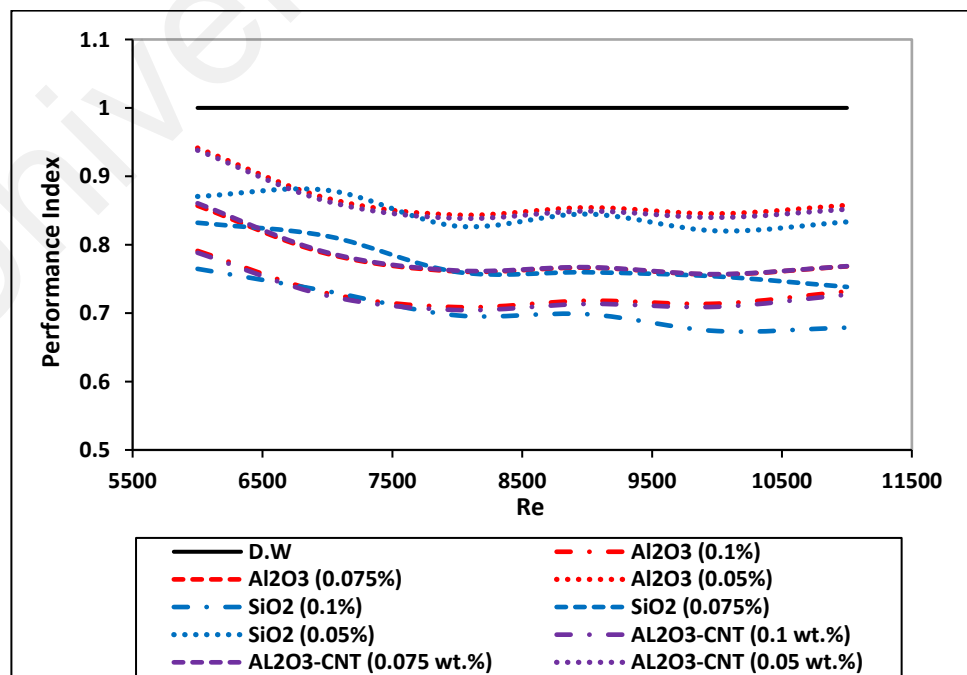
Figure 4-27: Performance index based on pumping power for the circular pipe.

4.3.2 Square pipe

The experimental data obtained from the square test section, such as Nusselt number, convection heat transfer coefficient, and pressure drop, have the same trend as those obtained from the circular test section for the same Re range. Figure 4-28 shows the average Nusselt number of different nanofluids in the square pipe, where the order of Nu number enhancement is the same as in the circular pipe, but its values are different due to the geometry shape effect.

For 0.05 wt.% concentration, the percentages enhancement of Nusselt number for SiO_2/DW, hybrid, and Al_2O_3/DW are 1.55%, 1.43%, and 1.15%, respectively. The average enhancement of the Nusselt number is 5.26%, 5.20%, and 4.63% for the nanofluids SiO_2/DW, Al_2O_3/DW, and hybrid, respectively, at 0.075 wt.%. For the highest concentration, 0.1 wt.%, the nanofluids SiO_2/DW, Al_2O_3/DW, and hybrid have an average increment of 7.13%, 6.63%, and 5.24%, respectively.

Figure 4-29 shows the average convection heat transfer coefficient, where the average percentage enhancement of the convection heat transfer coefficient is 8.16%, 8.03%, and 8.00 for the hybrid nanofluid at 0.1 wt.%, Al_2O_3/DW at 0.1 wt.%, and SiO_2/DW at 0.1 wt.% concentration, respectively. For 0.075 wt.% concentration, the Al_2O_3/DW nanofluid shows the highest average enhancement of 6.23%, followed by hybrid with 6.16%, and finally the SiO_2/DW nanofluid with 5.77%. For 0.05 wt.% concentration, the hybrid nanofluid shows the highest average enhancement of 2.26%, followed by the SiO_2/DW nanofluid with 1.88% and finally the Al_2O_3/DW with 1.81%.
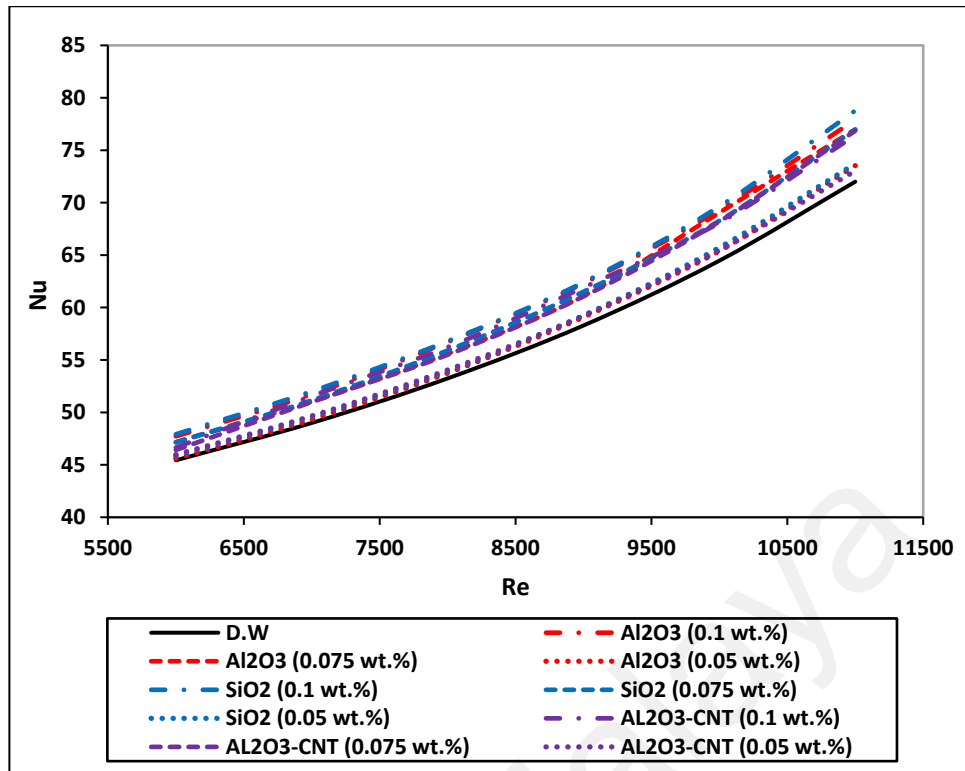
Figure 4-28: Average Nusselt number of DW and nanofluids in the square duct.
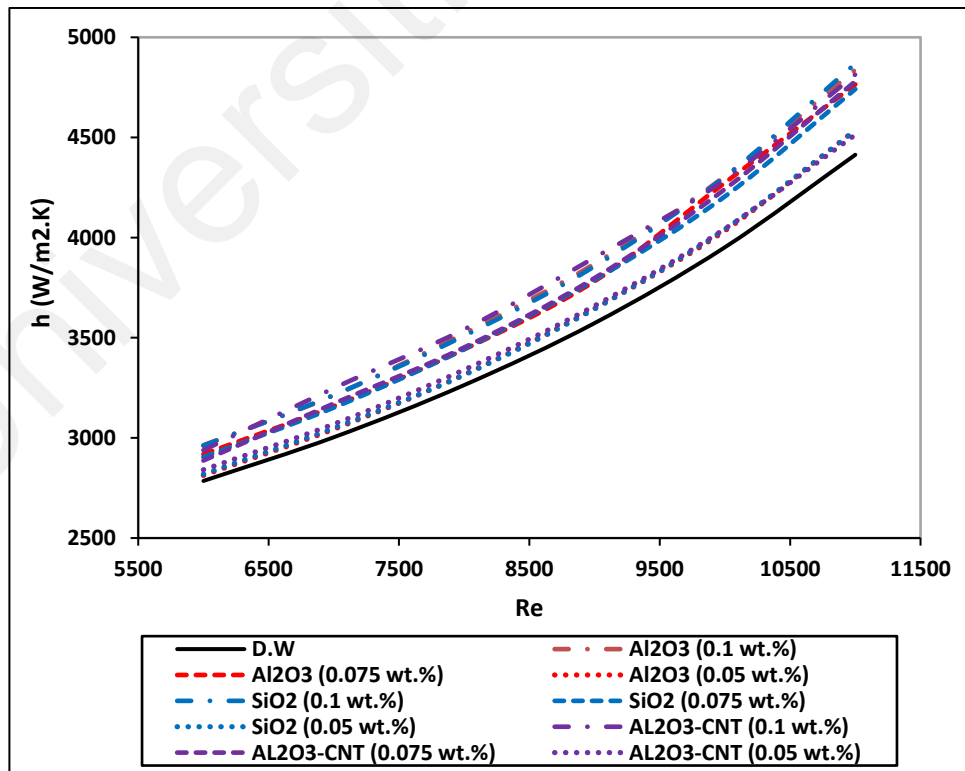
Figure 4-29: Average convection heat transfer coefficient of DW and nanofluids in the square duct.

Figure 4-30 shows the pressure drop profile for different nanofluids in the square test section. As in the circular test section, the SiO_2/DW nanofluid has the highest pressure drop increment compared to the similar wt.% concentration followed by hybrid nanofluid and Al_2O_3/DW nanofluid, respectively, which confirm the significant effect of dynamic and kinematic viscosities of nanofluids on the pressure drop. For 0.05 wt.% concentration, the SiO_2/DW, hybrid, and Al_2O_3/DW have an average increment of 11.18%, 9.70%, and 4.70%, respectively. The average increments are 18.95%, 16.95%, and 15.25% for the nanofluids SiO_2/DW, hybrid, and Al_2O_3/DW of 0.075 wt.%, respectively. For the highest concentration, 0.1 wt.%, the nanofluids SiO_2/DW, hybrid, and Al_2O_3/DW have an average increment of 27.50%, 26.10%, and 23.50%, respectively.
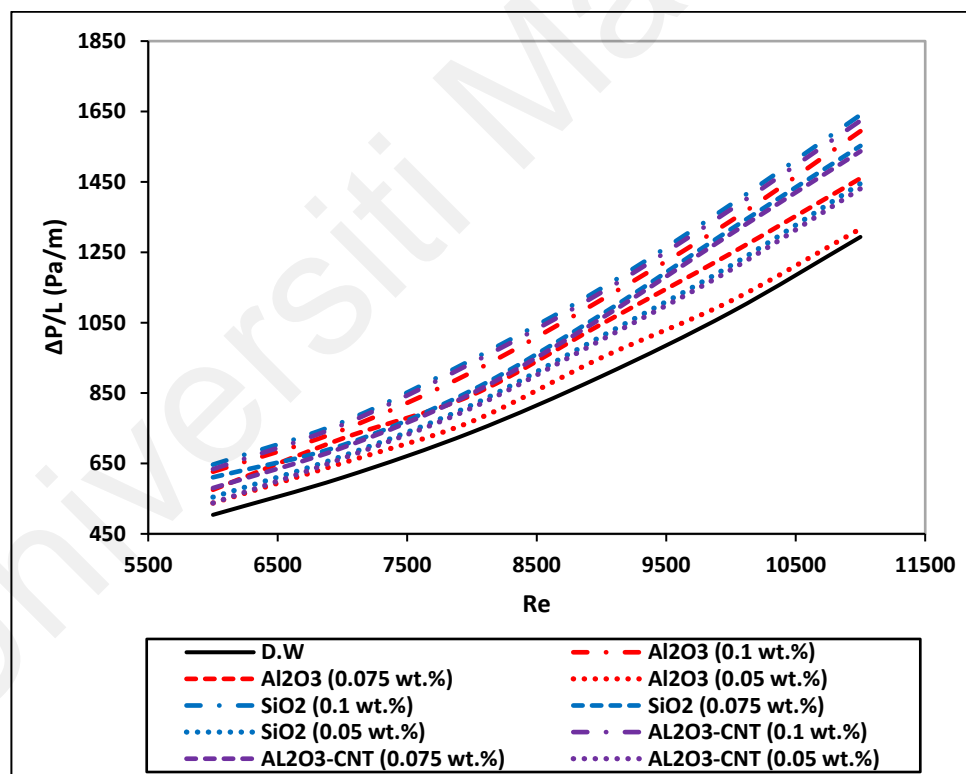
Figure 4-30: Pressure drop of DW and nanofluids in the square duct.

Table 4-2 shows the enhancement percentage for Nusselt number, convection heat transfer, and pressure drop of all nanofluid samples for the circular and square test sections.

Table 4-2: The percentage enhancement for different parameters in the experimental study.

Nanofluid	Nu number		h (W/m^2.K)		$\Delta P/L$ (Pa/m)	
	Cir	Sq	Cir	Sq	Cir	Sq
Al$_2$O$_3$ (0.1%)	6.32 %	6.63 %	7.72 %	8.03 %	29.71 %	23.50 %
Al$_2$O$_3$ (0.075%)	3.79 %	5.20 %	4.81 %	6.23 %	20.1 %	15.25 %
Al$_2$O$_3$ (0.05%)	1.38 %	1.15 %	2.04 %	1.81 %	11.26 %	4.70 %
SiO$_2$ (0.1%)	7.46 %	7.13 %	8.83 %	8.00 %	33.42 %	27.50 %
SiO$_2$ (0.075%)	5.83 %	5.26 %	6.35 %	5.77 %	22.67 %	18.95 %
SiO$_2$ (0.05%)	3.29 %	1.55 %	3.63 %	1.88 %	13.24 %	11.18 %
AL$_2$O$_3$-MWCNTs (0.1 wt.%)	6.08 %	5.24 %	9.02 %	8.16 %	31.22 %	26.10 %
AL$_2$O$_3$-MWCNTs (0.075 wt.%)	3.73 %	4.63 %	5.25 %	6.16 %	20.29 %	16.95 %
AL$_2$O$_3$-MWCNTs (0.05 wt.%)	2.32 %	1.43%	3.16 %	2.26 %	11.83 %	9.70 %

The performance index evaluation as in Figure 4-31 and Figure 4-32 shows that the performance of the nanofluid in the square pipe is higher than that of the circular one either on a pressure drop or pumping power basis. The increment of performance index in the square duct may belong to the increment percentage of heat transfer enhancement and the reduction of pressure drop increment compared to the data of the circular one.

From the present investigation, DW still has the best thermal performance compared with the data from different nanofluids and concentrations in the circular pipe configuration. The lowest nanofluid concentration has the best performance compared with the other concentrations of the same nanofluid.
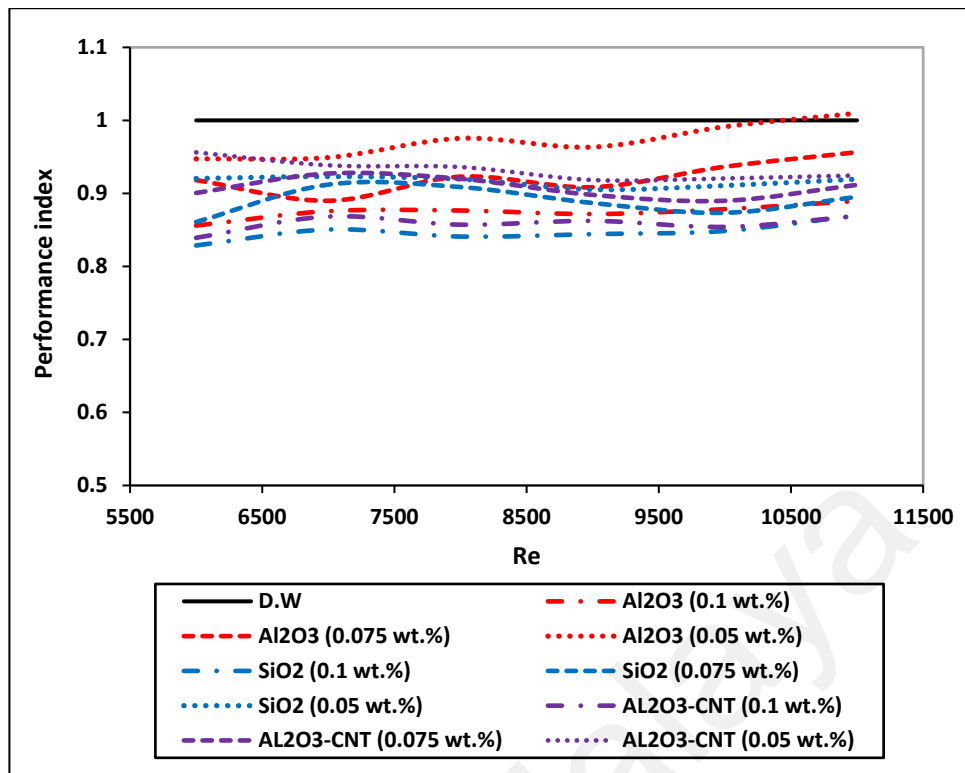
Figure 4-31: Performance index based on the pressure drop for the square duct.
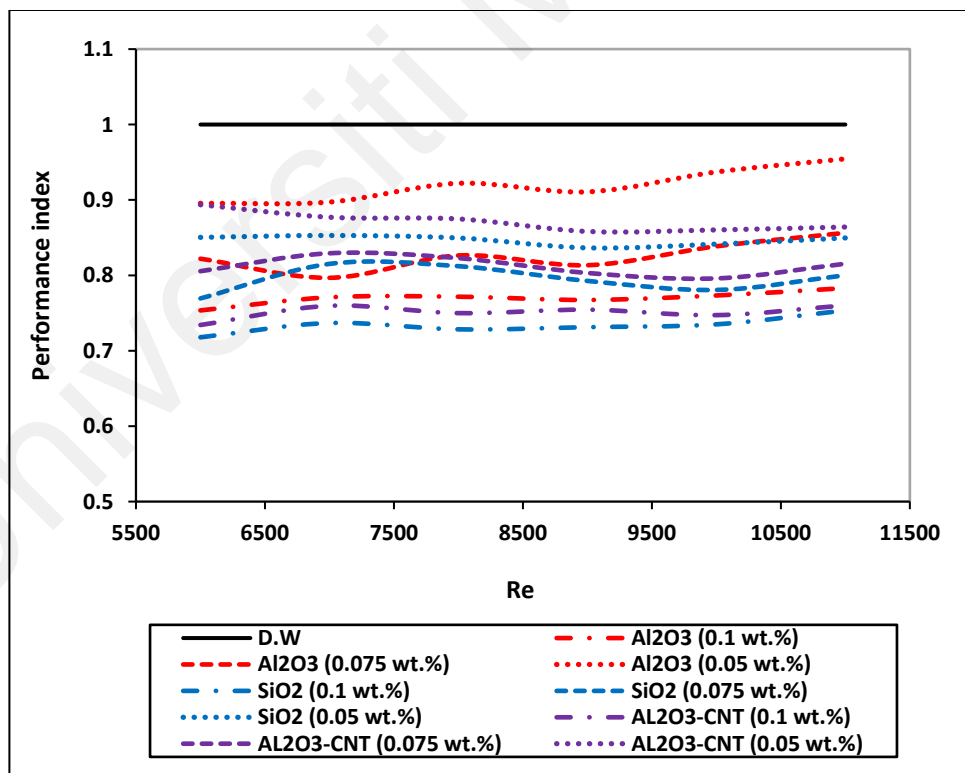
Figure 4-32: Performance index based on pumping power for the square duct.

4.4 Numerical Results

4.4.1 Circular and square pipes

4.4.1.1 Validation and mesh dependency

the Nusselt number values obtained from both the circular and square pipe models were compared at different mesh densities for the DW run at the same Reynolds number range to ensure that the current study's numerical results are mesh independent. The change in the mesh element density was done by keeping the number of longitudinal elements constant and the bias factor. Only the number of circumferential elements was increased to increase the total mesh elements number. Figure 4-33 shows the effect of mesh density on the DW Nusselt number, where the mesh densities of 968016, 1337232, and 5476460 gave nearly the same values of the Nusselt number. Therefore, the model of circular pipe with a mesh density of 968016 elements was selected to save the running time. Figure 4-34 shows the results of the mesh independency test of the square pipe model, where there was no noticeable change in the Nusselt number for the mesh densities of 600000, 864000, and 1563000 elements. Therefore, the mesh density of 600000 elements was selected.
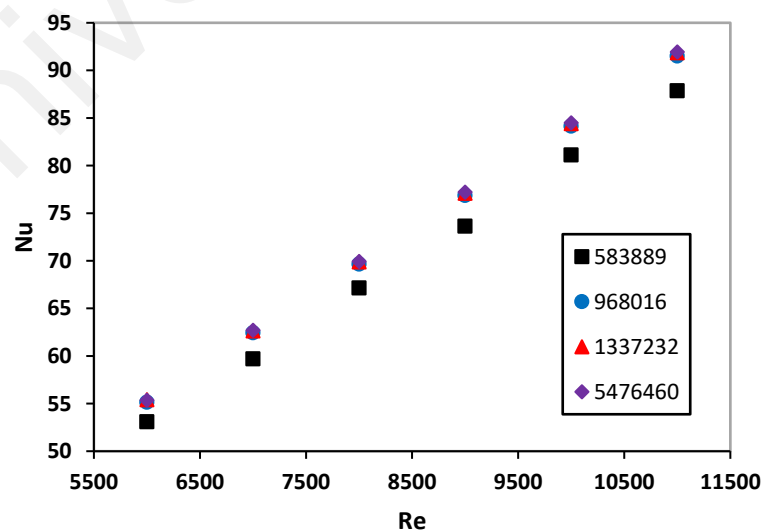
Figure 4-33: Nusselt number of DW at different mesh densities for circular pipe model.
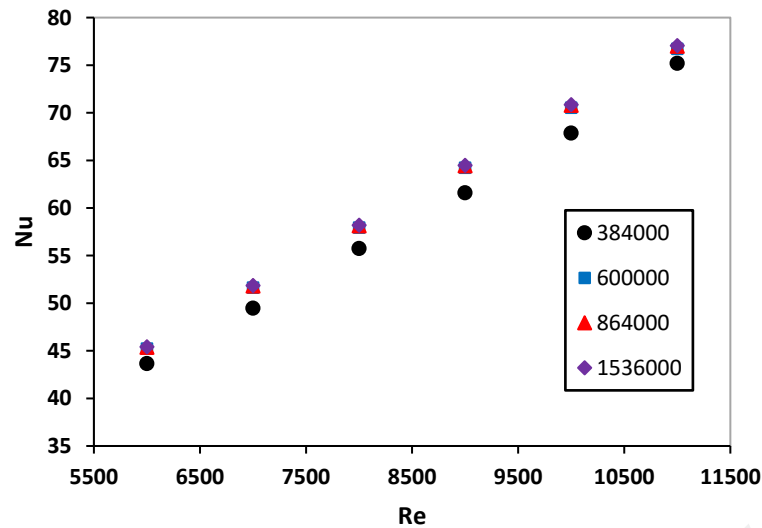
Figure 4-34: Nusselt number of DW at different mesh densities for square pipe model.

Validation of numerical models for the circular and the square pipes was done by comparing the Nusselt number and pressure drop obtained from the models with those obtained experimentally as shown in Figures 4-35 and 4-36, respectively. For the square duct, the Nusselt number and pressure drop obtained numerically showed a good agreement with those obtained experimentally with an average error of 6.8% and 2.49% for Nu number and ΔP/L, respectively. For circular pipe, the average Nusselt number and pressure drop errors were 9.34 % and 5.92 %, respectively. Therefore, the numerical solution obtained by the ANSYS Fluent models has been accepted for both models as the average errors were less than 10%.
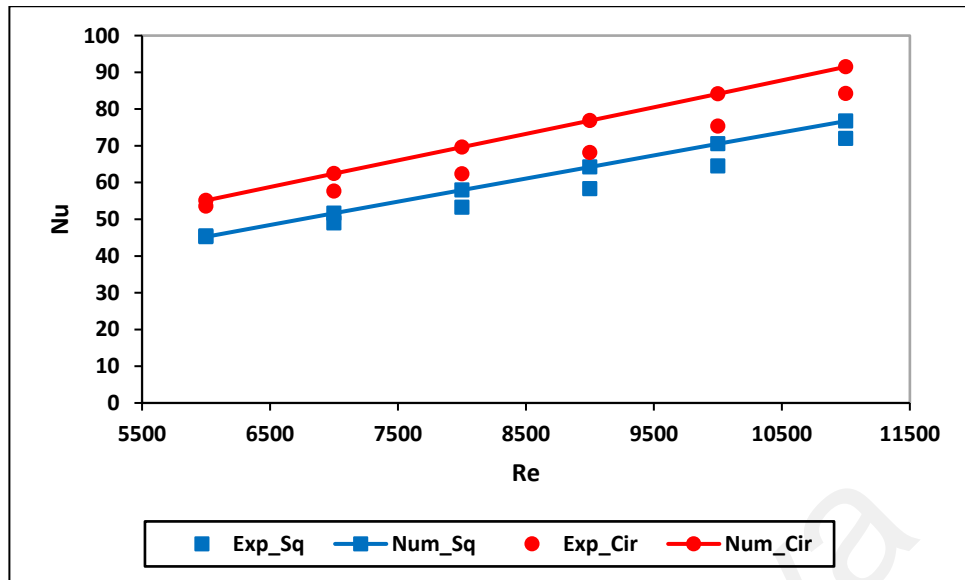
Figure 4-35: The average Nusselt number obtained experimentally and numerically for circular and square pipes.
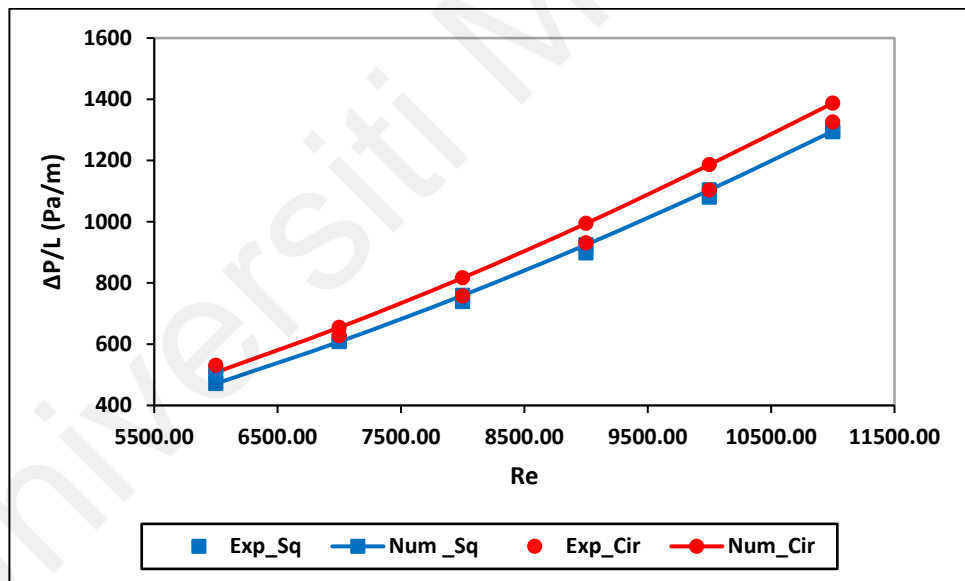
Figure 4-36: Pressure drop per unit length for the circular and the square pipes.

4.4.1.2 Thermal and flow characteristics

In this section, the thermal and fluid flow characteristics inside the circular and square pipes during the water run were discussed to show the different phenomena that affect the heat transfer and pressure drop in both configurations with no facilities to capture them in the experimental work. In the turbulent flow, the sharp edge corners in the square pipe cause a secondary flow formation and Reynolds's stress gradient. In the circular pipe

flow, there is no secondary flow, and the flow is more uniform, as shown in Figure 4-37, which displays the velocity vectors at the outlet section for both pipes.

The wall temperature contours for the circular and square pipe are shown in Figures 4-38 and 4-39, respectively. The temperature distribution is uniform on the circular pipe surface, and hot temperature spots appear along the edges of the square duct due to the formation of the secondary flow.
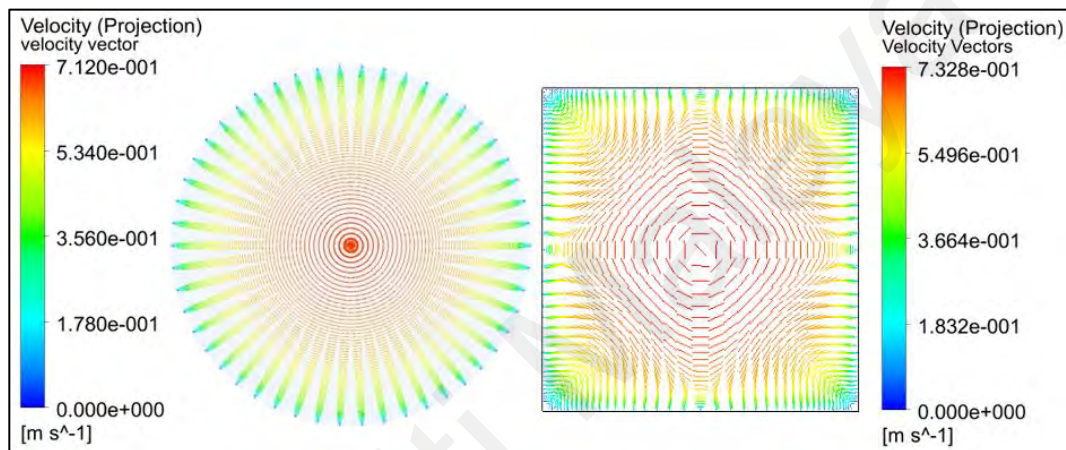
Figure 4-37: Velocity vectors for DW at the outlet section of the square and circular pipes at Re = 6000.
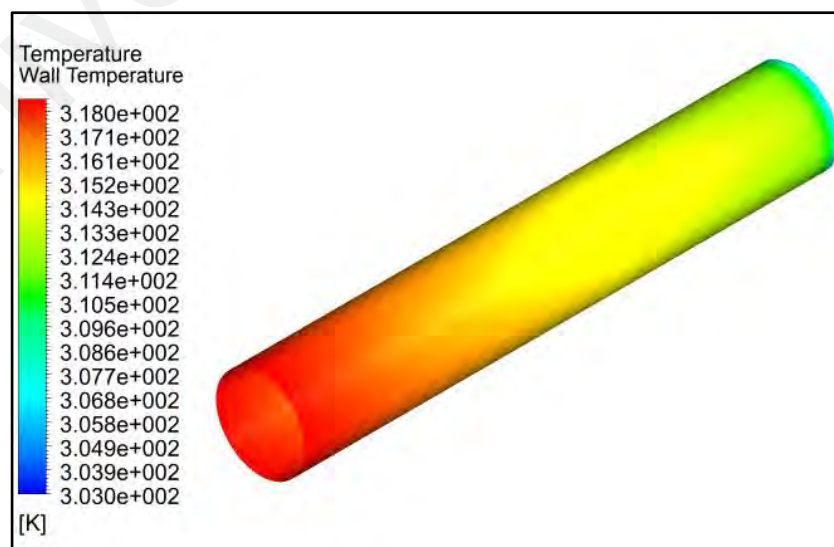
Figure 4-38: Temperature contours at the wall of the circular pipe with DW at Re = 11000.
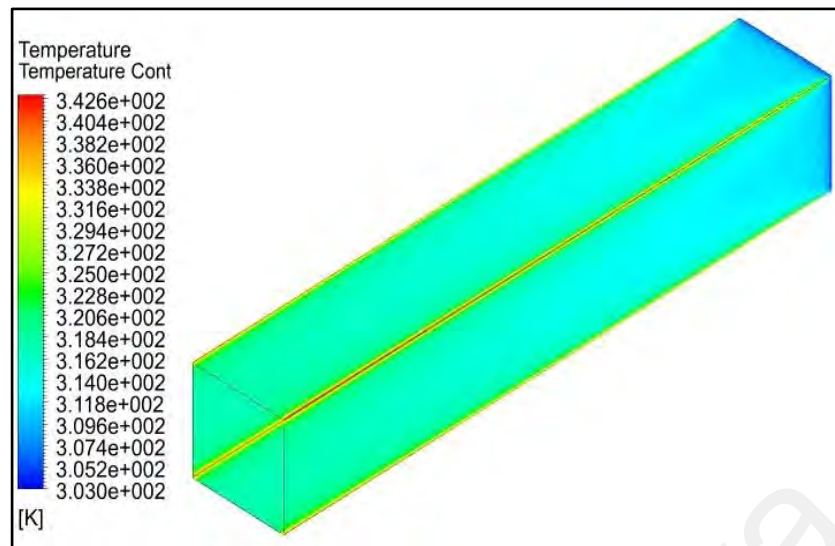
Figure 4-39: Temperature contours at the wall of the square pipe with DW at Re = 11000.

Figure 4-40 and Figure 4-41 show the flow development in the circular and square pipe, respectively, where the flow became fully developed at $x/D_h \geq 10$. Figure 4-42 shows the local Nusselt number and friction factor variation along the pipe length for both pipes configurations. The Nu number and friction factor became nearly straight and horizontal in the fully developed region. These profiles confirm that the current study models match the standard considerations for internal turbulent flow of incompressible fluids presented by (Cengel, 2007; Diessler, 1953).
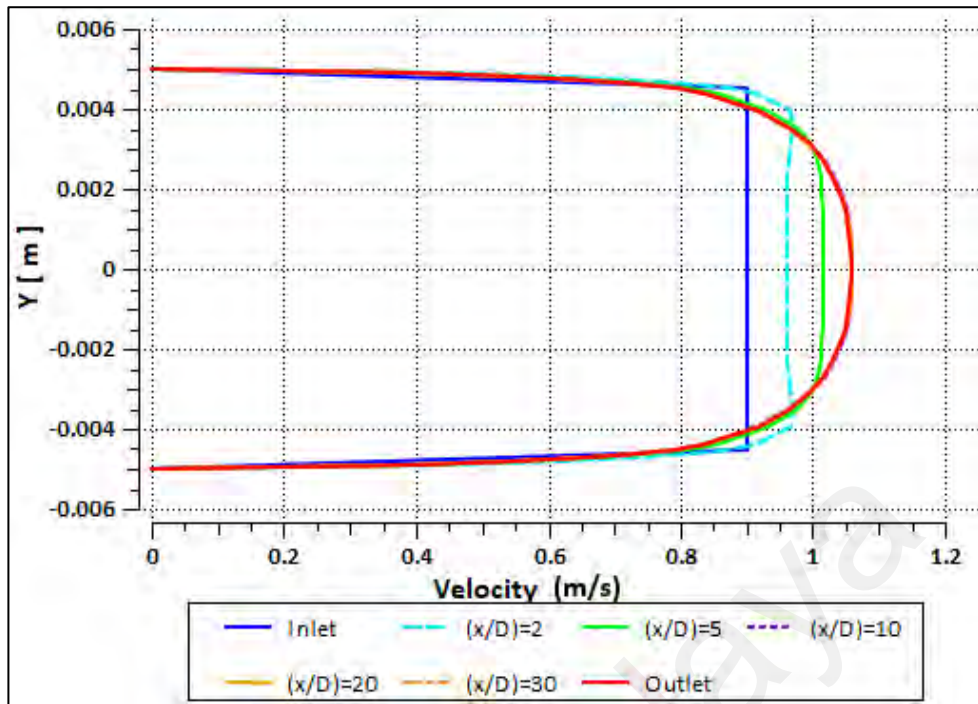
Figure 4-40: Velocity profile of DW at different locations in the circular pipe at Re = 11000.
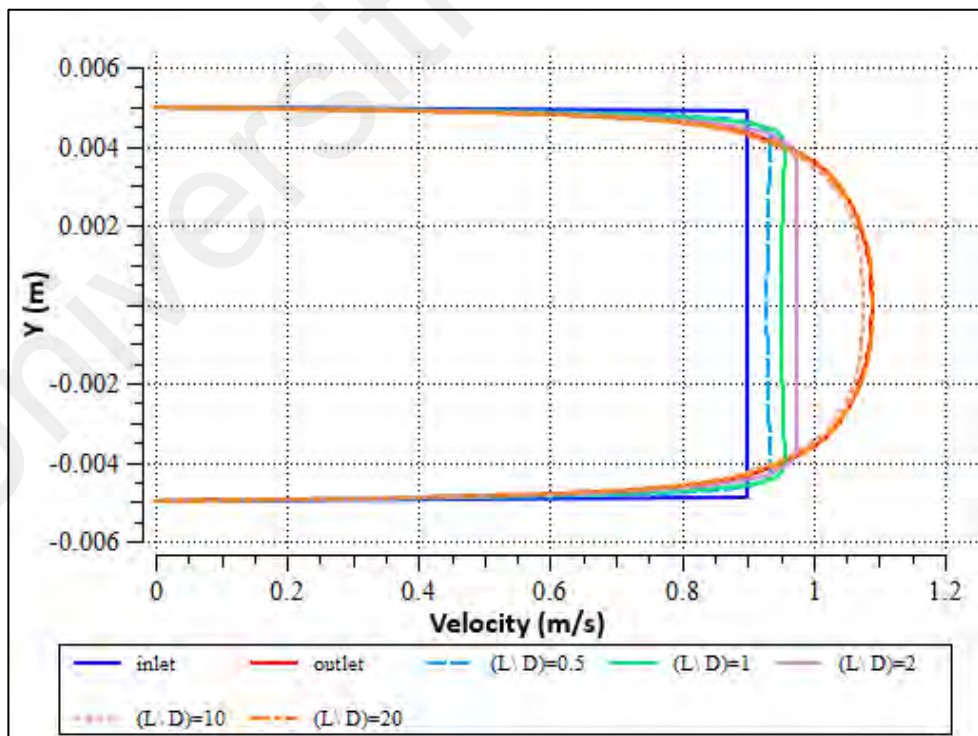
Figure 4-41: Velocity profile of DW at different locations in the square pipe at Re = 11000.
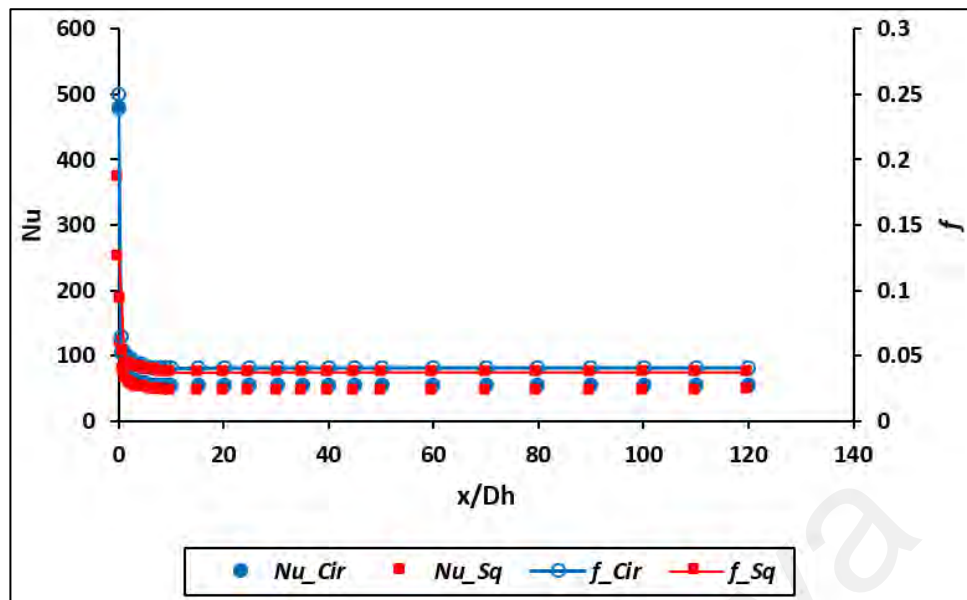
Figure 4-42: Local Nusselt number and friction factor profiles of DW at Re = 6000.

4.4.1.3 Heat transfer and pressure drop of nanofluids

In the CFD post module, the local Nusselt number was calculated using equation (3-22) by replacing the local fluid temperature with the fluid bulk temperature. The average Nusselt number over the turbulent flow region was calculated by getting the average of its local values in the fully developed region. Hence, the average heat transfer coefficient was calculated. The pressure drop along the pipe was calculated by getting the difference between the average pressure value at the inlet and the outlet sections of the pipe.

Figure 4-43 and Figure 4-44 show the average Nusselt number profiles of all nanofluid samples for circular and square pipe, respectively. The Nusselt number enhancement in both figures has the same order, not value, as obtained from the experimental work, which confirms the effect of nanofluid's Prandtl number on the Nusselt number values. Moreover, the convection heat transfer coefficient in Figure 4-45 and Figure 4-46 and the pressure drop in Figure 4-47 and Figure 4-48 have similar trends as those obtained from the experimental work, which confirm the vision of the current study towards the main factors affecting the heat transfer and pressure drop performance of nanofluids. Table 4-3

114

shows the average enhancement percentages for all the nanofluid concentrations based on the numerically obtained results that have the same trend in the experimental results.
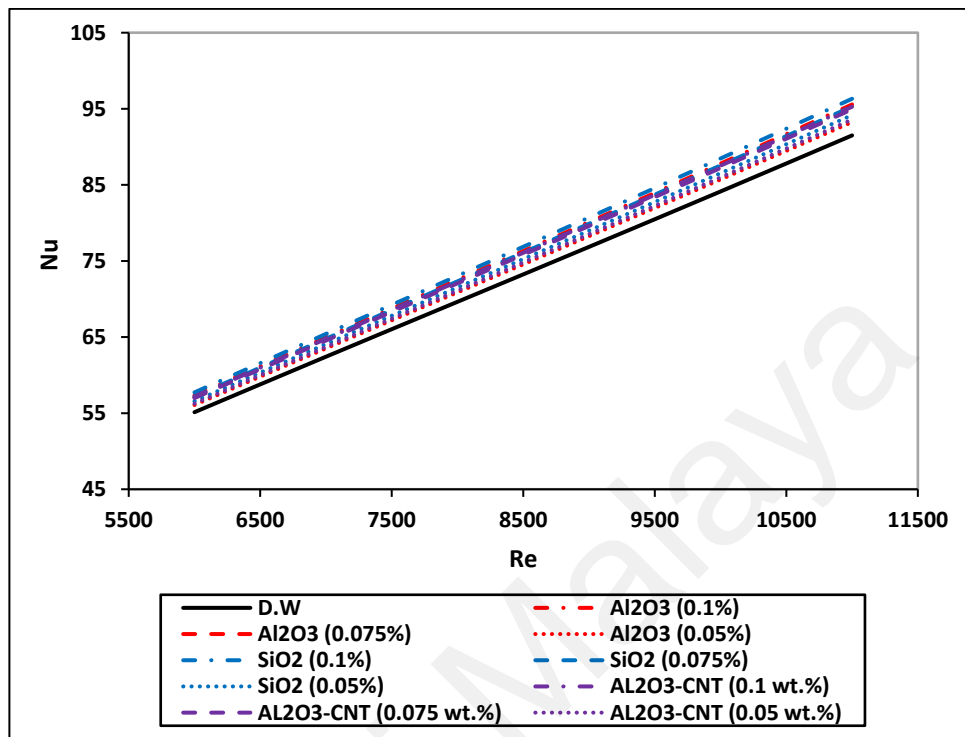
Figure 4-43: Average Nusselt number obtained numerically for the circular pipe.
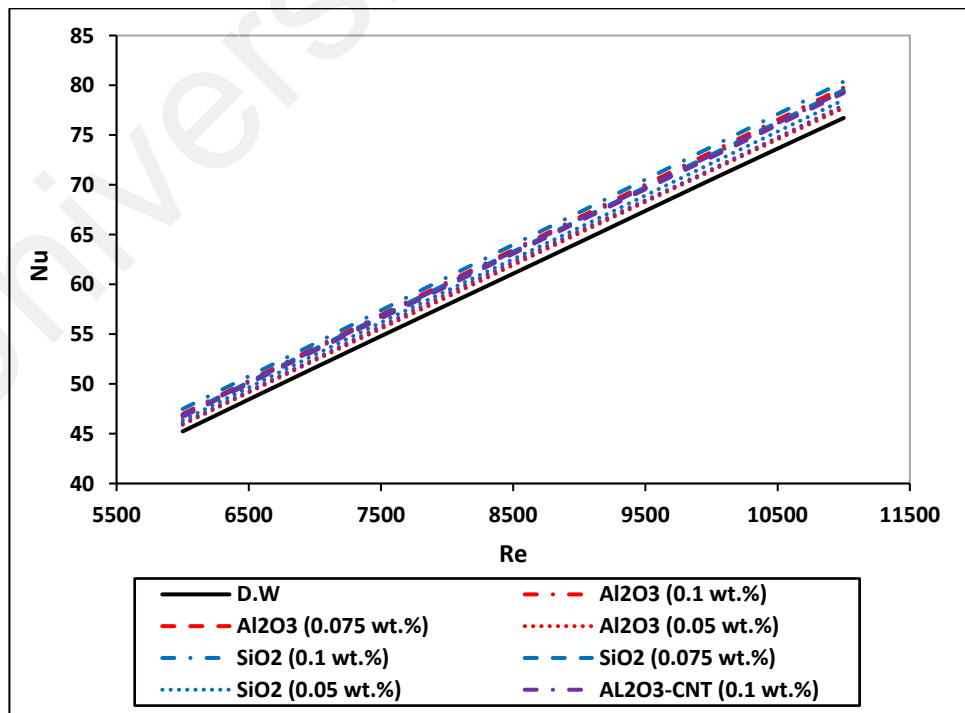
Figure 4-44: Average Nusselt number obtained numerically for the square pipe.
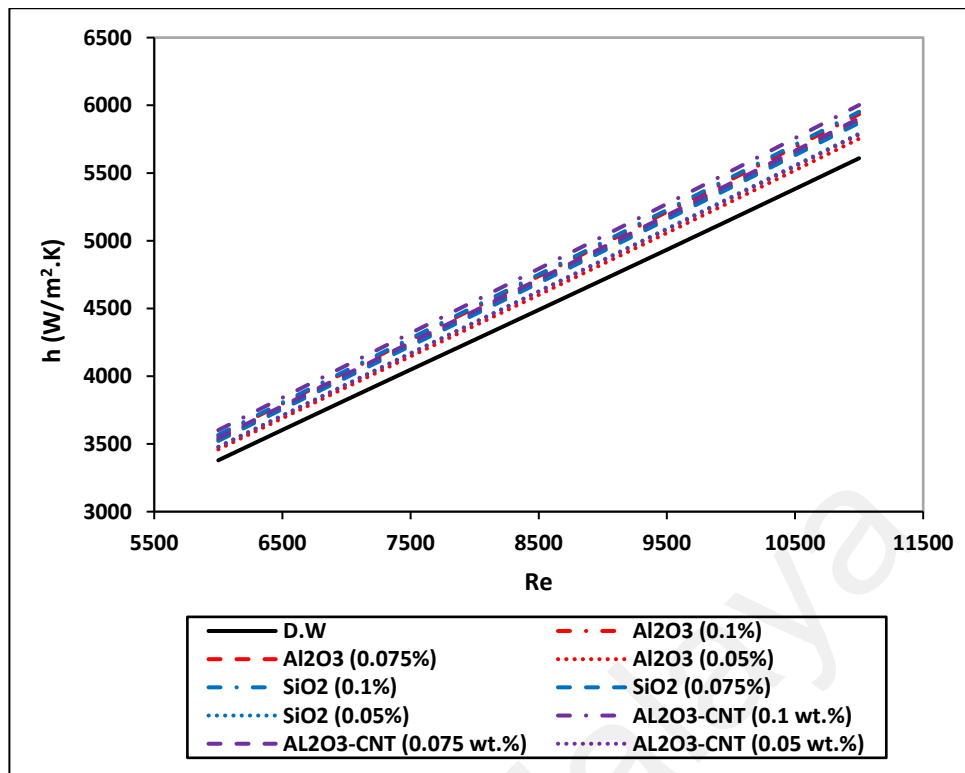
Figure 4-45: Average heat transfer coefficient obtained numerically for the circular pipe.
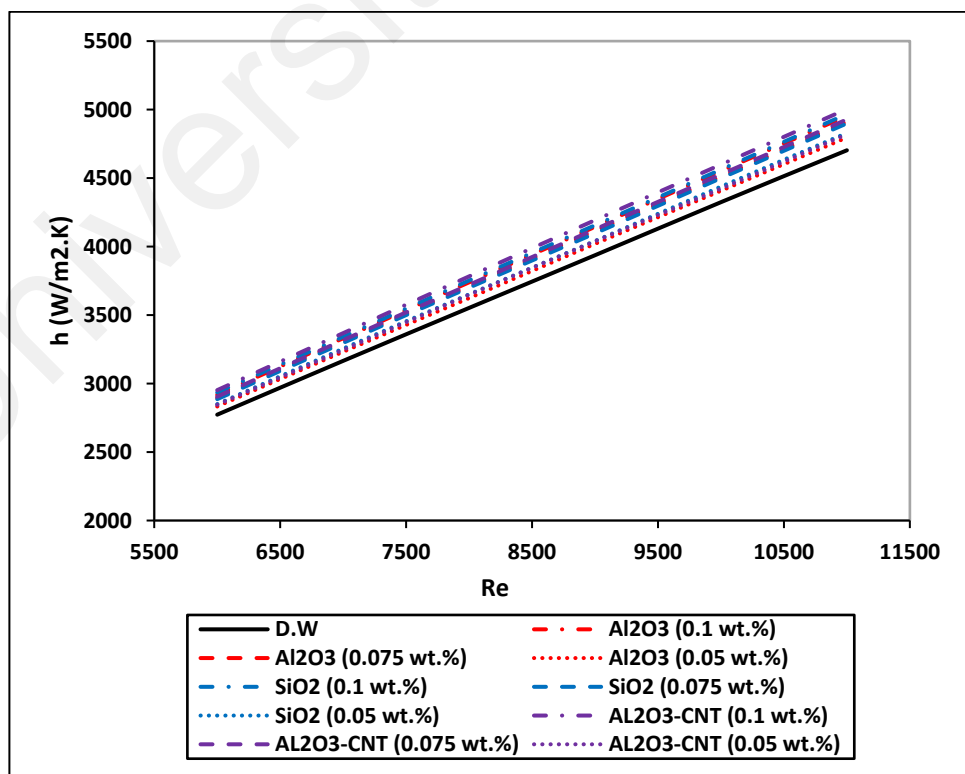
Figure 4-46: Average heat transfer coefficient obtained numerically for the square pipe.

Figure 4-47: Pressure drop per unit length obtained numerically for the circular pipe.

Figure 4-48: Pressure drop per unit length obtained numerically for the square pipe.

Nanofluid	Nu number		h (W/m^2.K)		$\Delta P/L$ (Pa/m)	
	Cir	Sq	Cir	Sq	Cir	Sq
Al_2O_3 (0.1%)	4.20 %	3.90 %	5.56 %	5.26 %	29.22 %	29.14 %
Al_2O_3 (0.075%)	3.69 %	3.43 %	4.70 %	4.44 %	24.89 %	24.81 %
Al_2O_3 (0.05%)	1.80 %	1.38 %	2.47 %	2.04 %	12.03 %	11.95 %
SiO_2 (0.1%)	4.97 %	4.76 %	5.83 %	5.62 %	33.42 %	33.33 %
SiO_2 (0.075%)	3.93 %	3.61 %	4.43 %	4.12 %	25.30 %	25.22 %
SiO_2 (0.05%)	2.76 %	2.40 %	3.09 %	2.74 %	17.24 %	17.16 %
AL_2O_3-MWCNTs (0.1 wt.%)	3.89 %	3.56 %	6.78 %	6.43 %	30.84 %	30.76 %
AL_2O_3-MWCNTs (0.075 wt.%)	3.54 %	3.24 %	5.06 %	4.76 %	25.13 %	25.05 %
AL_2O_3-MWCNTs (0.05 wt.%)	2.15 %	1.71 %	2.98 %	2.54 %	14.58 %	14.52 %

Figure 4-49 and Figure 4-50 show the performance index that was evaluated
numerically based on the equation (3-23) for both circular and square pipe, respectively.
From the performance index evaluation for both pipes, the numerical results confirmed
the results obtained experimentally, where the DW has the highest performance index
compared to the other nanofluids in the current study. Also, the lower concentration
showed the highest performance index for each nanofluid.
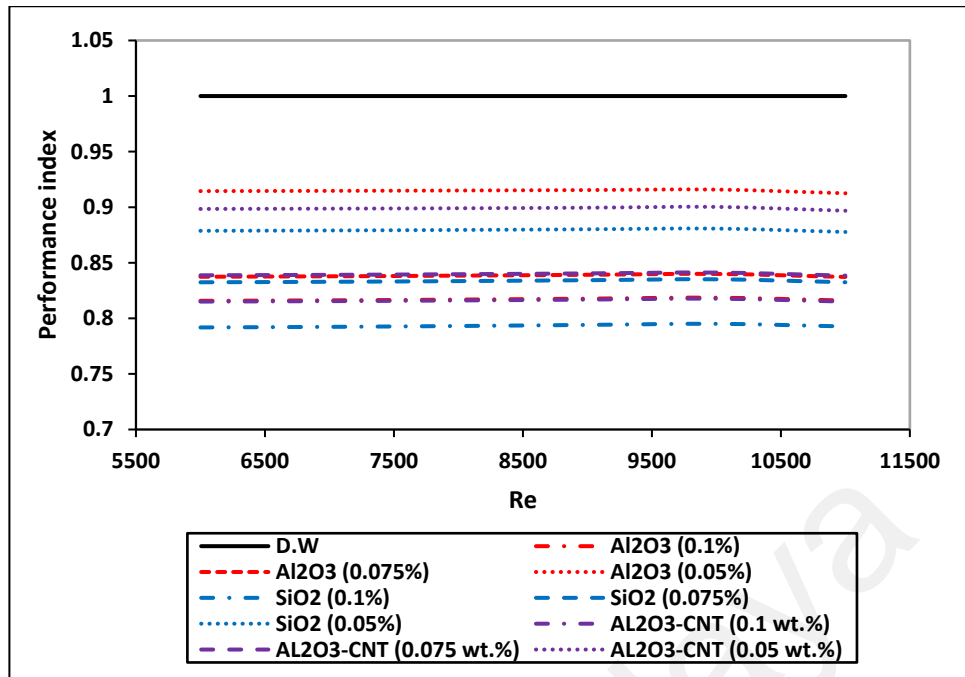
Figure 4-49: Performance index based on the pressure drop for the circular pipe.
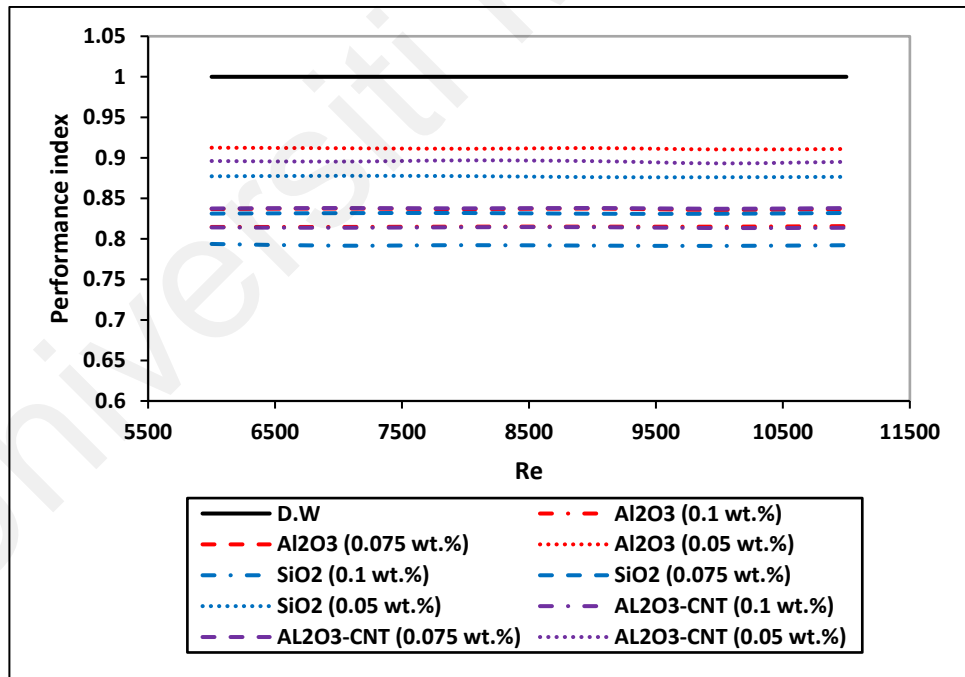
Figure 4-50: Performance index based on the pressure drop for the square pipe.

4.4.2   Annular pipe

In the current study, the performance of all nanofluids was evaluated at the same Reynolds number range of the circular and square pipes at different eccentricities starting from $e^* = 0.0$ (concentric case) to $e^* = 0.6$. All the nanofluids were tested for the concentric case, and only the highest and lowest concentration for each nanofluid were evaluated at the higher eccentricities. The model was validated using the concentric case results, and the different thermal and flow characteristics of the annular flow were investigated using the DW for comparison purposes.

4.4.2.1   Validation and mesh dependency

As shown in Fig. 4-51, the grid distribution was tested for the concentric case ($e^* = 0.0$) by computing the average outlet temperature at Reynolds number of 11000. Several mesh densities from 500000 elements up to 2000000 elements were tested to ensure that the solution is mesh-independent. The mesh independence was confirmed, and the numerical solution became steady and independent at the number of grid elements equals 1000000 (one million). Therefore, a grid distribution of 1000000 elements was employed to save running time.
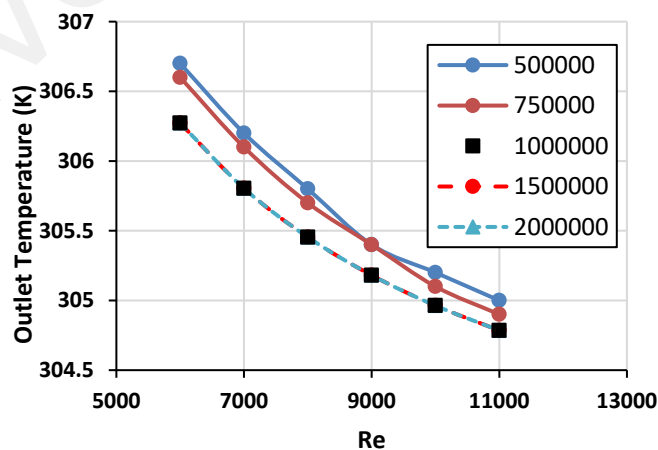
Figure 4-51: Outlet temperature profile at different mesh densities.

The numerical model validation was done for the concentric case by comparing the Nusselt number, and the friction factor of the DW run with those determined from the

empirical correlations. For annular geometry, various correlations were used to calculate the Nusselt number and friction factor at different Reynolds number ranges under the fully developed turbulent flow conditions. Table 3-1 shows the different empirical correlations that have been used to calculate the Nusselt number for annular geometry based on the hydraulic diameter of the annulus, and the friction factor of the annular space was evaluated by the equation (3-30).

A wide variation in the Nusselt number values that was obtained from the different empirical correlations mentioned in Table 3-1as shown in Figure 4-52(a). Therefore, the results obtained from the numerical model of this study are acceptable as it has a similar trend and mediating the curves of the other empirical correlation for the same Reynolds number range. Moreover, the friction factor obtained numerically showed a perfect agreement with that calculated by Gnielinski's correlation (2009), where the average error was 8.46%, as presented in Figure 4-52(b).
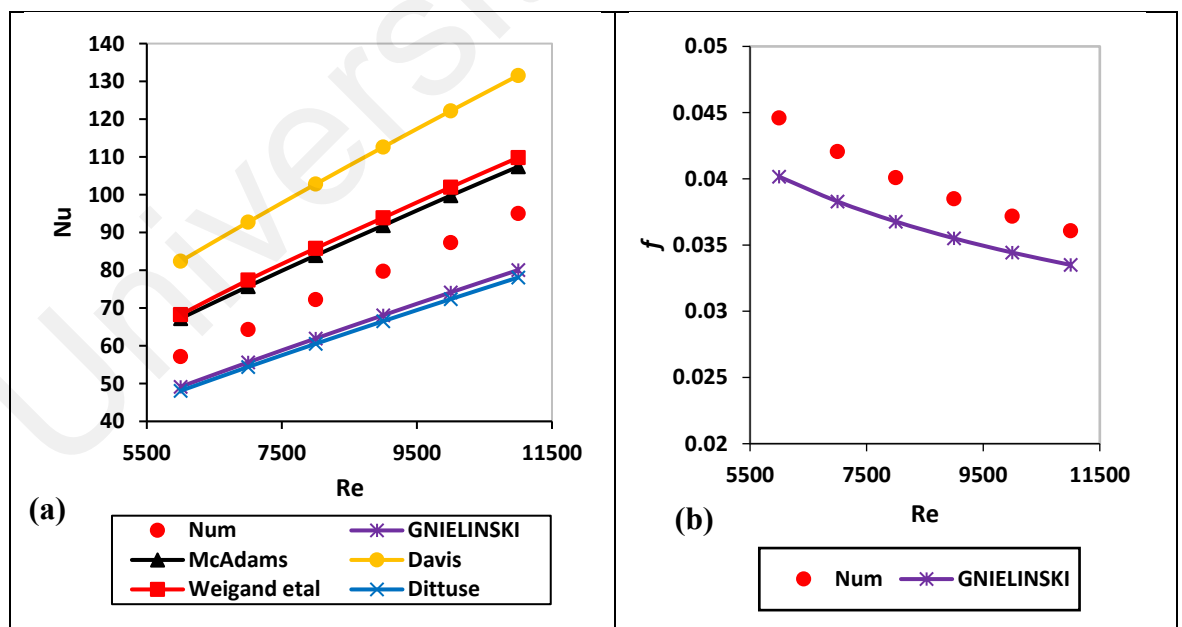
Figure 4-52: Validation curves of the numerical results: (a) Average Nusselt number and (b) Average friction factor.

4.4.2.2   Thermal and flow characteristics of the annular flow

Evaluation of the average Nusselt number and friction factor under turbulent flow conditions inside a circular annulus is still debated. Some researchers tend to use the same correlations of the circular tube by replacing the hydraulic diameter with the physical diameter of the circular pipe. In contrast, others reject that treatment due to the effect of annulus diameter ratios. Gnielinski (2009) modified the equation presented by Petukhov and Kirillov for the circular pipes to suit the evaluation of the Nusselt number inside the annular passages by multiplying the equation with the entrance correction factor. That factor was greater than unity, which refers to the higher Nusselt number for annular passage compared to circular cross-sections of the same hydraulic diameter. Also, Gnielinski (2015) and Barrow (1955) concluded that the average friction inside the annulus is higher than inside the circular tube for the same Reynolds number and hydraulic diameter and, accordingly, the pressure drop. Those conclusions were tested for the numerical results of the current study using the DW.

Figure 4-53(a) shows the average Nusselt number evaluated numerically for all configurations in the current study. The average Nusselt number of the annular concentric passage is higher than the circular and square tubes of the same hydraulic diameter. The average Nu number in the concentric annulus was higher than the circular pipe with 3.5%, matching Deissler and Taylor's results (1955). Figure 4-53(b) shows the pressure drop per unit length profiles for all configurations in the current study. The average increment percentage between the annular passage and the circular tube was 7.12%.
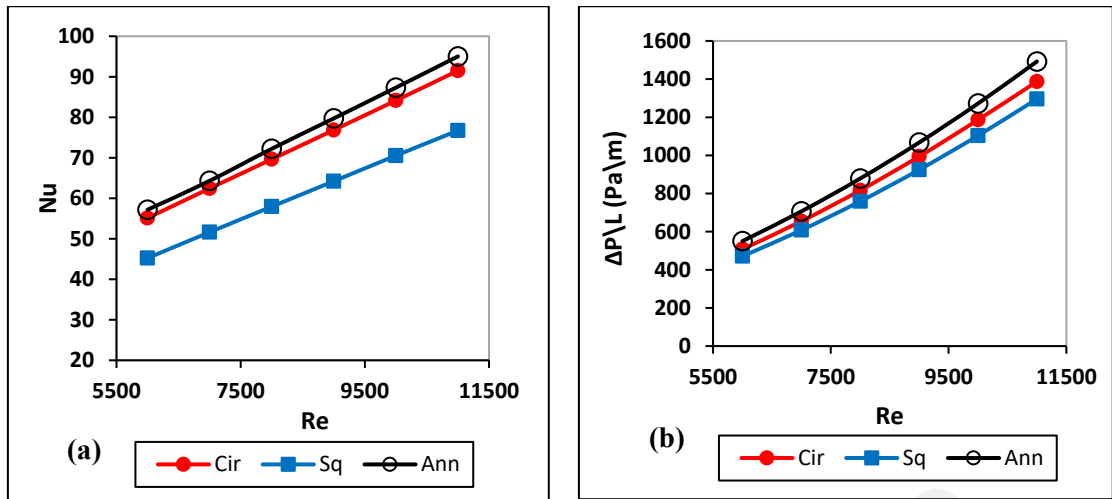
Figure 4-53: A comparison between the numerically evaluated parameters for different configurations of the same D_h: (a) Average Nusselt number, (b) pressure drop per unit length.

Figures 4-54 and 4-55 show the velocity profiles of the distilled water inside the annulus at different axial distances for the zero-eccentricity case (concentric case) and the maximum eccentricity case ($e^* = 0.6$) at the highest Reynolds number (Re = 11000), respectively. The velocity profile for the concentric case in Fig. 4-54 shows that the entrance length is nearly ten times the hydraulic diameter, which matches the standard conditions of the internal turbulent flow (Cengel, 2007). Figure 4-55 shows the effect of the eccentricity on the velocity profile. The lower side of the annulus became narrow, the flow resistance increased, and the top side became wider, decreasing the flow resistance at that side. Therefore, the fluid velocity in the narrow space decreased gradually when the eccentricity increased, which increased the fluid temperature in the narrow area than that in the wide area of the annulus, as shown in Figure 4-56.

Figure 4-57 shows the contour map of the flow separation that occurs in the eccentric annulus and increases with the eccentricity value. This flow separation leads to a nonuniform temperature distribution along the annulus for the inner tube surface or the fluid, as shown in Figure 4-58. Due to the nonuniform temperature distribution, the convection heat transfer coefficient and the Nusselt number were calculated using equations (3-21) and (3-22), respectively, based on the bulk average surface temperature

of the inner tube surface and the inlet and outlet flow temperature as recommended by

Deissler and Taylor (1955).
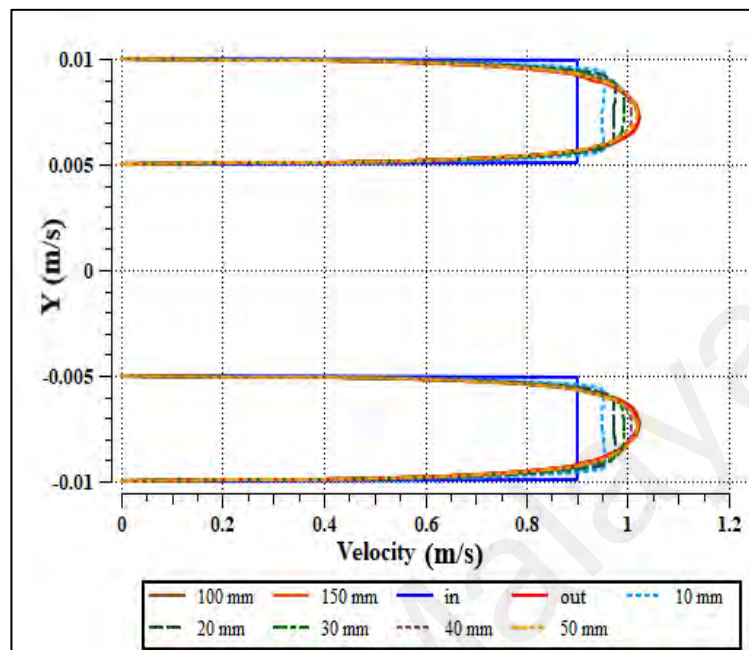
Figure 4-54: The Concentric velocity profile development in the annular space for the DW Run at Re = 11000.
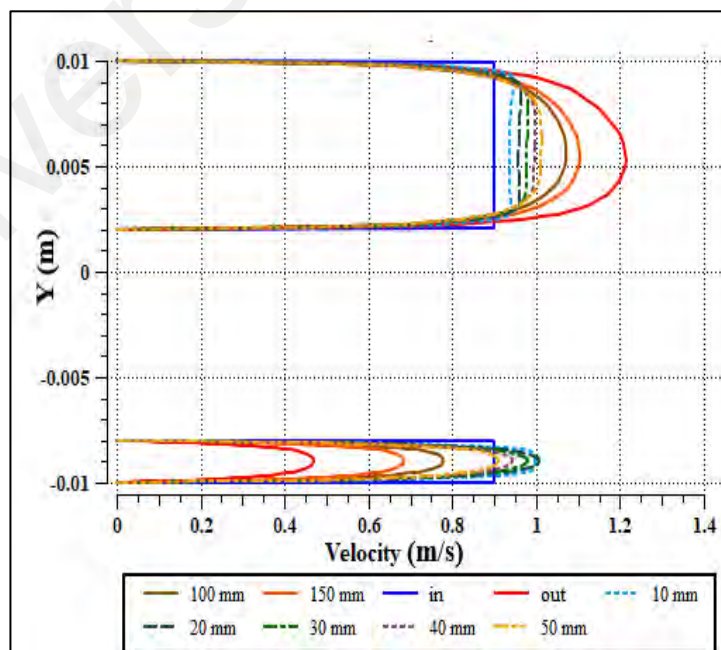
Figure 4-55: The velocity profile development in the annular space for the DW Run at Re = 11000 and (b) e* = 0.6.
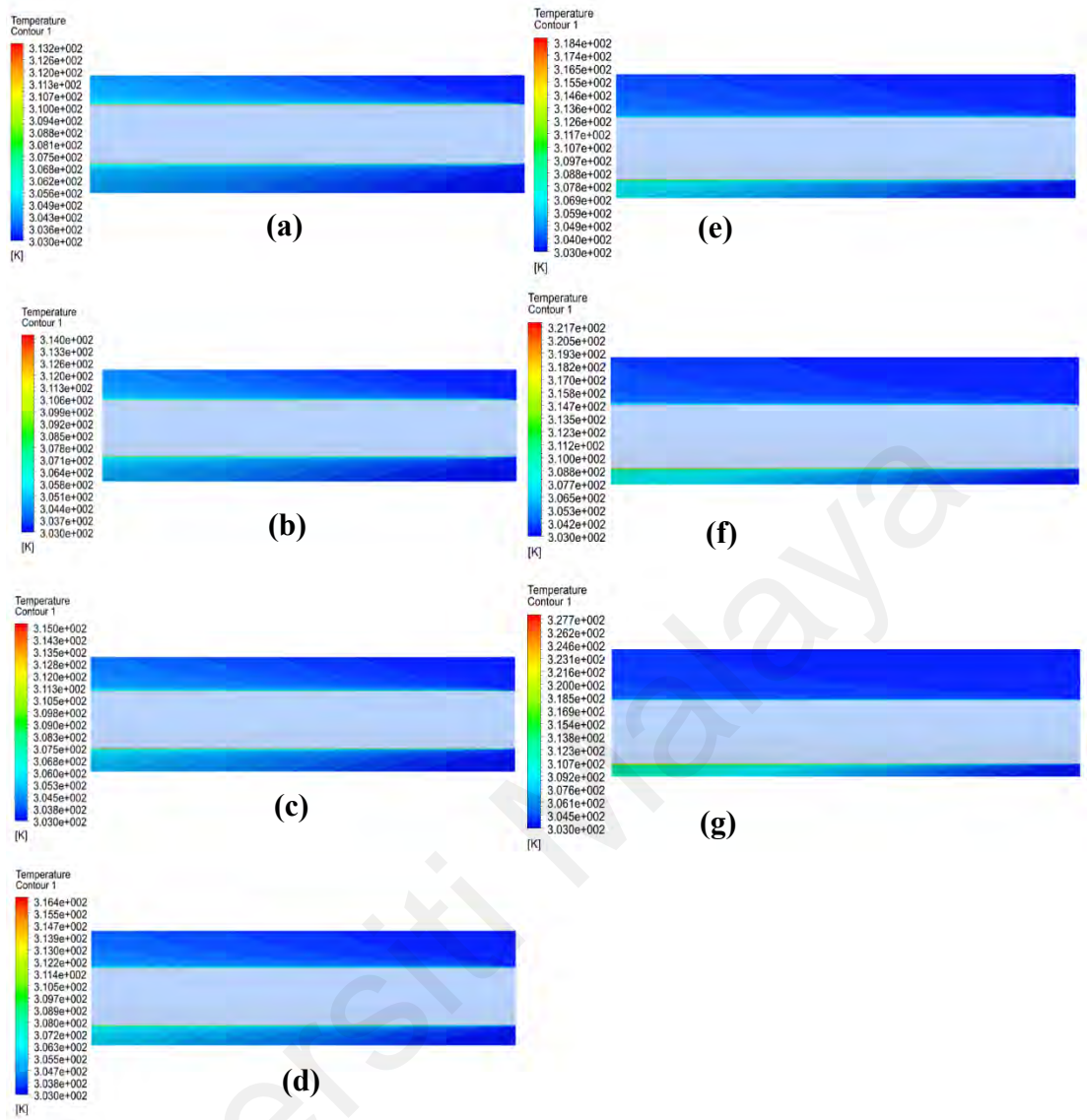
Figure 4-56: The temperature contours of the DW Run at Re = 11000: (a) e* = 0.0, (b) e*** = 0.1, (c) e*** = 0.2, (d) e*** = 0.3, (e) e*** =0.4, (f) e*** = 0.5, and (g) e*** = 0.6.**
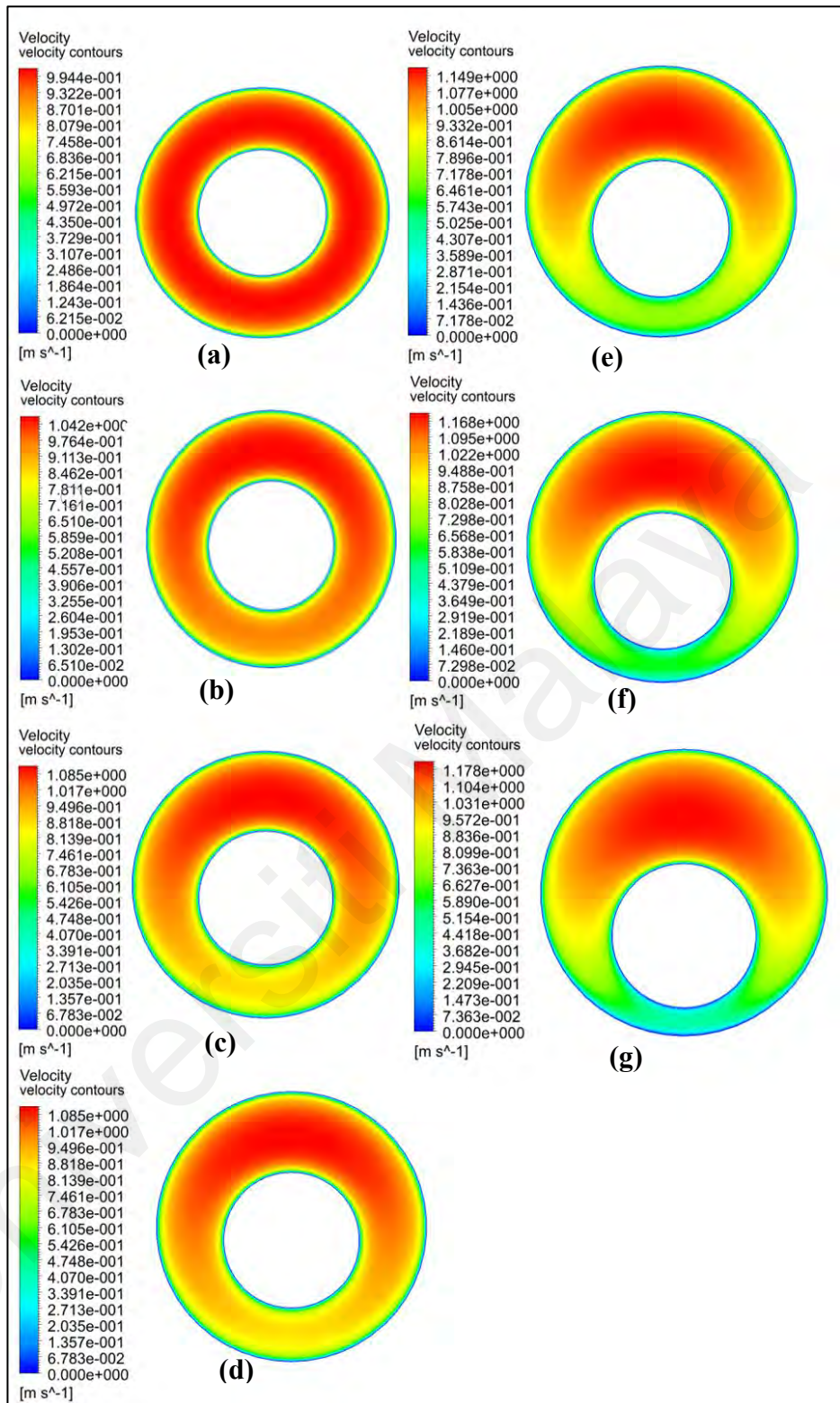
Figure 4-57: The outlet velocity contours of the DW Run at Re = 11000: (a) e* = 0.0, (b) e* = 0.1, (c) e* = 0.2, (d) e* = 0.3, (e) e* =0.4, (f) e* = 0.5, and (g) e* = 0.6.
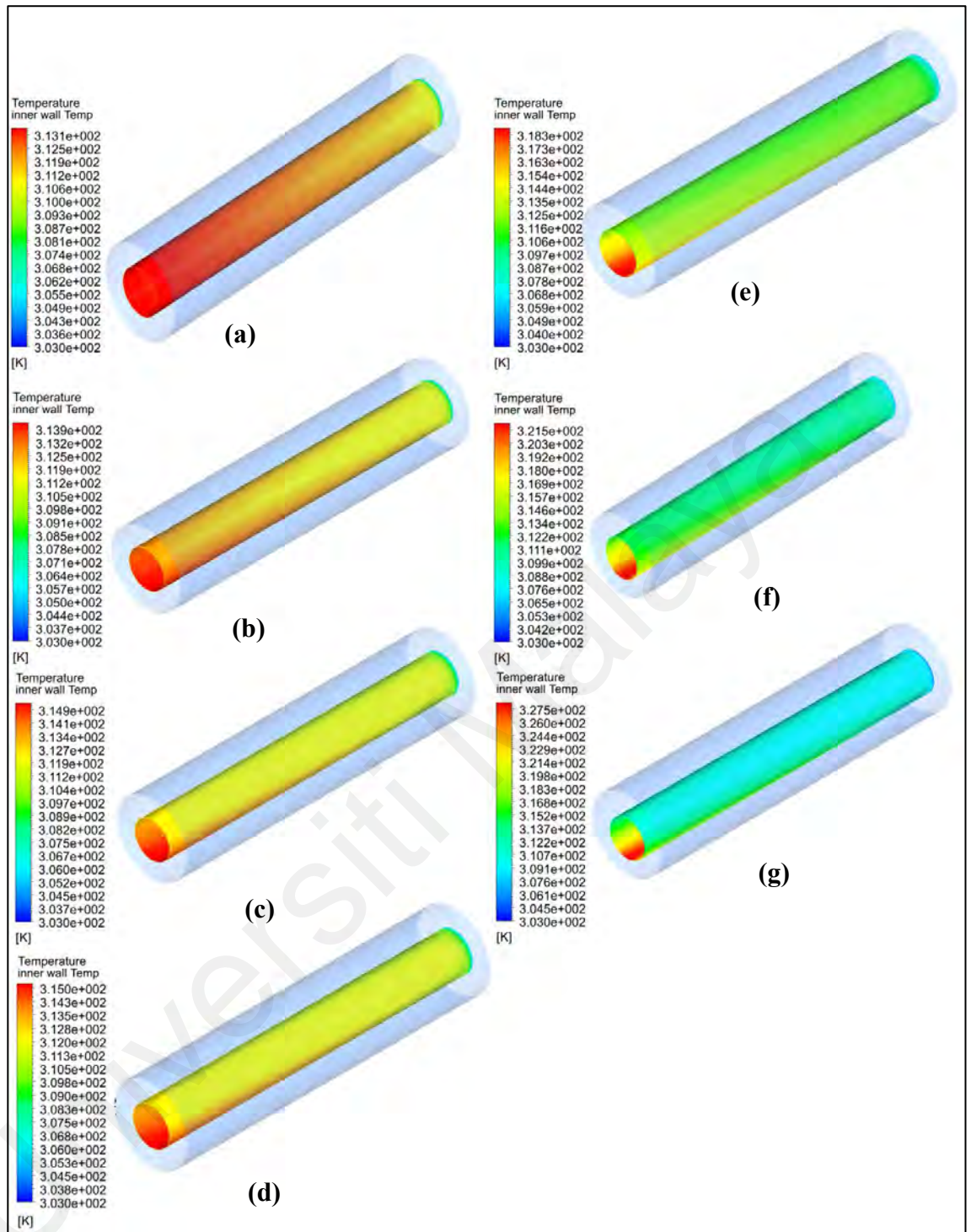
Figure 4-58: The contours of the inner wall temperature of the DW Run at Re = 11000: (a) $e^* = 0.0$, (b) $e^* = 0.1$, (c) $e^* = 0.2$, (d) $e^* = 0.3$, (e) $e^* = 0.4$, (f) $e^* = 0.5$, and (g) $e^* = 0.6$.

The deterioration in the temperature distribution caused a drop in the heat transfer rate in comparison with the concentric case, as shown in Figure 4-59(a), where the average Nusselt number decreased when the eccentricity increased, which agrees with the published work of Lee and Barrow (1963), Deissler and Taylor (1955), Kline and

Tavoularis (2015), and Alassar (2017). Figure 4-59-a also shows that the difference between the Nusselt number for the concentric and eccentric cases increases as the Reynolds number increases due to the increase of the flow separation at the high velocities. Also, the significant flow separation increases the collapse of the temperature distribution along the circumferential wall of the inner tube surface.

Deissler and Taylor (1955) stated that the wall shear stress should decrease when the eccentricity increases. Therefore, the friction factor will decrease accordingly. It is directly proportional to the wall shear stress according to equation (3-19) which is confirmed in the current study as shown in Figure 4-59(b).
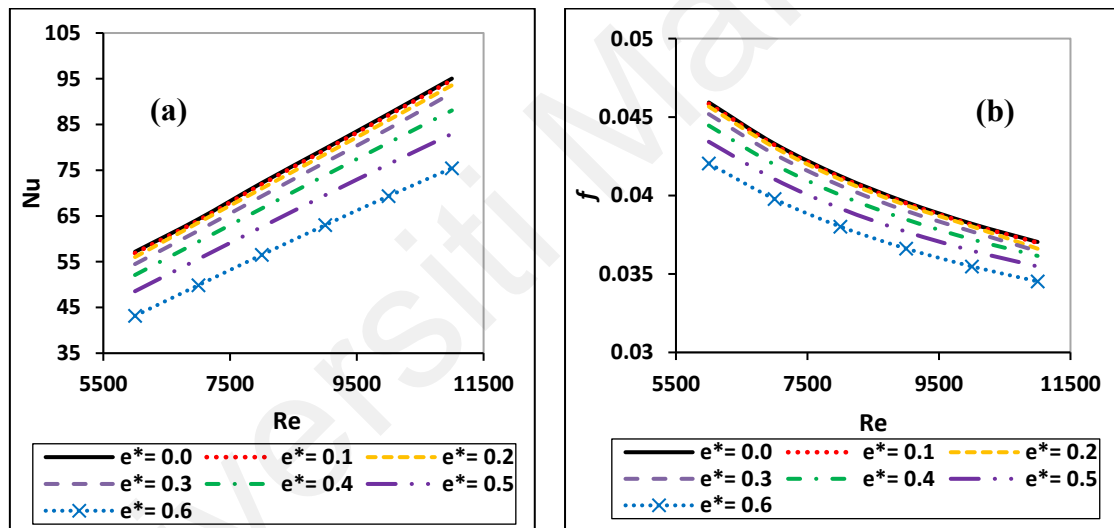
Figure 4-59: Profiles of (a) Average Nusselt number, (b) Average friction factor for the DW at different eccentricity values.

The average reduction percentages of the Nusselt number due to the eccentricity effect are 0.412 %, 1.586 %, 3.904 %, 7.69 %, 13.34 %, and 21.817 % for the eccentricities 0.1, 0.2, 0.3, 0.4, 0.5, and 0.6, respectively. The reduction of the friction factor due to eccentricity effect is an indication to the reduction of the pressure drop as well where, the friction factor reduction percentages for the eccentricities 0.1, 0.2, 0.3, 0.4, 0.5, and 0.6 are 0.164 %, 0.617 %, 1.479 %, 2.824 %, 4.852 %, and 7.627 %, respectively. Therefore, the performance evaluation of the nanofluids in the eccentric heat exchanger

is important to know if the nanofluids can compensate for the reduction of the convection heat transfer due to the eccentricity effect.

4.4.2.3 Heat transfer and pressure drop of nanofluids in the concentric annulus.

Figure 4-60 shows the profiles of Nusselt number for different nanofluid concentrations used in this study. As discussed earlier with the circular and square pipe, the Prandtl number has the main effect on the Nusselt number enhancement at the same Reynolds number, where the SiO_2 /DW nanofluid showed the highest enhancement percentages of 5.26%, 4.19%, and 3.02% for the concentrations 0.1 wt.%, 0.075 wt.%, and 0.05 wt.%, respectively. The Al_2O_3 / DW nanofluid showed an enhancement of 4.54%, 3.99%, and 2.02% for the concentrations 0.1 wt.%, 0.075 wt.%, and 0.05 wt.%, respectively. When using the hybrid nanofluid, the enhancement occurred was 4.22%, 3.75%, and 2.39%, for the concentrations 0.1 wt.%, 0.075 wt.%, and 0.05 wt.%, respectively.

Figure 4-61 shows the pressure drop per unit length variation with the Reynolds number for all nanofluid concentrations. The SiO_2 /DW nanofluid showed the highest pressure drop increment percentage, followed by the hybrid nanofluid, and the lowest increment percentages were obtained from the Al_2O_3 / DW nanofluid. For 0.1 wt.% concentration, the SiO_2 /DW nanofluid caused an average percentage increase in pressure drop of 22.24%. The hybrid nanofluid caused an increment of 20.71%, and the percentage increasing was 19.72% in the case of Al_2O_3 / DW nanofluid. A 17.2% average increment was obtained with the SiO_2 /DW nanofluid of 0.075 wt.% concentration, and the hybrid nanofluid of the same concentration caused an average increment of 17.09%, and the Al_2O_3 / DW nanofluid of 0.075 wt.% caused a 16.93% average increment. Average increments of 11.51%, 9.47%, and 7.39% were obtained with the SiO_2 /DW nanofluid,

hybrid nanofluid, and Al₂O₃ / DW nanofluid, respectively, for the 0.05 wt.% concentration.
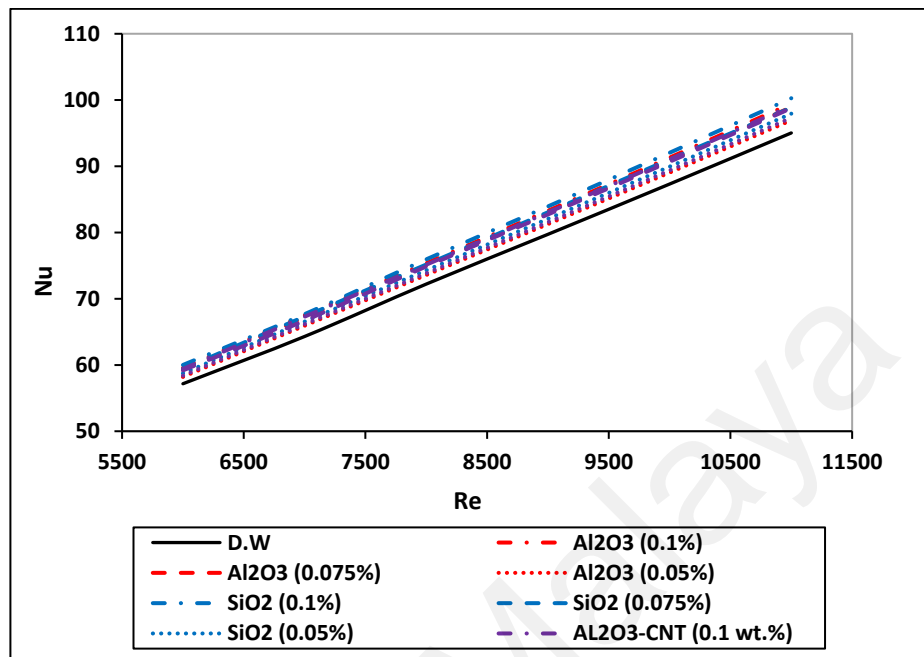
Figure 4-60: Average Nusselt number obtained numerically for the concentric annular heat exchanger.
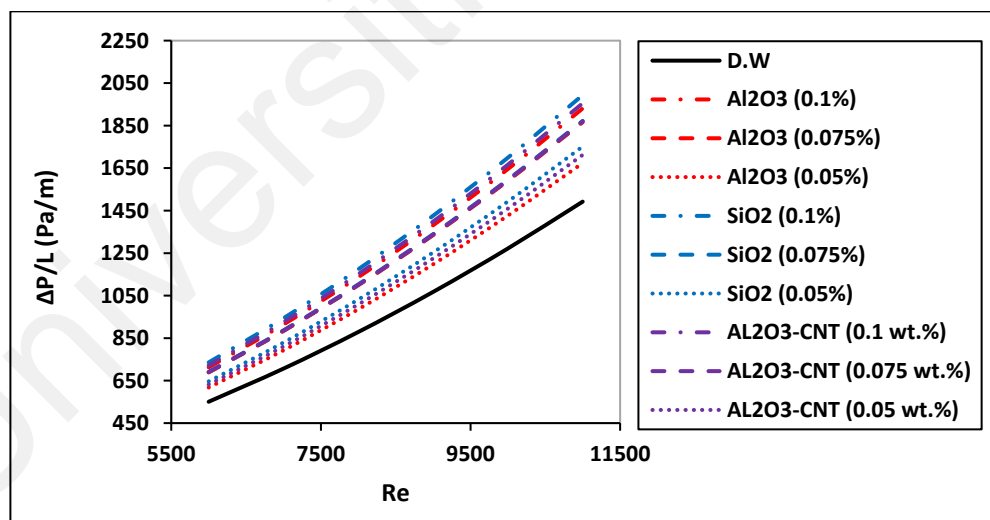
Figure 4-61: pressure drop per unit length obtained numerically for the concentric annular heat exchanger.

A comparison was made to investigate the effect of the same hydraulic diameter pipe configurations on the Nu number, convection heat transfer coefficient, pressure drop, and thermal performance for all nanofluid concentrations. Figure 4-62 shows all pipe configurations' percentage enhancement Nu number, convection heat transfer coefficient,

and pressure drop. Even though the differences were too small, the annular heat exchanger showed the highest enhancement percentages compared to the circular and square cross-sections. Figure 4-63 shows the average performance index that performed numerically for all nanofluid concentrations in the three pipes configurations. The data in the figure represents the average value of the performance index at different Reynolds numbers for all nanofluid concentrations in the different pipe configurations. As shown in the figure, there are no significant differences between the performance index of each nanofluid concentration through any of the three pipe configurations. The 0.05 wt.% concentration of Al_2O_3 / DW nanofluid has the highest performance index in all pipe configurations either evaluated based on the pressure drop or the pumping power. On the other hand, the 0.1 wt.% SiO_2 /DW nanofluid has the lowest performance index compared to the other nanofluid concentrations for all pipe configurations.
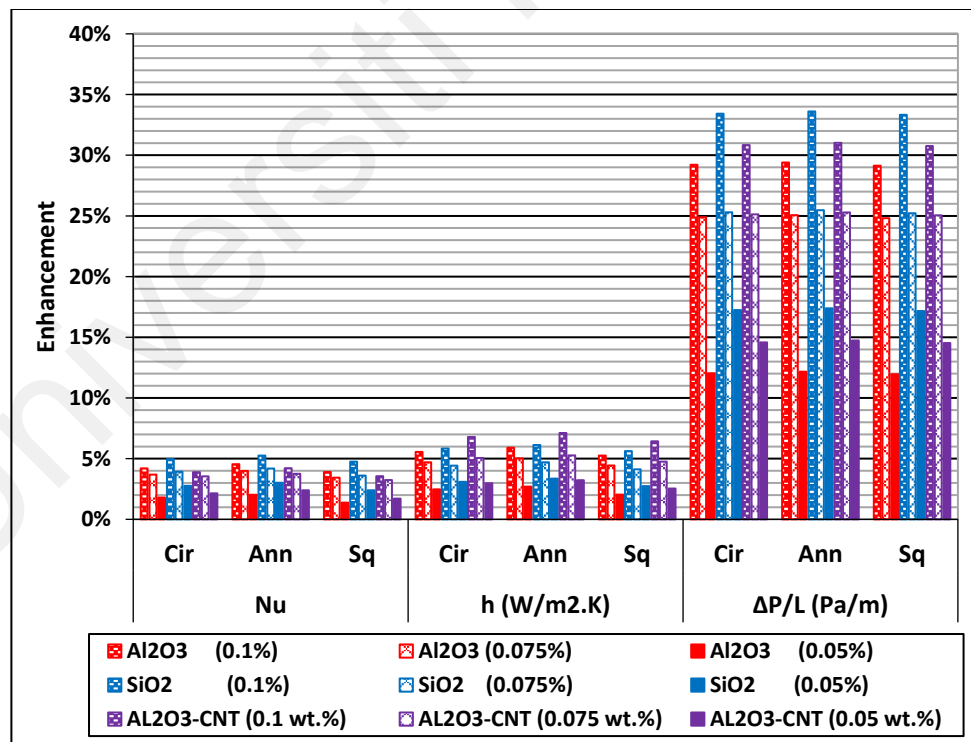
Figure 4-62: The average increment in the heat transfer and pressure drop for all pipe configurations.
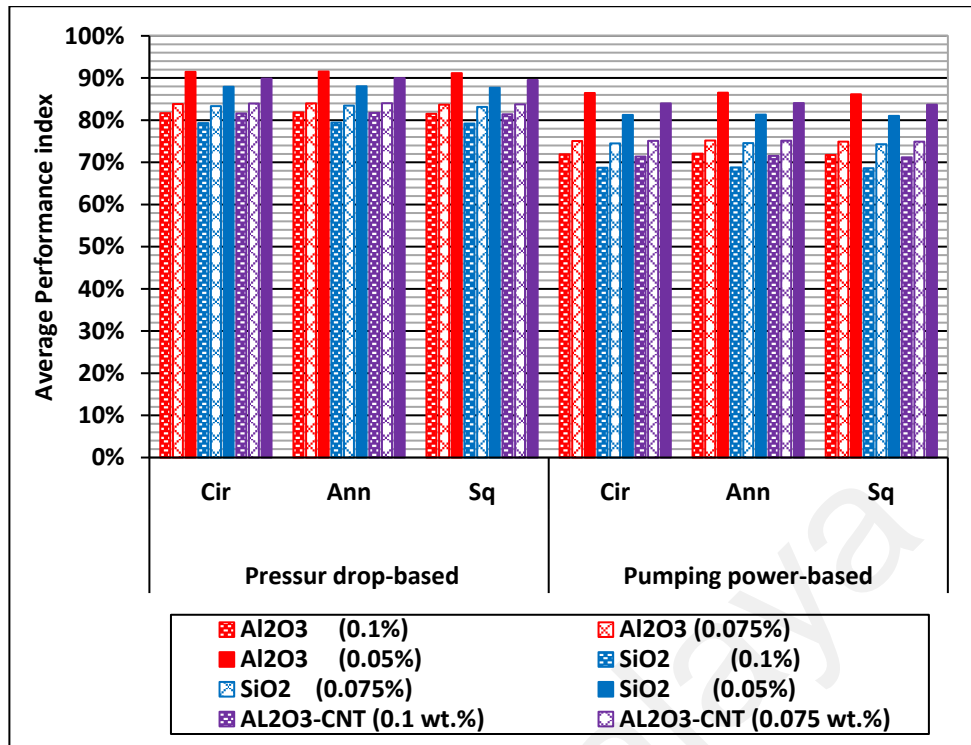
Figure 4-63: The numerically evaluated average performance index for all pipe configurations.

4.4.2.4 Heat transfer and pressure drop of nanofluids in the eccentric annulus

As discussed in part 4.4.2.2, convection heat transfer and pressure drop decrease when the eccentricity of the annular passage increases. Figure 4-64 (a) and (b) show the effect of the eccentricity on the convection heat transfer coefficient and pressure drop of the Al_2O_3 / DW nanofluid of 0.1 wt.% concentration, respectively. The average reduction percentages of the convection heat transfer at the same Reynolds number range due to eccentricity effect were 0.40%, 1.67%, 3.92%, 7.69%, 13.27%, and 21.64% for the eccentricities 0.1, 0.2, 0.3, 0.4, 0.5, and 0.6, respectively. For pressure drop, the average reduction percentages due to eccentricity effect were 0.17%, 0.68%, 1.60%, 3.02%, 5.04%, and 7.81% for the eccentricities 0.1, 0.2, 0.3, 0.4, 0.5, and 0.6, respectively.

Figure 4-65 presents the effect of the eccentricity on the on the convection heat transfer coefficient and pressure drop of the SiO_2 / DW nanofluid of 0.1 wt.% concentration. The average reduction percentages of the convection heat transfer due to eccentricity effect were 0.36%, 1.59%, 3.91%, 7.60%, 13.18%, and 21.53% for the eccentricities 0.1, 0.2,

0.3, 0.4, 0.5, and 0.6, respectively. The pressure drop reduction percentages were 0.17%, 0.68%, 1.60%, 3.02%, 5.04%, and 7.81% for the eccentricities 0.1, 0.2, 0.3, 0.4, 0.5, and 0.6, respectively.

Figure 4-66 presents the effect of the eccentricity on the on the convection heat transfer coefficient and pressure drop of the hybrid nanofluid of 0.1 wt.% concentration. The average reduction percentages of the convection heat transfer due to eccentricity effect were 0.36%, 1.59%, 3.91%, 7.60%, 13.18%, and 21.53% for the eccentricities 0.1, 0.2, 0.3, 0.4, 0.5, and 0.6, respectively. The pressure drop reduction percentages were 0.17%, 0.68%, 1.60%, 3.02%, 5.04%, and 7.81% for the eccentricities 0.1, 0.2, 0.3, 0.4, 0.5, and 0.6, respectively.

According to the above results, the eccentricity significantly impacts the convection heat transfer coefficient compared to pressure drop. This effect is nearly the same for all fluids, reflecting the considerable effect of the flow separation on the convection heat transfer compared to the pressure drop.

A comparison was made between the eccentric convection heat transfer of nanofluids and the DW's concentric convection heat transfer coefficient to investigate if the nanofluids can compensate for the reduction in the convection heat transfer of the DW due to eccentricity effect or not. The highest and lowest concentration of all nanofluids were selected for this comparison, and the results are shown in Figure 4-67. For 0.05 wt.%, the Al_2O_3 / DW nanofluid showed a higher convection heat transfer coefficient at the eccentricities 0.1 and 0.2 than DW's convection coefficient at the concentric case. The SiO_2 / DW and the hybrid nanofluids showed a higher convection heat transfer coefficient at the same eccentricities. For the 0.1 wt.%, all nanofluids showed a higher convection heat transfer coefficient at the eccentricities 0.1, 0.2, and 0.3 than the DW's convection coefficient at the concentric case. These results showed that the nanofluid, even with a

very low concentration, can be used as an alternative heat transfer fluid in eccentric heat exchanger applications because it can compensate for some heat transfer loss due to the eccentricity effect.
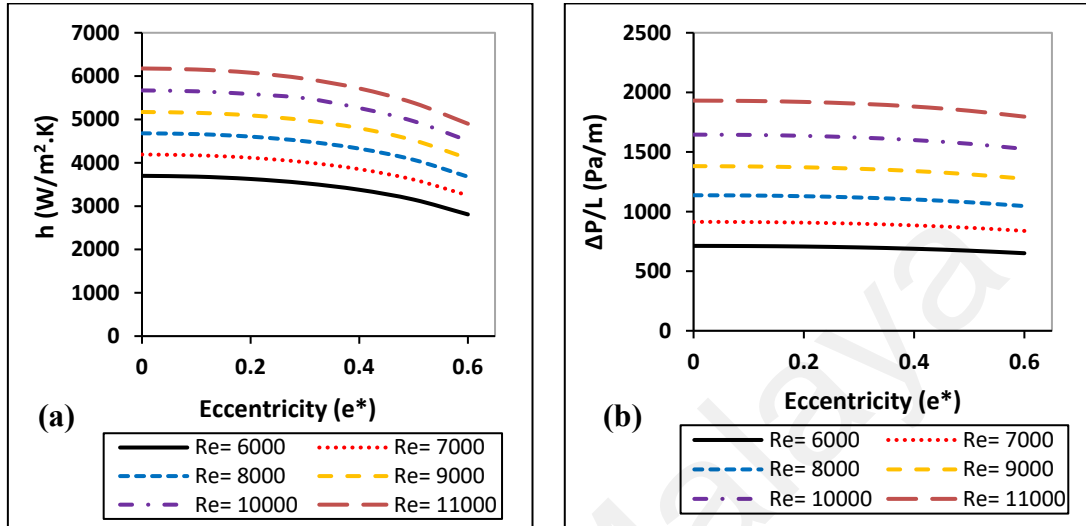
Figure 4-64: The eccentricity effect on the: (a) convection heat transfer coefficient, (b) pressure drop per unit length of the Al_2O_3 /DW nanofluid with 0.1 wt.% concentration.
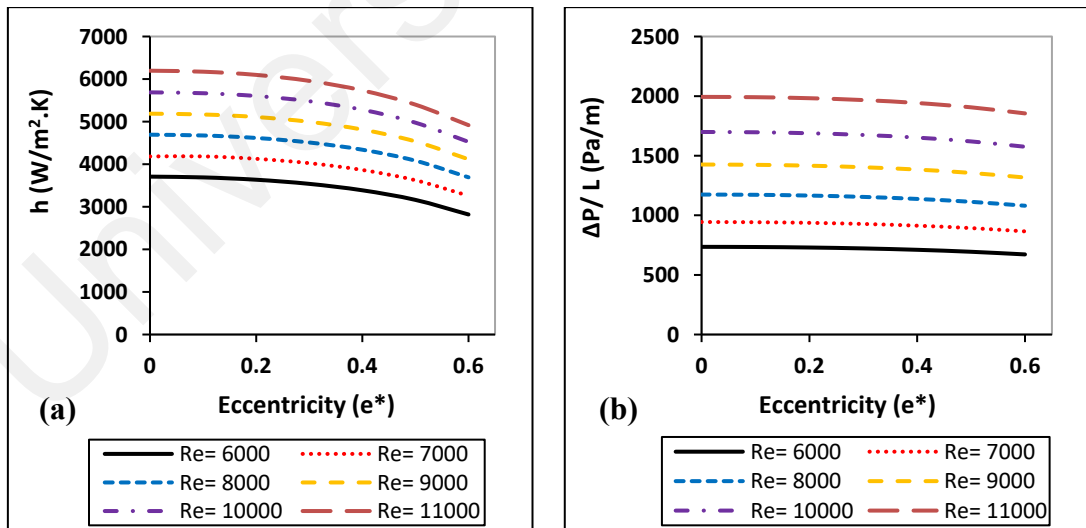
Figure 4-65: The eccentricity effect on the: (a) convection heat transfer coefficient, (b) pressure drop per unit length of the SiO_2 nanofluid with 0.1 wt.% concentration.
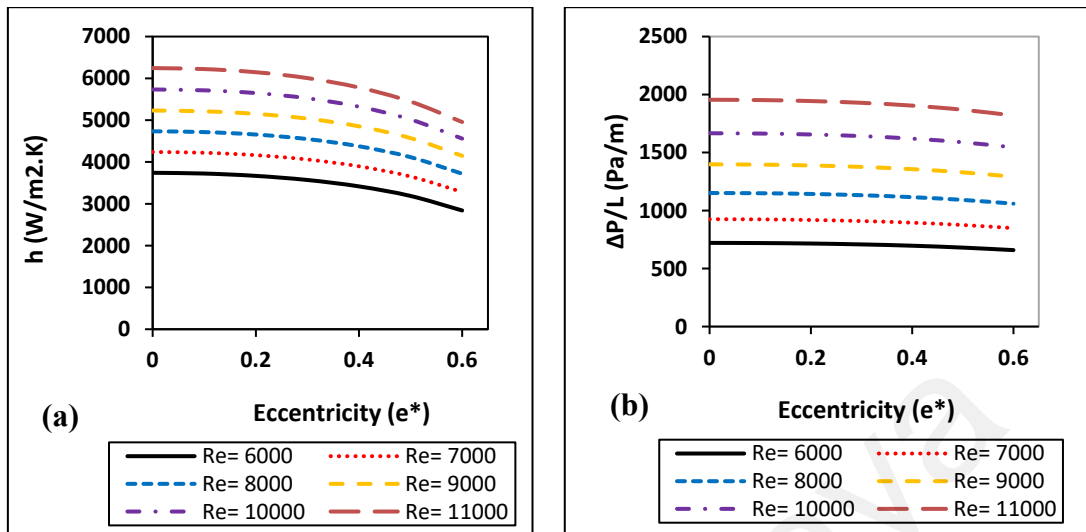
Figure 4-66: The eccentricity effect on the: (a) convection heat transfer coefficient, (b) pressure drop per unit length of the Hybrid nanofluid with 0.1 wt.% concentration.
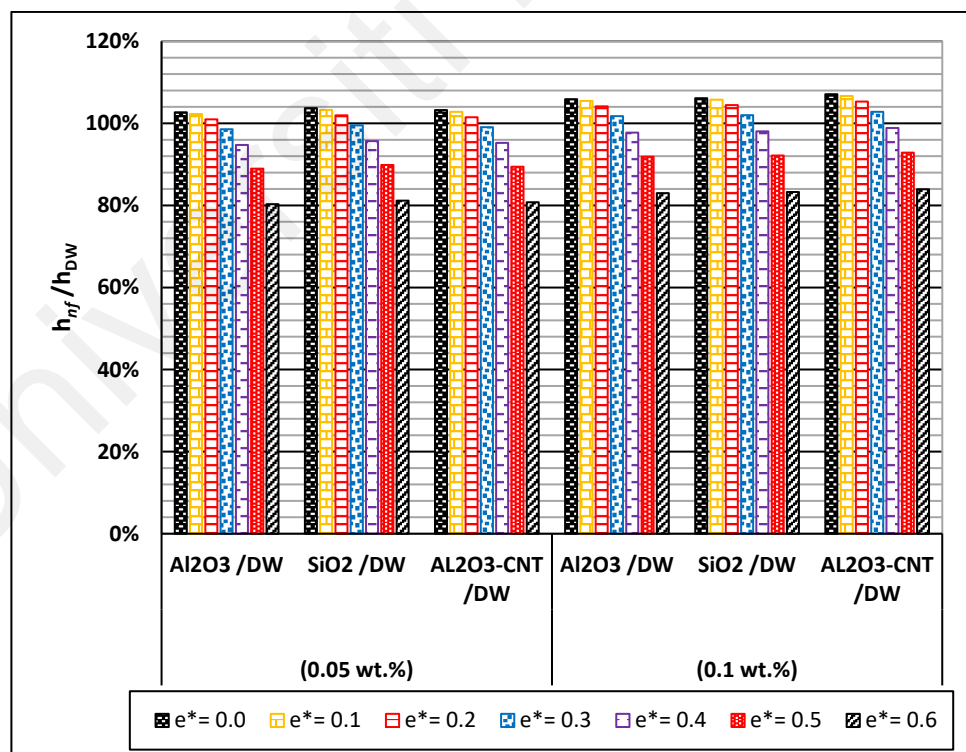
Figure 4-67: The average convection heat transfer coefficents ratio at different eccentricities.

CHAPTER 5: CONCLUSIONS AND FUTURE WORK

5.1   Introduction

The objectives of the current study were achieved by preparing three different nanofluids and evaluating their thermal performance experimentally and numerically compared to the DW. Characterization, stability, and thermophysical evaluation were performed for all nanofluid samples. The thermal performance for DW and all nanofluids was performed experimentally and numerically for different pipe geometries of the same hydraulic diameter. The experimental part covers the nanofluids' thermal performance evaluation in pipes with circular and square cross-sections. The numerical part covers the nanofluids' thermal performance evaluation in circular, square, and annular pipe cross-sections. The experimental and numerical work was conducted under the same forced turbulent flow conditions with Re numbers range from 6000 to 11000. In this chapter, the research findings will be pointed out, and the recommendation for future work will be presented.

5.2   Research conclusions

Based on the experimental and numerical results of the current study, all the objectives are achievable and being confirmed, and the findings can be concluded as follow:

1. Two single and one hybrid composite aqua-based nanofluids were prepared in different nanofluid concentrations of 0.1, 0.075, and 0.05 wt.% using the two-step method. Silica, Alumina, and Pristine MWCNTs nanopowder were purchased commercially to prepare the metal oxide nanofluid, and the Alumina coated f-MWCNTs hybrid nanofluid at different mixing ratios. The acid treatment method was employed to functionalize the MWCNTs. The synthesizing and functionalization processes were successful based on the different results of FTIR, RAMAN, FESEM, and SDS analysis. Based

on the (UV-Vis) spectrum evaluation, the stability test showed that all the nanofluid samples were dispersed well over 15 days. All nanofluid concentrations showed a stability ratio over 93%.

2. Based on the thermophysical properties evaluation at 30 °C for all nanofluid concentrations in comparison with the DW, the hybrid nanofluid showed the highest enhancement in thermal conductivity (2.77%, 1.47%, and 0.815%), followed by the Alumina (1.31%, 0.978%, and 0.653%), and finally the Silica nanofluids (0.816%, 0.489%, and 0.326%). In contrast, the Prandtl number showing a different trend for the same nanofluids where its % enhancement for the silica nanofluid concentrations were the highest (33.31%, 26.57%, and 21.58%), followed by the Alumina (30.5%, 25.96%, and 20.68%), and finally the hybrid nanofluid (29.58%, 25.58%, and 20.64%). Our results showed that the Prandtl number has the most significant effect on the Nusselt number, which interfered with the impact of thermal conductivity on the convection heat transfer coefficient. Therefore, it is not necessary that the higher the thermal conductivity, the higher the Nusselt number. The results also showed that the dynamic and kinematic viscosity product has the most significant effect on the pressure drop. So, the dynamic viscosity can be considered as a critical parameter, where it has a considerable impact on the Prandtl number and pressure drop.

3. The thermal performance comparison for the current experimental work showed that the max enhancement in h $(W/m^2.K)$ was 9.02% for the circular pipe and 8.16% for the square duct. The max pressure drop %increment was 33.42 and 27.5 for the circular and square duct, respectively. Moreover, the performance index evaluation for all nanofluid

concentrations showed that the DW was economically efficient compared to the nanofluids unless we target the enhancement in heat transfer regardless of the cost of pressure drop or pumping power. The numerical results showed the geometry effect on the Nu number and pressure drop, where the concentric annular pipe showed an average increment of Nu (3.5% and 19.7%) and pressure drop increment of (7.12%, 13.61%) for the same Re number range compared to the circular and square pipe, respectively.

4. Evaluation of heat transfer and pressure drop in the annular pipe with different vertical eccentricities ($e^* = 0.1$ to $e^* = 0.6$) were conducted numerically. The results showed that the heat transfer and friction loss decrease when the eccentricity increased. The convection heat transfer coefficient recorded the lowest average reduction of 0.40% and the highest average reduction of 21.64% at the eccentricities 0.1 and 0.6, respectively. The pressure drop recorded the lowest average reduction of 0.17% and the highest average reduction of 7.81% at the eccentricities 0.1 and 0.6, respectively. Another comparison was made between the convection heat transfer coefficient of the lowest and highest nanofluid concentrations at different eccentricities and the convection heat transfer coefficient of the DW at the concentric case. This comparison showed that all nanofluids at the concentration 0.05 wt.% gave a higher convection heat transfer coefficient at the eccentricities 0.1 and 0.2 than the DW at the concentric case. Also, it showed that all nanofluids at the concentration 0.1 wt.% gave a higher convection heat transfer coefficient at the eccentricities 0.1, 0.2, and 0.3 compared to the DW at the concentric case.

5. Finally, the nanofluids' thermal performance in all pipe configurations showed that the DW is still considered the best choice as a convective medium unless heat transfer enhancement is targeted, regardless of the penalty due to pumping power or pressure drop increment.

5.3   Recommendations for future work

Based on the findings of the current study, some specific subjects may be addressed for future work on nanofluid studies, as stated below:

1. The researchers could focus on synthesizing a new nanocomposite material with high specific heat and thermal conductivity to enhance the Prandtl number of nanofluids. Mixing three or more nanoparticles in a stable colloid may be helpful for controlling more, the nanofluid thermophysical properties.

2. The researchers are advised to perform an optimization study for the hybrid nanofluid with different mixing ratios to get the best mixing ratio that can give the best thermal performance.

3. The researchers could perform an extension for the current numerical work by fabricating an annular passage with various eccentricities and evaluate the thermal performance of nanofluids in the eccentric annular conduit experimentally.

4. A comparative and optimization study using different cross-sections configuration of the annular conduit may be performed experimentally under different boundary conditions.

REFERENCES

Abareshi, M., Goharshiadi, E. K., Zebarjad, S. M., Fadafan, H. K., & Youssefi, A. (2010). Fabrication, characterization and measurement of thermal conductivity of Fe3O4 nanofluids. *Journal of Magnetism and Magnetic Materials, 322*. doi:10.1016/j.jmmm.2010.08.016

Abdolbaqi, M. K., Azmi, W. H., Mamat, R., Sharma, K. V., & Najafi, G. (2016). Experimental investigation of thermal conductivity and electrical conductivity of BioGlycol–water mixture based Al2O3 nanofluid. *Applied Thermal Engineering, 102*(Supplement C), 932-941. doi:https://doi.org/10.1016/j.applthermaleng.2016.03.074

Abdolbaqi, M. K., Azwadi, C. S. N., & Mamat, R. (2014). Heat transfer augmentation in the straight channel by using nanofluids. *Case Studies in Thermal Engineering, 3*, 59-67. doi:https://doi.org/10.1016/j.csite.2014.04.001

Abdolbaqi, M. K., Sidik, N. A. C., Rahim, M. F. A., Mamat, R., Azmi, W. H., Yazid, M. N. A. W. M., & Najafi, G. (2016). Experimental investigation and development of new correlation for thermal conductivity and viscosity of BioGlycol/water based SiO2 nanofluids. *International Communications in Heat and Mass Transfer, 77*(Supplement C), 54-63. doi:https://doi.org/10.1016/j.icheatmasstransfer.2016.07.001

Akilu, S., Sharma, K. V., Baheta, A. T., & Mamat, R. (2016). A review of thermophysical properties of water based composite nanofluids. *Renewable & Sustainable Energy Reviews, 66*, 654-678. doi:10.1016/j.rser.2016.08.036

Alassar, R. S. (2017). Slip Flow in Eccentric Annuli. *Journal of Fluids Engineering, 139*(4), 041201-041201-041207. doi:10.1115/1.4035115

Alawi, O. A., Sidik, N. A., Che Xian, Wei, H., Kean, T. H., & Kazi, S. N. (2018). Thermal conductivity and viscosity models of metallic oxides nanofluids. *International Journal of Heat and Mass Transfer, 116*(Supplement C), 1314-1325. doi:https://doi.org/10.1016/j.ijheatmasstransfer.2017.09.133

Angayarkanni, S. A., & Philip, J. (2015). Review on thermal properties of nanofluids: Recent developments. *Advances in Colloid and Interface Science, 225*, 146-176. doi:http://dx.doi.org/10.1016/j.cis.2015.08.014

Arzani, H. K. A., Ahmad Kazi, S. N. Chew, B. T. Badarudin, A. (2015). Experimental and numerical investigation of thermophysical properties, heat transfer and pressure drop of covalent and noncovalent functionalized graphene nanoplatelet-based water nanofluids in an annular heat exchanger. *International Communications in Heat and Mass Transfer, 68*, 267-275. doi:http://dx.doi.org/10.1016/j.icheatmasstransfer.2015.09.007

Bahmani, M. H. S., Ghanbarali; Zarringhalam, Majid; Akbari, Omid Ali; Alrashed, Abdullah A. A. A.; Shabani, Gholamreza Ahmadi Sheikh; Goodarzi, Marjan. (2018). Investigation of turbulent heat transfer and nanofluid flow in a double pipe

heat exchanger. *Advanced Powder Technology, 29*(2), 273-282. doi:https://doi.org/10.1016/j.apt.2017.11.013

Barrow, H. (1955). Fluid Flow and Heat Transfer in an Annulus with a Heated Core Tube. *Proceedings of the Institution of Mechanical Engineers, 169*(1), 1113-1124. doi:10.1243/PIME_PROC_1955_169_109_02

Batchelor, G. K. (2006). The effect of Brownian motion on the bulk stress in a suspension of spherical particles. *Journal of Fluid Mechanics, 83*(1), 97-117. doi:10.1017/S0022112077001062

Beck, M., Yuan, Y., Warrier, P., & Teja, A. (2009). The effect of particle size on the thermal conductivity of alumina nanofluids. *Journal of Nanoparticle Research, 11*(5), 1129-1136. doi:10.1007/s11051-008-9500-2

Bergman, T. L., Incropera, F. P., DeWitt, D. P., & Lavine, A. S. (2011). *Fundamentals of heat and mass transfer*: John Wiley & Sons.

Bisht, P., Joshi, M., & Gupta, A. (2014). Comparison of Heat Transfer between a Circular and Rectangular Tube Heat Exchanger by using Ansys Fluent. *International Journal of Thermal Technologies, 4*(2), 88-92.

Boertz, H., J. Baars, A., Cieśliński, J. T., & Smolen, S. (2018). Numerical Study of Turbulent Flow and Heat Transfer of Nanofluids in Pipes. *Heat Transfer Engineering, 39*(3), 241-251. doi:10.1080/01457632.2017.1295739

Bönnemann, H., Botha, S. S., Bladergroen, B., & Linkov, V. M. (2005). Monodisperse copper- and silver-nanocolloids suitable for heat-conductive fluids. *Applied Organometallic Chemistry, 19*(6), 768-773. doi:10.1002/aoc.889

Branch, C. A. (1991). *Heat transfer and heat transfer fouling in evaporators with Kraft pulp black liquor.* (PhD), The University of Auckland, Auckland, New Zealand. Retrieved from https://researchspace.auckland.ac.nz/handle/2292/50996

Brinkman, H. C. (1952). The Viscosity of Concentrated Suspensions and Solutions. *The Journal of Chemical Physics, 20*(4), 571-571. doi:10.1063/1.1700493

Cantab, B. A. (1963). *Turbulent flow in concentric and eccentric annuli.* (Master of Applied Science), The University of Britich Colombia, Vancover, Canada.

Cengel, Y. A. (2007). *Heat and Mass Transfer: A Practical Approach*: McGraw-Hill Education (India) Pvt Limited.

Chandrasekar, M., Suresh, S., & Chandra Bose, A. (2010). Experimental investigations and theoretical determination of thermal conductivity and viscosity of Al2O3/water nanofluid. *Experimental Thermal and Fluid Science, 34*(2), 210-216. doi:https://doi.org/10.1016/j.expthermflusci.2009.10.022

Chen, L., & Xie, H. (2010). Surfactant-free nanofluids containing double- and single-walled carbon nanotubes functionalized by a wet-mechanochemical reaction. *Thermochimica Acta, 497*(1), 67-71. doi:https://doi.org/10.1016/j.tca.2009.08.009

Chen, L., Xie, H., Li, Y., & Yu, W. (2008). Nanofluids containing carbon nanotubes treated by mechanochemical reaction. *Thermochimica Acta, 477*(1), 21-24. doi:https://doi.org/10.1016/j.tca.2008.08.001

Cho, S., Kikuchi, K., & Kawasaki, A. (2012). On the role of amorphous intergranular and interfacial layers in the thermal conductivity of a multi-walled carbon nanotube–copper matrix composite. *Acta Materialia, 60*(2), 726-736. doi:https://doi.org/10.1016/j.actamat.2011.09.056

Choi, S.-K., Kim, S.-O., Lee, T.-H., & Dohee, H. (2014). Computation of the Natural Convection of Nanofluid in a Square Cavity with Homogeneous and Nonhomogeneous Models. *Numerical Heat Transfer, Part A: Applications, 65*(4), 287-301. doi:10.1080/10407782.2013.831695

Choudhary, R., Khurana, D., Kumar, A., & Subudhi, S. (2017). Stability analysis of Al2O3/water nanofluids. *Journal of Experimental Nanoscience, 12*(1), 140-151. doi:10.1080/17458080.2017.1285445

Darzi, A. A. R., Farhadi, M., & Sedighi, K. (2013). Heat transfer and flow characteristics of AL2O3–water nanofluid in a double tube heat exchanger. *International Communications in Heat and Mass Transfer, 47*, 105-112. doi:https://doi.org/10.1016/j.icheatmasstransfer.2013.06.003

Das, S. K., Choi, S. U. S., Yu, W., & Pradeep, T. (2008). *Nanofluids: Science and Technology*. New Jersey: Wiley.

Das, S. K., Putra, N., Theisen, P., & Roetzel, W. (2003). Temperature dependence of thermal conductivity enhancement for nanofluids. *Journal of Heat Transfer, 125*. doi:10.1115/1.1571080

Davis, E. S. (1943). Heat Transfer and Pressure Drop in Annuli. *Trans. ASME*, 775-760.

Deissler, R. G. (1959). *Analysis of turbulent flow and heat transfer in noncircular passages*: US Government Printing Office.

Deissler, R. G., & Taylor, M. F. (1955). Analysis of fully developed turbulent heat transfer and flow in an annulus with various eccentricities. *NACA Tech. Note, National Advisory Committee for Aeronautics, 3451*.

Diebold, U. (2003). The surface science of titanium dioxide. *Surface Science Reports, 48*(5), 53-229. doi:https://doi.org/10.1016/S0167-5729(02)00100-0

Diessler, R. G. (1953). *Analysis of Turbulent Heat Transfer and Flow in the Entrance Regions of Smooth Passages* (pp. 88). Retrieved from https://books.google.com.my/books?id=YVa-7XIXlyQC

Ding, Y., Alias, H., Wen, D., & Williams, R. A. (2006). Heat transfer of aqueous suspensions of carbon nanotubes (CNT nanofluids). *Int J Heat Mass Transf, 49*. doi:10.1016/j.ijheatmasstransfer.2005.07.009

Dirker, J., & Meyer, J. P. (2004). Convection heat transfer in concentric annuli. *Experimental Heat Transfer, 17*(1), 19-29. doi:10.1080/08916150490246528

Duan, Z., Yovanovich, M. M., & Muzychka, Y. S. (2012). Pressure Drop for Fully Developed Turbulent Flow in Circular and Noncircular Ducts. *Journal of Fluids Engineering, 134*(6), 061201-061201-061210. doi:10.1115/1.4006861

Eastman, J. A., Choi, S. U. S., Li, S., Yu, W., & Thompson, L. J. (2001). Anomalously increased effective thermal conductivities of ethylene glycol-based nanofluids containing copper nanoparticles. *Applied Physics Letters, 78*(6), 718-720. doi:doi:http://dx.doi.org/10.1063/1.1341218

Einstein, A. (1906). Eine neue Bestimmung der Moleküldimensionen. *Annalen der Physik, 324*(2), 289-306. doi:10.1002/andp.19063240204

El-Maghlany, W. M., & Elazm, M. M. A. (2016). Influence of nanoparticles on mixed convection heat transfer in an eccentric horizontal annulus with rotating inner cylinder. *Journal of the Taiwan Institute of Chemical Engineers, 63*, 259-270. doi:https://doi.org/10.1016/j.jtice.2016.03.014

Fedele, L., Colla, L., & Bobbo, S. (2012). Viscosity and thermal conductivity measurements of water-based nanofluids containing titanium oxide nanoparticles. *International Journal of Refrigeration, 35*(5), 1359-1366. doi:https://doi.org/10.1016/j.ijrefrig.2012.03.012

Fedele, L., Colla, L., Bobbo, S., Barison, S., & Agresti, F. (2011). Experimental stability analysis of different water-based nanofluids. *Nanoscale Research Letters, 6*(1), 300-300. doi:10.1186/1556-276X-6-300

Fernández-Seara, J., Uhía, F. J., Sieres, J., & Campo, A. (2007). A general review of the Wilson plot method and its modifications to determine convection coefficients in heat exchange devices. *Applied Thermal Engineering, 27*(17), 2745-2757. doi:https://doi.org/10.1016/j.applthermaleng.2007.04.004

Fertman, V. E., Golovicher, L. E., & Matusevich, N. P. (1987). Thermal conductivity of magnetite magnetic fluids. *Journal of Magnetism and Magnetic Materials, 65*(2), 211-214. doi:https://doi.org/10.1016/0304-8853(87)90034-5

Gavili, A., Zabihi, F., Isfahani, T. D., & Sabbaghzadeh, J. (2012). The thermal conductivity of water base ferrofluids under magnetic field. *Experimental Thermal and Fluid Science, 41*, 94-98. doi:https://doi.org/10.1016/j.expthermflusci.2012.03.016

Ghadimi, A., Saidur, R., & Metselaar, H. S. C. (2011). A review of nanofluid stability properties and characterization in stationary conditions. *International Journal of Heat And Mass Transfer, 54*(17-18), 4051-4068. doi:10.1016/j.ijheatmasstransfer.2011.04.014

Gnielinski, V. (1975). New equations for heat and mass transfer in the turbulent flow in pipes and channels. *NASA STI/recon technical report A, 41*(1), 8-16.

Gnielinski, V. (2009). Heat Transfer Coefficients for Turbulent Flow in Concentric Annular Ducts. *Heat Transfer Engineering, 30*(6), 431-436. doi:10.1080/01457630802528661

Gnielinski, V. (2015). Turbulent Heat Transfer in Annular Spaces—A New Comprehensive Correlation. *Heat Transfer Engineering, 36*(9), 787-789. doi:10.1080/01457632.2015.962953

Habibi Matin, M., & Pop, I. (2013). Natural convection flow and heat transfer in an eccentric annulus filled by Copper nanofluid. *International Journal of Heat And Mass Transfer, 61*, 353-364. doi:https://doi.org/10.1016/j.ijheatmasstransfer.2013.01.061

Hamilton, R. L., & Crosser, O. K. (1962). Thermal conductivity of heterogeneous two-component systems. *Industrial Engineering and Chemistry Fundamentals, 1*. doi:10.1021/i160003a005

Hamzah, M. H., Sidik, N. A. C., Ken, T. L., Mamat, R., & Najafi, G. (2017). Factors affecting the performance of hybrid nanofluids: A comprehensive review. *International Journal of Heat and Mass Transfer, 115*(Part A), 630-646. doi:https://doi.org/10.1016/j.ijheatmasstransfer.2017.07.021

Hejazian, M., & Moraveji, M. K. (2013). A Comparative Analysis of Single and Two-Phase Models of Turbulent Convective Heat Transfer in a Tube for TiO2 Nanofluid with CFD. *Numerical Heat Transfer, Part A: Applications, 63*(10), 795-806. doi:10.1080/10407782.2013.756759

Hemmat Esfe, M., Saedodin, S., & Mahmoodi, M. (2014). Experimental studies on the convective heat transfer performance and thermophysical properties of MgO–water nanofluid under turbulent flow. *Experimental Thermal and Fluid Science, 52*, 68-78. doi:https://doi.org/10.1016/j.expthermflusci.2013.08.023

Heyhat, M. M. K., F. Rashidi, A. M. Alem Varzane Esfehani, S. Amrollahi, A. (2012). Experimental investigation of turbulent flow and convective heat transfer characteristics of alumina water nanofluids in fully developed flow regime. *International Communications in Heat and Mass Transfer, 39*(8), 1272-1278. doi:https://doi.org/10.1016/j.icheatmasstransfer.2012.06.024

Ho, C. J., Liu, W. K., Chang, Y. S., & Lin, C. C. (2010). Natural convection heat transfer of alumina-water nanofluid in vertical square enclosures: An experimental study. *International Journal of Thermal Sciences, 49*(8), 1345-1353. doi:https://doi.org/10.1016/j.ijthermalsci.2010.02.013

Ho, C. J., Wei, L. C., & Li, Z. W. (2010). An experimental investigation of forced convective cooling performance of a microchannel heat sink with Al2O3/water nanofluid. *Applied Thermal Engineering, 30*(2), 96-103. doi:https://doi.org/10.1016/j.applthermaleng.2009.07.003

Hu, Y. L., Decai; Shu, Shi; Niu, Xiaodong. (2017). Natural convection in a nanofluid-filled eccentric annulus with constant heat flux wall: A lattice Boltzmann study with immersed boundary method. *International Communications in Heat and Mass Transfer, 86*, 262-273. doi:https://doi.org/10.1016/j.icheatmasstransfer.2017.05.015

Hussein, A. M., Sharma, K. V., Bakar, R. A., & Kadirgama, K. (2013). The Effect of Nanofluid Volume Concentration on Heat Transfer and Friction Factor inside a Horizontal Tube. *Journal of Nanomaterials, 2013*, 12. doi:10.1155/2013/859563

Inkyo, M., Tokunaga, Y., Tahara, T., Iwaki, T., Iskandar, F., Hogan, C. J., & Okuyama, K. (2008). Beads Mill-Assisted Synthesis of Poly Methyl Methacrylate (PMMA)-TiO2 Nanoparticle Composites. *Industrial & Engineering Chemistry Research, 47*(8), 2597-2604. doi:10.1021/ie071069j

Jabbari, F., Rajabpour, A., & Saedodin, S. (2017). Thermal conductivity and viscosity of nanofluids: A review of recent molecular dynamics studies. *Chemical Engineering Science, 174*, 67-81. doi:10.1016/j.ces.2017.08.034

Jafarimoghaddam, A., & Aberoumand, S. (2017). A Comparison between heat transfer performance of rectangular and semicircular tubes considering boundary effects on Brownian motions in the presence of Ag / water nanofluids: Applicable in the design of cooling system of photovoltaic cells. *PLOS ONE, 12*(7), e0180883-e0180883. doi:10.1371/journal.pone.0180883

Jang, S. P., & Choi, S. U. S. (2004). Role of Brownian motion in the enhanced thermal conductivity of nanofluids. *Applied Physics Letters, 84*. doi:10.1063/1.1756684

Jarahnejad, M., Haghighi, E. B., Saleemi, M., Nikkam, N., Khodabandeh, R., Palm, B., . . . Muhammed, M. (2015). Experimental investigation on viscosity of water-based Al2O3 and TiO2 nanofluids. *Rheologica Acta, 54*(5), 411-422. doi:10.1007/s00397-015-0838-y

Jiang, L., Gao, L., & Sun, J. (2003). Production of aqueous colloidal dispersions of carbon nanotubes. *Journal of Colloid and Interface Science, 260*(1), 89-94. doi:https://doi.org/10.1016/S0021-9797(02)00176-5

Joni, I. M., Purwanto, A., Iskandar, F., & Okuyama, K. (2009). Dispersion Stability Enhancement of Titania Nanoparticles in Organic Solvent Using a Bead Mill Process. *Industrial & Engineering Chemistry Research, 48*(15), 6916-6922. doi:10.1021/ie801812f

Kakaç, S., & Pramuanjaroenkij, A. (2009). Review of convective heat transfer enhancement with nanofluids. *International Journal of Heat and Mass Transfer, 52*(13–14), 3187-3196. doi:http://dx.doi.org/10.1016/j.ijheatmasstransfer.2009.02.006

Kanakia, S. T., Jimmy D.; Chowdhury, Sayan Mullick; Lalwani, Gaurav; Tembulkar, Tanuf; Button, Terry; Shroyer, Kenneth R.; Moore, William; Sitharaman, Balaji. (2013). Physicochemical characterization of a novel graphene-based magnetic resonance imaging contrast agent. *International journal of nanomedicine, 8*, 2821-2833. doi:10.2147/IJN.S47062

Kanaras, A. G., Kamounah, F. S., Schaumburg, K., Kiely, C. J., & Brust, M. (2002). Thioalkylated tetraethylene glycol: a new ligand for water soluble monolayer protected gold clusters. *Chemical Communications*(20), 2294-2295. doi:10.1039/B207838B

Keblinski, P., Phillpot, S. R., Choi, S. U. S., & Eastman, J. A. (2002). Mechanisms of heat flow in suspensions of nano-sized particles (nanofluids). *International Journal of Heat and Mass Transfer, 45*(4), 855-863. doi:http://dx.doi.org/10.1016/S0017-9310(01)00175-2

Keblinski, P., & Thomin, J. (2006). Hydrodynamic field around a Brownian particle. *PHYSICAL REVIEW E, 73*(1), 010502.

Kenjereš, S., & Hanjalić, K. (1995). Prediction of turbulent thermal convection in concentric and eccentric horizontal annuli. *International Journal of Heat and Fluid Flow, 16*(5), 429-439. doi:https://doi.org/10.1016/0142-727X(95)00051-Q

Khairul, M. A., Shah, K., Doroodchi, E., Azizian, R., & Moghtaderi, B. (2016). Effects of surfactant on stability and thermo-physical properties of metal oxide nanofluids. *International Journal of Heat and Mass Transfer, 98*(Supplement C), 778-787. doi:https://doi.org/10.1016/j.ijheatmasstransfer.2016.03.079

Khanafer, K., & Vafai, K. (2011). A critical synthesis of thermophysical characteristics of nanofluids. *International Journal of Heat and Mass Transfer, 54*(19–20), 4410-4428. doi:http://dx.doi.org/10.1016/j.ijheatmasstransfer.2011.04.048

Khoshvaght-Aliabadi, M., Rahnama, P., Zanganeh, A., & Akbari, M. H. (2016). Experimental study on metallic water nanofluids flow inside rectangular duct equipped with circular pins (pin channel). *Experimental Thermal and Fluid Science, 72*, 18-30. doi:https://doi.org/10.1016/j.expthermflusci.2015.10.029

Kim, H. J., Bang, I. C., & Onoe, J. (2009). Characteristic stability of bare Au-water nanofluids fabricated by pulsed laser ablation in liquids. *Optics and Lasers in Engineering, 47*(5), 532-538. doi:https://doi.org/10.1016/j.optlaseng.2008.10.011

Kline, N., & Tavoularis, S. (2015). An Experimental Study of Forced Heat Convection in Concentric and Eccentric Annular Channels. *Journal of Heat Transfer, 138*(1), 012502-012502-012511. doi:10.1115/1.4031160

Kline, S. (1953). Describing Uncertainties in Single-Sample Experiments. *Mechanical Engineering, 75*, 3-8.

Kole, M., & Dey, T. K. (2013). Investigation of thermal conductivity, viscosity, and electrical conductivity of graphene based nanofluids. *Journal of Applied Physics, 113*(8), 084307. doi:doi:http://dx.doi.org/10.1063/1.4793581

Kumar, A., Joshi, H. M., Mandale, A. B., Srivastava, R., Adyanthaya, S. D., Pasricha, R., & Sastry, M. (2004). Phase transfer of platinum nanoparticles from aqueous to organic solutions using fatty amine molecules. *Journal of Chemical Sciences, 116*(5), 293-300. doi:10.1007/bf02708280

Kumar, G., Banu, G. S., Pappa, P. V., Sundararajan, M., & Pandian, M. R. (2004). Hepatoprotective activity of Trianthema portulacastrum L. against paracetamol and thioacetamide intoxication in albino rats. *Journal of Ethnopharmacology, 92*(1), 37-40. doi:https://doi.org/10.1016/j.jep.2003.12.009

Kumar, S. A., Meenakshi, K. S., Narashimhan, B. R. V., Srikanth, S., & Arthanareeswaran, G. (2009). Synthesis and characterization of copper nanofluid by a novel one-step method. *Materials Chemistry and Physics, 113*(1), 57-62. doi:https://doi.org/10.1016/j.matchemphys.2008.07.027

Launder, B. E., & Spalding, D. B. (1972). *Lectures in mathematical models of turbulence*. London ;: Academic Press.

Lee, D., Kim, J.-W., & Kim, B. G. (2006). A New Parameter to Control Heat Transport in Nanofluids: Surface Charge State of the Particle in Suspension. *The Journal of Physical Chemistry B, 110*(9), 4323-4328. doi:10.1021/jp057225m

Lee, J.-H., Hwang, K. S., Jang, S. P., Lee, B. H., Kim, J. H., Choi, S. U. S., & Choi, C. J. (2008). Effective viscosities and thermal conductivities of aqueous nanofluids containing low volume concentrations of Al2O3 nanoparticles. *International Journal of Heat and Mass Transfer, 51*(11–12), 2651-2656. doi:http://dx.doi.org/10.1016/j.ijheatmasstransfer.2007.10.026

Lee, S., & Choi, S. U. S. (1999). Measuring thermal conductivity of fluids containing oxide nanoparticles. *Journal of Heat Transfer, 121*. doi:10.1115/1.2825978

Lee, S. W., Park, S. D., & Bang, I. C. (2012). Critical heat flux for CuO nanofluid fabricated by pulsed laser ablation differentiating deposition characteristics. *International Journal of Heat and Mass Transfer, 55*(23), 6908-6915. doi:https://doi.org/10.1016/j.ijheatmasstransfer.2012.07.004

Lee, Y., & Barrow, H. (1963). Paper 12: Turbulent Flow and Heat Transfer in Concentric and Eccentric Annuli. *Proceedings of the Institution of Mechanical Engineers, Conference Proceedings, 178*(9), 1-16. doi:10.1243/pime_conf_1963_178_231_02

Li, C. H., & Peterson, G. P. (2006). Experimental investigation of temperature and volume fraction variations on the effective thermal conductivity of nanoparticle suspensions (nanofluids). *Journal of Applied Physics, 99*(8), 084314. doi:doi:http://dx.doi.org/10.1063/1.2191571

Li, C. H., & Peterson, G. P. (2007). The effect of particle size on the effective thermal conductivity of Al2O3-water nanofluids. *Journal of Applied Physics, 101*(4), 044312. doi:doi:http://dx.doi.org/10.1063/1.2436472

Li, X., Zhu, D., & Wang, X. (2007). Evaluation on dispersion behavior of the aqueous copper nano-suspensions. *Journal of Colloid and Interface Science, 310*(2), 456-463. doi:https://doi.org/10.1016/j.jcis.2007.02.067

Liu, M., Lin, M. C., & Wang, C. (2011). Enhancements of thermal conductivities with Cu, CuO, and carbon nanotube nanofluids and application of MWNT/water nanofluid on a water chiller system. *Nanoscale Research Letters, 6*(1), 297-297. doi:10.1186/1556-276X-6-297

Lo, C.-H., Tsung, T.-T., & Chen, L.-C. (2005). Shape-controlled synthesis of Cu-based nanofluid using submerged arc nanoparticle synthesis system (SANSS). *Journal of Crystal Growth, 277(1),* 636-642. doi:https://doi.org/10.1016/j.jcrysgro.

Lo, C.-H., Tsung, T.-T., & Lin, H.-M. (2007). Preparation of silver nanofluid by the submerged arc nanoparticle synthesis system (SANSS). *Journal of Alloys and Compounds, 434-435* (SupplementC), 659-662. doi:https://doi.org/10.1016/j.jallcom.2006.08.217

Lotfi, R., Saboohi, Y., & Rashidi, A. M. (2010). Numerical study of forced convective heat transfer of Nanofluids: Comparison of different approaches. *International Communications in Heat and Mass Transfer, 37*(1), 74-78. doi:https://doi.org/10.1016/j.icheatmasstransfer.2009.07.013

Ma, M., Zhu, Y.-J., Cheng, G., & Huang, Y. (2008). Solvothermal Synthesis of Boehmite and γ-Alumina Nanorods. *Journal of Materials Science and Technology, 24*.

Mahian, O., Kianifar, A., Heris, S. Z., & Wongwises, S. (2016). Natural convection of silica nanofluids in square and triangular enclosures: Theoretical and experimental study. *International Journal of Heat and Mass Transfer, 99*(Supplement C), 792-804. doi:https://doi.org/10.1016/j.ijheatmasstransfer.2016.03.045

Maïga, S. E. B. P., Samy Joseph Nguyen, Cong Tam Roy, Gilles Galanis, Nicolas. (2005). Heat transfer enhancement by using nanofluids in forced convection flows. *International Journal of Heat and Fluid Flow, 26*(4), 530-546. doi:https://doi.org/10.1016/j.ijheatfluidflow.2005.02.004

Masuda, H., Ebata, A., Teramea, K., & Hishinuma, N. (1993). Alteration of thermal conductivity and viscosity of liquid by dispersing ultra-fine particles. *Netsu Bussei, 4*. doi:10.2963/jjtp.7.227

Matin, M. H., & Pop, I. (2014). Numerical Study of Mixed Convection Heat Transfer of a Nanofluid in an Eccentric Annulus. *Numerical Heat Transfer, Part A: Applications, 65*(1), 84-105. doi:10.1080/10407782.2013.812000

Maxwell, J. C. (1891). *A Treatise on Electricity and Magnetism*. Oxford: Clarendon.

Mayerhöfer, T. G., & Popp, J. (2019). Beer's law derived from electromagnetic theory. *Spectrochimica Acta Part A: Molecular and Biomolecular Spectroscopy, 215*, 345-347. doi:https://doi.org/10.1016/j.saa.2019.02.103

McAdams, W. H. (1954). *Heat Transmissions* (3rd ed.). New York: McGraw-Hill , Inc.

Mehrali, M., Sadeghinezhad, E., Latibari, S. T., Kazi, S. N., Mehrali, M., Zubir, M. N. B. M., & Metselaar, H. S. C. (2014). Investigation of thermal conductivity and rheological properties of nanofluids containing graphene nanoplatelets. *Nanoscale Research Letters, 9*(1), 15. doi:10.1186/1556-276x-9-15

Mirzaee, M., & Lakzian, E. (2017). Entropy generation analysis of eccentric cylinders pair sources on nanofluid natural convection with non-Boussinesq state. *Advanced Powder Technology, 28*(12), 3172-3183. doi:https://doi.org/10.1016/j.apt.2017.09.034

Missana, T., & Adell, A. (2000). On the Applicability of DLVO Theory to the Prediction of Clay Colloids Stability. *Journal of Colloid and Interface Science, 230*(1), 150-156. doi:https://doi.org/10.1006/jcis.2000.7003

Moffat, R. J. (1988). Describing the uncertainties in experimental results. *Experimental Thermal and Fluid Science, 1*(1), 3-17. doi:https://doi.org/10.1016/0894-1777(88)90043-X

Mohanrajhu, N., Purushothaman, K., & Kulasekharan, N. (2015). Numerical Heat Transfer and Pressure Drop Studies of Turbulent Al2O3 - Ethylene Glycol/Water Nanofluid Flow in an Automotive Radiator Tube. *Applied Mechanics and Materials, 787*, 152-156. doi:10.4028/www.scientific.net/AMM.787.152

Munson, B. R. (2013). *Fundamentals of fluid mechanics*: Seventh edition. Hoboken, NJ : John Wiley & Sons, Inc., [2013].

Namburu, P. K., Kulkarni, D. P., Dandekar, A., & Das, D. K. (2007). Experimental investigation of viscosity and specific heat of silicon dioxide nanofluids. *IET Micro & Nano Letters, 2*(3), 67-71. doi:10.1049/mnl:20070037

Nasiri, A., Shariaty-Niasar, M., Rashidi, A., Amrollahi, A., & Khodafarin, R. (2011). Effect of dispersion method on thermal conductivity and stability of nanofluid. *Experimental Thermal and Fluid Science, 35*(4), 717-723. doi:https://doi.org/10.1016/j.expthermflusci.2011.01.006

Nasiri, A., Shariaty-Niasar, M., Rashidi, A. M., & Khodafarin, R. (2012). Effect of CNT structures on thermal conductivity and stability of nanofluid. *International Journal of Heat and Mass Transfer, 55*(5), 1529-1535. doi:https://doi.org/10.1016/j.ijheatmasstransfer.2011.11.004

Nasiri, M., Etemad, S. G., & Bagheri, R. (2011). Experimental heat transfer of nanofluid through an annular duct. *International Communications in Heat and Mass Transfer, 38*(7), 958-963. doi:https://doi.org/10.1016/j.icheatmasstransfer.2011.04.011

Nikitin, N., Wang, H., & Chernyshenko, S. (2009). Turbulent flow and heat transfer in eccentric annulus. *Journal of Fluid Mechanics, 638*, 95-116. doi:10.1017/S002211200900812X

Niyogi, S., Hamon, M. A., Hu, H., Zhao, B., Bhowmik, P., Sen, R., . . . Haddon, R. C. (2002). Chemistry of single-walled carbon nanotubes. *Acc Chem Res, 35*(12), 1105-1113. doi:10.1021/ar010155r

Ogino, F., Sakano, T., & Mizushina, T. (1987). Momentum and heat transfers from fully developed turbulent flow in an eccentric annulus to inner and outer tube walls. *Wärme - und Stoffübertragung, 21*(2), 87-93. doi:10.1007/BF01377564

Pak, B. C., & Cho, Y. I. (1998). Hydrodynamic and heat transfer study of dispersed fluids with submicron metallic oxide particles. *Experimental Heat Transfer, 11*(2), 151-170. doi:10.1080/08916159808946559

Parekh, K., & Lee, H. S. (2010). Magnetic field induced enhancement in thermal conductivity of magnetite nanofluid. *Journal of Applied Physics, 107*(9), 09A310. doi:10.1063/1.3348387

Pasquali, R. C., Taurozzi, M. P., & Bregni, C. (2008). Some considerations about the hydrophilic–lipophilic balance system. *International Journal of Pharmaceutics, 356*(1), 44-51. doi:https://doi.org/10.1016/j.ijpharm.2007.12.034

Petukhov, B. S. (1970). Heat Transfer and Friction in Turbulent Pipe Flow with Variable Physical Properties. In J. P. Hartnett & T. F. Irvine (Eds.), *Advances in Heat Transfer* (Vol. 6, pp. 503-564): Elsevier.

Philip, J., Shima, P. D., & Raj, B. (2007). Enhancement of thermal conductivity in magnetite based nanofluid due to chainlike structures. *Applied Physics Letters, 91*(20), 203108. doi:10.1063/1.2812699

Phuoc, T. X., Soong, Y., & Chyu, M. K. (2007). Synthesis of Ag-deionized water nanofluids using multi-beam laser ablation in liquids. *Optics and Lasers in Engineering, 45*(12), 1099-1106. doi:https://doi.org/10.1016/j.optlaseng.2007.06.005

Popiel, C. O., & Wojtkowiak, J. (1998). Simple Formulas for Thermophysical Properties of Liquid Water for Heat Transfer Calculations (from 0°C to 150°C). *Heat Transfer Engineering, 19*(3), 87-101. doi:10.1080/01457639808939929

Ranjbarzadeh, R., Karimipour, A., Afrand, M., Isfahani, A. H. M., & Shirneshan, A. (2017). Empirical analysis of heat transfer and friction factor of water/graphene oxide nanofluid flow in turbulent regime through an isothermal pipe. *Applied Thermal Engineering, 126*, 538-547. doi:https://doi.org/10.1016/j.applthermaleng.2017.07.189

Rastogi, R. K., Rahul; Tripathi, S. K.; Sharma, Amit L.; Kaur, Inderpreet; Bharadwaj, Lalit M. (2008). Comparative study of carbon nanotube dispersion using surfactants. *Journal of Colloid and Interface Science, 328*(2), 421-428. doi:https://doi.org/10.1016/j.jcis.2008.09.015

Razzaq, M. Y., Anhalt, M., Frormann, L., & Weidenfeller, B. (2007). Thermal, electrical and magnetic studies of magnetite filled polyurethane shape memory polymers. *Materials Science and Engineering: A, 444*(1), 227-235. doi:https://doi.org/10.1016/j.msea.2006.08.083

Rohsenow, W., Rohsenow, W. M., Hartnett, J. P., & Ganić, E. N. (1985). *Handbook of Heat Transfer Applications*: McGraw-Hill.

Rostamani, M., Hosseinizadeh, S. F., Gorji, M., & Khodadadi, J. M. (2010). Numerical study of turbulent forced convection flow of nanofluids in a long horizontal duct considering variable properties. *International Communications in Heat and Mass Transfer, 37*(10), 1426-1431. doi:https://doi.org/10.1016/j.icheatmasstransfer.2010.08.007

Sadeghinezhad, E., Mehrali, M., Tahan Latibari, S., Mehrali, M., Kazi, S. N., Oon, C. S., & Metselaar, H. S. C. (2014). Experimental Investigation of Convective Heat

Transfer Using Graphene Nanoplatelet Based Nanofluids under Turbulent Flow Conditions. *Industrial & Engineering Chemistry Research, 53*(31), 12455-12465. doi:10.1021/ie501947u

Sadri, R., Hosseini, M., Kazi, S. N., Bagheri, S., Abdelrazek, A. H., Ahmadi, G., . . . Abidin, N. I. Z. (2017). A facile, bio-based, novel approach for synthesis of covalently functionalized graphene nanoplatelet nano-coolants toward improved thermo-physical and heat transfer properties. *Journal of Colloid and Interface Science*. doi:https://doi.org/10.1016/j.jcis.2017.07.052

Sadri, R., Hosseini, M., Kazi, S. N., Bagheri, S., Zubir, N., Solangi, K. H., . . . Badarudin, A. (2017). A bio-based, facile approach for the preparation of covalently functionalized carbon nanotubes aqueous suspensions and their potential as heat transfer fluids. *Journal of Colloid and Interface Science, 504*(Supplement C), 115-123. doi:https://doi.org/10.1016/j.jcis.2017.03.051

Sadri, R., Mallah, A. R., Hosseini, M., Ahmadi, G., Kazi, S. N., Dabbagh, A., . . . Yaakup, N. A. (2018). CFD modeling of turbulent convection heat transfer of nanofluids containing green functionalized graphene nanoplatelets flowing in a horizontal tube: Comparison with experimental data. *Journal of Molecular Liquids, 269*, 152-159. doi:https://doi.org/10.1016/j.molliq.2018.06.011

Saha, G., & Paul, M. C. (2014). Numerical analysis of the heat transfer behaviour of water based Al2O3 and TiO2 nanofluids in a circular pipe under the turbulent flow condition. *International Communications in Heat and Mass Transfer, 56*, 96-108. doi:https://doi.org/10.1016/j.icheatmasstransfer.2014.06.008

Sahoo, B. C., Vajjha, R. S., Ganguli, R., Chukwu, G. A., & Das, D. K. (2009). Determination of Rheological Behavior of Aluminum Oxide Nanofluid and Development of New Viscosity Correlations. *Petroleum Science and Technology, 27*(15), 1757-1770. doi:10.1080/10916460802640241

Saidur, R., Leong, K. Y., & Mohammed, H. A. (2011). A review on applications and challenges of nanofluids. *Renewable and Sustainable Energy Reviews, 15*(3), 1646-1668. doi:https://doi.org/10.1016/j.rser.2010.11.035

Sarkar, J., Ghosh, P., & Adil, A. (2015). A review on hybrid nanofluids: Recent research, development and applications. *Renewable and Sustainable Energy Reviews, 43*, 164-177. doi:http://dx.doi.org/10.1016/j.rser.2014.11.023

Sarsam W. S., A. A., Zubir M. N. M., Yarmand H., Kazi S. N., Badarudin A. (2016). Stability and thermophysical properties of water-based nanofluids containing triethanolamine-treated graphene nanoplatelets with different specific surface areas. *Colloids and Surfaces a-Physicochemical and Engineering Aspects, 500*, 17-31. doi:10.1016/j.colsurfa.2016.04.016

Sekhar, Y. R., & Sharma, K. V. (2015). Study of viscosity and specific heat capacity characteristics of water-based Al2O3 nanofluids at low particle concentrations. *Journal of Experimental Nanoscience, 10*(2), 86-102. doi:10.1080/17458080.2013.796595

Selvam, C., Lal, D. M., & Harish, S. (2016). Thermal conductivity enhancement of ethylene glycol and water with graphene nanoplatelets. *Thermochimica Acta, 642*(Supplement C), 32-38. doi:https://doi.org/10.1016/j.tca.2016.09.002

Şenay, G., Kaya, M., Gedik, E., & Kayfeci, M. (2019). Numerical investigation on turbulent convective heat transfer of nanofluid flow in a square cross-sectioned duct. *International Journal of Numerical Methods for Heat and Fluid Flow*. doi:10.1108/HFF-06-2018-0260

Shahsavar, A., & Bahiraei, M. (2017). Experimental investigation and modeling of thermal conductivity and viscosity for non-Newtonian hybrid nanofluid containing coated CNT/Fe3O4 nanoparticles. *Powder Technology, 318*, 441-450. doi:https://doi.org/10.1016/j.powtec.2017.06.023

Shahzadi, I., & Nadeem, S. (2017). Stimulation of metallic nanoparticles under the impact of radial magnetic field through eccentric cylinders: A useful application in biomedicine. *Journal of Molecular Liquids, 225*, 365-381. doi:https://doi.org/10.1016/j.molliq.2016.11.062

Shanbedi, M., Zeinali Heris, S., & Maskooki, A. (2015). Experimental investigation of stability and thermophysical properties of carbon nanotubes suspension in the presence of different surfactants. *Journal of Thermal Analysis and Calorimetry, 120*(2), 1193-1201. doi:10.1007/s10973-015-4404-8

Sharma, K., Sarm, PK, Azmi, WH, Mamat, Rizalman, Kadirgama, K. (2012). Correlations to predict friction and forced convection heat transfer coefficients of water based nanofluids for turbulent flow in a tube. *International Journal of Microscale and Nanoscale Thermal and Fluid Transport Phenomena, 3*(4), 25.

Sheikholeslami, M., Gorji-Bandpy, M., & Ganji, D. D. (2014). MHD free convection in an eccentric semi-annulus filled with nanofluid. *Journal of the Taiwan Institute of Chemical Engineers, 45*(4), 1204-1216. doi:https://doi.org/10.1016/j.jtice.2014.03.010

Shima, P. D., Philip, J., & Raj, B. (2010). Influence of aggregation on thermal conductivity in stable and unstable nanofluids. *Applied Physics Letters, 97*(15), 153113. doi:10.1063/1.3497280

Siginer, D. A., & Wang, H. P. (1995). *Developments and Applications of Non-Newtonian Flows.* Paper presented at the Asme International Mechanical Engineering Congress and Exposition, San Francisco, California.

Silambarasan, M., Manikandan, S., & Rajan, K. S. (2012). Viscosity and thermal conductivity of dispersions of sub-micron TiO2 particles in water prepared by stirred bead milling and ultrasonication. *International Journal of Heat and Mass Transfer, 55*(25), 7991-8002. doi:https://doi.org/10.1016/j.ijheatmasstransfer.2012.08.030

Singh, A. K., & Raykar, V. S. (2008). Microwave synthesis of silver nanofluids with polyvinylpyrrolidone (PVP) and their transport properties. *Colloid and Polymer Science, 286*(14), 1667-1673. doi:10.1007/s00396-008-1932-9

Sonawane, S. S., Khedkar, R. S., & Wasewar, K. L. (2013). Study on concentric tube heat exchanger heat transfer performance using Al2O3 – water based nanofluids. *International Communications in Heat and Mass Transfer, 49*, 60-68. doi:https://doi.org/10.1016/j.icheatmasstransfer.2013.10.001

Sridhara, V., & Satapathy, L. N. (2011). Al(2)O(3)-based nanofluids: a review. *Nanoscale Research Letters, 6*(1), 456-456. doi:10.1186/1556-276X-6-456

Syam Sundar, L., Singh, M. K., & Sousa, A. C. M. (2013). Investigation of thermal conductivity and viscosity of Fe3O4 nanofluid for heat transfer applications. *International Communications in Heat and Mass Transfer, 44*(Supplement C), 7-14. doi:https://doi.org/10.1016/j.icheatmasstransfer.2013.02.014

Taler, D. (2016). Determining velocity and friction factor for turbulent flow in smooth tubes. *International Journal of Thermal Sciences, 105*, 109-122. doi:https://doi.org/10.1016/j.ijthermalsci.2016.02.011

Tang, E., Cheng, G., Ma, X., Pang, X., & Zhao, Q. (2006). Surface modification of zinc oxide nanoparticle by PMAA and its dispersion in aqueous system. *Applied Surface Science, 252*(14), 5227-5232. doi:https://doi.org/10.1016/j.apsusc.2005.08.004

Tawfik, M. M. (2017). Experimental studies of nanofluid thermal conductivity enhancement and applications: A review. *Renewable & Sustainable Energy Reviews, 75*, 1239-1253. doi:10.1016/j.rser.2016.11.111

Teimouri, H. S., Ghanbar Ali; Afrand, Masoud; Fakhari, Mohammad Mahdi. (2017). Mixed convection in a rotating eccentric annulus containing nanofluid using bi-orthogonal grid types: A finite volume simulation. *Journal of Molecular Liquids, 227*, 114-126. doi:https://doi.org/10.1016/j.molliq.2016.11.094

Timofeeva, E. (2011). Nanofluids for heat transfer–potential and engineering strategies. In: Two phase flow, phase change and numerical modelling. *InTech, Croatia*, 15.

Trisaksri, V., & Wongwises, S. (2007). Critical review of heat transfer characteristics of nanofluids. *Renewable and Sustainable Energy Reviews, 11*(3), 512-523. doi:https://doi.org/10.1016/j.rser.2005.01.010

Tsai, T.-H., Kuo, L.-S., Chen, P.-H., & Yang, C.-T. (2008). Effect of viscosity of base fluid on thermal conductivity of nanofluids. *Applied Physics Letters, 93*(23), 233121. doi:10.1063/1.3046732

Usui, H., & Tsuruta, K. (1980). Analysis of fully developed turbulent flow in an eccentric annulus. *Journal of Chemical Engineering of Japan, 13*(6), 445-450. doi:10.1252/jcej.13.445

Vajjha, R. S., & Das, D. K. (2012). A review and analysis on influence of temperature and concentration of nanofluids on thermophysical properties, heat transfer and pumping power. *International Journal of Heat and Mass Transfer, 55*(15), 4063-4078. doi:https://doi.org/10.1016/j.ijheatmasstransfer.2012.03.048

Vandsburger, L. (2009). Synthesis and covalent surface modification of carbon nanotubes for preparation of stabilized nanofluid suspensions.

Wamkam, C. T., Opoku, M. K., Hong, H., & Smith, P. (2011). Effects of pH on heat transfer nanofluids containing ZrO2 and TiO2 nanoparticles. *Journal of Applied Physics, 109*(2), 024305. doi:10.1063/1.3532003

Wang, C., Yang, J., & Ding, Y. (2013). Phase transfer based synthesis and thermophysical properties of Au/Therminol VP-1 nanofluids. *Progress in Natural Science: Materials International, 23*(3), 338-342. doi:https://doi.org/10.1016/j.pnsc.2013.04.006

Wang, X.-Q., & Mujumdar, A. S. (2007). Heat transfer characteristics of nanofluids: a review. *International Journal of Thermal Sciences, 46*(1), 1-19. doi:http://dx.doi.org/10.1016/j.ijthermalsci.2006.06.010

Wang, X., Xu, S., Zhou, J., & Xu, W. (2010). A rapid phase transfer method for nanoparticles using alkylamine stabilizers. *Journal of Colloid and Interface Science, 348*(1), 24-28. doi:https://doi.org/10.1016/j.jcis.2010.03.068

Wang, X. W., Xu, X. F., & Choi, S. U. S. (1999). Thermal conductivity of nanoparticle-fluid mixture. *Journal of Thermalphysics and Heat Transfer, 13*. doi:10.2514/2.6486

Wen, D., & Ding, Y. (2004). Experimental investigation into convective heat transfer of nanofluids at the entrance region under laminar flow conditions. *International Journal of Heat and Mass Transfer, 47*(24), 5181-5188. doi:http://dx.doi.org/10.1016/j.ijheatmasstransfer.2004.07.012

Wen, D. L., Guiping; Vafaei, Saeid; Zhang, Kai. (2009). Review of nanofluids for heat transfer applications. *Particuology, 7*(2), 141-150. doi:https://doi.org/10.1016/j.partic.2009.01.007

Wiegand, J. H., McMillen, E. L., & E., L. R. (1945). Discussion on: Annular Heat Transfer Coefficients for Turbulent Flow. *American Institute of Chemical Engineers, 41*, 147–153.

Williams, W., Buongiorno, J., & Hu, L.-W. (2008). Experimental Investigation of Turbulent Convective Heat Transfer and Pressure Loss of Alumina/Water and Zirconia/Water Nanoparticle Colloids (Nanofluids) in Horizontal Tubes. *Journal of Heat Transfer, 130*(4), 042412-042412. doi:10.1115/1.2818775

Wilson, E. (1915). A basis for rational design of heat transfer apparatus. *The J. Am. Soc. Mech. Engrs., 37*, 546-551.

Wozniak, M., Danelska, A., Rutkowski, P., & Kata, D. (2013). Thermal conductivity of highly loaded aluminium nitride–poly(propylene glycol) dispersions. *International Journal of Heat and Mass Transfer, 65*(Supplement C), 592-598. doi:https://doi.org/10.1016/j.ijheatmasstransfer.2013.06.048

Xia, G., Jiang, H., Liu, R., & Zhai, Y. (2014). Effects of surfactant on the stability and thermal conductivity of Al2O3/de-ionized water nanofluids. *International*

Journal of Thermal Sciences, 84, 118-124. doi:http://dx.doi.org/10.1016/j.ijthermalsci.2014.05.004

Xie, H., Lee, H., Youn, W., & Choi, M. (2003). Nanofluids containing multiwalled carbon nanotubes and their enhanced thermal conductivities. *Journal of Applied Physics, 94*(8), 4967-4971. doi:10.1063/1.1613374

Xie, H., Wang, J., Xi, T., Liu, Y., Ai, F., & Wu, Q. (2002). Thermal conductivity enhancement of suspensions containing nanosized alumina particles. *Journal of Applied Physics, 91*(7), 4568-4572. doi:doi:http://dx.doi.org/10.1063/1.1454184

Xuan, Y., & Roetzel, W. (2000). Conceptions for heat transfer correlation of nanofluids. *International Journal of Heat and Mass Transfer, 43*(19), 3701-3707. doi:http://dx.doi.org/10.1016/S0017-9310(99)00369-5

Yang, J., Sargent, E., Kelley, S., & Ying, J. Y. (2009). A general phase-transfer protocol for metal ions and its application in nanocrystal synthesis. *Nature Materials, 8*, 683. doi:https://doi.org/10.1038/nmat2490

Yang, L., Xu, J., Du, K., & Zhang, X. (2017). Recent developments on viscosity and thermal conductivity of nanofluids. *Powder Technology, 317*(Supplement C), 348-369. doi:https://doi.org/10.1016/j.powtec.2017.04.061

Yarmand, H., Gharehkhani, S., Shirazi, S. F. S., Amiri, A., Alehashem, M. S., Dahari, M., & Kazi, S. N. (2016). Experimental investigation of thermo-physical properties, convective heat transfer and pressure drop of functionalized graphene nanoplatelets aqueous nanofluid in a square heated pipe. *Energy Conversion and Management, 114*, 38-49. doi:https://doi.org/10.1016/j.enconman.2016.02.008

Yarmand, H., Zulkifli, N. W. B. M., Gharehkhani, S., Shirazi, S. F. S., Alrashed, A. A. A. A., Ali, M. A. B., . . . Kazi, S. N. (2017). Convective heat transfer enhancement with graphene nanoplatelet/platinum hybrid nanofluid. *International Communications in Heat and Mass Transfer, 88*, 120-125. doi:https://doi.org/10.1016/j.icheatmasstransfer.2017.08.010

Yu, F., Chen, Y., Liang, X., Xu, J., Lee, C., Liang, Q., . . . Deng, T. (2017). Dispersion stability of thermal nanofluids. *Progress in Natural Science: Materials International, 27*(5), 531-542. doi:https://doi.org/10.1016/j.pnsc.2017.08.010

Yu, W., & Choi, S. (2003). The role of interfacial layers in the enhanced thermal conductivity of nanofluids: a renovated Maxwell model. *J Nanoparticle Res, 5*. doi:10.1023/a:1024438603801

Yu, W., & Xie, H. (2012). A Review on Nanofluids: Preparation, Stability Mechanisms, and Applications. *Journal of Nanomaterials, 2012*, 17. doi:10.1155/2012/435873

Yu, W., Xie, H., Wang, X., & Wang, X. (2011). Highly Efficient Method for Preparing Homogeneous and Stable Colloids Containing Graphene Oxide. *Nanoscale Research Letters, 6*(1), 47-47. doi:10.1007/s11671-010-9779-7

Yu, W. F., David M.; Routbort, Jules L.; Choi, Stephen U. S. (2008). Review and Comparison of Nanofluid Thermal Conductivity and Heat Transfer

Enhancements. *Heat Transfer Engineering, 29*(5), 432-460. doi:10.1080/01457630701850851

Zawrah, M. F., Khattab, R. M., Girgis, L. G., El Daidamony, H., & Abdel Aziz, R. E. (2016). Stability and electrical conductivity of water-base Al2O3 nanofluids for different applications. *HBRC Journal, 12*(3), 227-234. doi:https://doi.org/10.1016/j.hbrcj.2014.12.001

Zhang, Z. M. (2007). *Nano/Microscale Heat Transfer* (1st ed.). USA: McGraw-Hill Comanies, Inc.

Zhou, S.-Q., & Ni, R. (2008). Measurement of the specific heat capacity of water-based Al2O3 nanofluid. *Applied Physics Letters, 92*(9), 093123. doi:10.1063/1.2890431

Zhu, H.-t., Lin, Y.-s., & Yin, Y.-s. (2004). A novel one-step chemical method for preparation of copper nanofluids. *Journal of Colloid and Interface Science, 277*(1), 100-103. doi:https://doi.org/10.1016/j.jcis.2004.04.026

Zhu, H., Zhang, C., Tang, Y., Wang, J., Ren, B., & Yin, Y. (2007). Preparation and thermal conductivity of suspensions of graphite nanoparticles. *Carbon, 45*(1), 226-228. doi:https://doi.org/10.1016/j.carbon.2006.07.005

LIST OF PUBLICATIONS AND PAPERS PRESENTED

Journal Articles related to thesis:

1- **Abdelrazek, A. H.**, Alawi, O. A., Kazi, S. N., & Yusoff, N. (2021). Thermal performance evaluation for alumina coated MWCNTs composite nanofluid in annular passage of various eccentricities. *Powder Technology*, *391*, 114-132.

2- Alawi, O. A., **Abdelrazek, A. H.**, Aldlemy, M. S., Ahmed, W., Hussein, O. A., Ghafel, S. T., ... & Yaseen, Z. M. (2021). Heat Transfer and Hydrodynamic Properties Using Different Metal-Oxide Nanostructures in Horizontal Concentric Annular Tube: An Optimization Study. *Nanomaterials*, *11*(8), 1979.

3- Ahmed, W., Chowdhury, Z. Z., Kazi, S. N., Johan, M. R. B., **Abdelrazek, A. H.**, Fayaz, H., ... & Khan, T. Y. (2021). Experimental evaluation and numerical verification of enhanced heat transportation by using ultrasonic assisted nanofluids in a closed horizontal circular passage. *Case Studies in Thermal Engineering*, 26, 101026.

4- AbdRabbuh, O. A., Oon, C. S., Kazi, S. N., **Abdelrazek, A. H.**, Ahmed, W., Mallah, A. R., ... & Kamangar, S. (2021). An experimental investigation of eco-friendly treated GNP heat transfer growth: circular and square conduit comparison. *Journal of Thermal Analysis and Calorimetry*, *145*(1), 139-151.

5- Ahmed, W., Chowdhury, Z. Z., Kazi, S. N., Johan, M. R., Akram, N., Oon, C. S., & **Abdelrazek, A. H.** (2021). Characteristics investigation on heat transfer growth of sonochemically synthesized ZnO-DW based nanofluids inside square heat exchanger. *Journal of Thermal Analysis and Calorimetry*, *144*(4), 1517-1534.

6- **Abdelrazek, A. H.**, Kazi, S. N., Alawi, O. A., Yusoff, N., Oon, C. S., & Ali, H. M. (2020). Heat transfer and pressure drop investigation through pipe with different shapes using different types of nanofluids. *Journal of Thermal Analysis and Calorimetry*, *139*(3), 1637-1653.

7- **Abdelrazek, A. H.**, Alawi, O. A., Kazi, S. N., Yusoff, N., Chowdhury, Z., & Sarhan, A. A. (2018). A new approach to evaluate the impact of thermophysical properties of nanofluids on heat transfer and pressure drop. *International Communications in Heat and Mass Transfer*, *95*, 161-170.

8- Hosseini, M., **Abdelrazek, A. H.**, Sadri, R., Mallah, A. R., Kazi, S. N., Chew, B. T., & Yusoff, N. (2018). Numerical study of turbulent heat transfer of nanofluids containing eco-friendly treated carbon nanotubes through a concentric annular heat exchanger. *International Journal of Heat and Mass Transfer*, *127*, 403-412.

Journal Articles not related to thesis:

1- **Abdelrazek, A. H.**, Choudhury, I. A., Nukman, Y., & Kazi, S. N. (2020). Metal cutting lubricants and cutting tools: a review on the performance improvement and sustainability assessment. *The International Journal of Advanced Manufacturing Technology*, *106*(9), 4221-4245.

2- Oon, C. S., Kazi, S. N., Hakimin, M. A., **Abdelrazek, A. H.**, Mallah, A. R., Low, F. W., ... & Kamanger, S. (2020). Heat transfer and fouling deposition investigation on the titanium coated heat exchanger surface. *Powder Technology*, *373*, 671-680.

3- Sadri, R., Hosseini, M., Kazi, S. N., Bagheri, S., **Abdelrazek, A. H.**, Ahmadi, G., ... & Abidin, N. I. Z. (2018). A facile, bio-based, novel approach for synthesis of covalently functionalized graphene nanoplatelet nano-coolants toward improved thermo-physical and heat transfer properties. *Journal of colloid and interface science*, 509, 140-152.

4- **Abdelrazek, A. H.,** Taha, I. S., Morsy, M. G., & Abdel-Rahman, A. K. (2014). The effect of using false ceiling on roof cooling load. *Journal of Engineering Sciences*, 42(3), 666-682.

Conference proceedings:

1- **Ali H. Abdelrazek**, S. N. Kazi, Nukman Yusoff, I. A. Choudhury, "Experimental investigation of Al_2O_3 nanofluid performance through different heat exchanger geometries under forced turbulent flow", *International Conference on Life and Engineering Sciences* (ICOLES 2019), Istanbul, Turkey.